Durham University

Durham E-Theses

Optical Deformation of Emulsion Droplets

HANNAH MARIE BUNYAN

How to cite:

BUNYAN, HANNAH MARIE (2010) Optical Deformation of Emulsion Droplets. Masters thesis, Durham University.

Use policy

The full-text may be used and/or reproduced, and given to third parties in any format or medium, without prior permission or charge, for personal research or study, educational, or not-for-profit purposes provided that:

- a full bibliographic reference is made to the original source
- a https://etheses.durham.ac.uk/id/eprint/220/ is made to the metadata record in Durham E-Theses
- the full-text is not changed in any way

The full-text must not be sold in any format or medium without the formal permission of the copyright holders.

Please consult the full Durham E-Theses policy for further details.

Academic Support Office, The Palatine Centre, Durham University, Stockton Road, Durham, DH1 3LE
e-mail: e-theses.admin@durham.ac.uk Tel: +44 0191 334 6107
https://etheses.durham.ac.uk

Table of Contents

Table of Contents **1**

1 Introduction **1**
1.1 Aims of the Project 1
1.2 Electromagnetic Radiation 1
1.3 Refraction 2
1.4 Radiation Pressure 3
1.5 Optical Trapping 4
1.6 Optical Tweezers [3] 7
1.7 Surface Free Energy [10] 10
1.8 Surfactants 11
1.9 Micelles and Solubilisation 13
1.10 Emulsions 14
1.11 Microemulsions 14
1.12 Previous Work with Optical Tweezers 16
1.13 Temperature – Insensitive Microemulsions 19
1.14 Microfluidics 24
1.15 Membrane Emulsification 30
References 37

2 Microfluidics **41**
2.1 Introduction 41
2.2 Design of microfluidic device 41
2.3 Microfabrication 45
2.4 Photolithography 47
2.5 Method 51
2.6 Testing of first device, results and improvements 55
2.7 Design of second device 58
2.8 Testing of second device, results and improvements 59
2.9 Future Work and Improvements to Design 61
2.10 Design of a microfluidic device with Epigem 63
References 66

3 Membrane Emulsification **68**
3.1 Droplet Formation and Detachment 68
3.2 Choice of Membrane 72
3.3 Structure of Ceramic Membranes 74
3.4 Design and Construction 74
3.5 Calculation of Shear Stress 76
3.6 Method 78
3.7 Experiments 79
3.8 Results 81
3.9 Discussion and Conclusions 87

3.10 Improvements to Design and Future Work 92
3.11 Premix Membrane Emulsification 93
3.12 Droplet Formation and Break-up 94
3.13 Method 97
3.14 Examination of Emulsions 98
3.15 Results 99
3.16 0.03M NaCl/1mM AOT Solution 103
3.17 Discussion 106
References 110

4 Multiple Optical Tweezers 113
4.1 Interference and Diffraction [1] 113
4.2 Polarisation [1] 116
4.3 Spatial Light Modulators 117
4.4 Birefringence 118
4.5 Multiple optical tweezers 120
4.6 Using the SLM as a Phase Grating 122
4.7 Creating phase grating patterns 125
4.8 Experiments, Results and Discussion 127
4.9 Conclusions and Future work 131
References 135

5 Optical Deformation 136
5.1 Temperature-sensitive System 136
5.2 Control of Optical Traps 136
5.3 Results 137
5.4 Microemulsion Phase Behaviour 141
5.5 Temperature-insensitive Microemulsions 142
5.6 CTAB/Brij-58/Butanol/Heptane 143
5.7 AOT/NaCl/Brij-35/Butanol/ Eucalyptus Oil 147
5.8 AOT/NaCl/$C_{12}E_5$/Heptane 152
5.9 Alkyl Glucoside Surfactants 159
5.10 Plantacare/Cetiol S/GMO 162
References 166

1 Introduction

1.1 Aims of the Project

This project aims to investigate the deformation of emulsion droplets using optical tweezers. Manipulation and deformation of the surface of an emulsion droplet is possible due to the ultralow interfacial tension found in a microemulsion system.

A spatial light modulator will enable the arrangement of several optical traps around a single emulsion droplet, in a three dimensional array. Deformation of the emulsion droplet in three dimensions will be investigated.

Various methods for producing emulsion droplets of an ideal size will be considered, including a microfluidic device and membrane emulsification.

A temperature insensitive microemulsion will be necessary in order for exothermic emulsion polymerisation to take place without disrupting the ultralow interfacial tension. Finding such a system and putting it to use is also an aim of the project.

1.2 Electromagnetic Radiation

Electromagnetic radiation is a self-propagating wave through space or matter, composed of an electric field and a magnetic field oscillating perpendicular to one another and to the direction of travel of the wave. Electromagnetic waves move with oscillating harmonic motion (like a sine wave), and the wavelength is the distance between successive wave crests. In three dimensions the crests form what is called a wavefront. The motion of a set of wavefronts can be indicated by rays, which are lines drawn perpendicular to the wavefront. At a great distance from the source of the wave, the wavefront can be approximated by a plane, and the rays are parallel lines. Such a wave is called a plane wave [1].

1.3 Refraction

The refractive index of a medium is described by a complex number, the imaginary part of which deals with absorption of light by the medium. The ratio of the speed of light in a vacuum to the speed of light in the medium is given by n. A higher refractive index indicates that light will travel more slowly through the medium than through one with a low refractive index. When an electromagnetic wave crosses a boundary from one region to another (with different refractive indexes) its wavelength and velocity change, i.e. it is refracted. The angle of refraction is measured relative to the normal (see Figure 1).

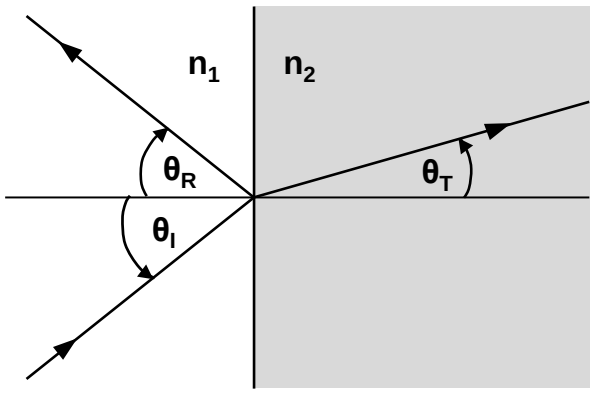

Figure 1: Reflection and refraction of a plane wave at the boundary between two dielectric media. Adapted from [2].

Snell's law (Equation 1.1) states that the ratio of the sine of the angle of incidence to the sine of the angle of refraction is a constant. Snell's law is

$$n_1 \sin\theta_I = n_2 \sin\theta_T \tag{1.1}$$

where n_1 and n_2 are the refractive indices of the two regions either side of the boundary, and θ_I and θ_T are the angles of incidence and transmission, respectively. The angle of reflection θ_R is equal to the angle of incidence θ_I. Hence if n_2 is greater than n_1, $\sin\theta_T$ must be smaller than $\sin\theta_I$, and θ', the angle of refraction, must be smaller than θ, the angle of incidence. A wave crossing a boundary from a low refractive index medium to a high refractive index medium is therefore 'bent' towards the normal.

1.4 Radiation Pressure

Radiation pressure is the force exerted on a surface exposed to electromagnetic radiation, such as a laser beam. The origin of this force is the momentum carried by light. We can regard an incident beam of light as a stream of photons. For light of frequency ν each photon has an energy

$$E = h\nu \tag{1.2}$$

and a momentum

$$p = \frac{E}{c} = \frac{h}{\lambda} \tag{1.3}$$

where h is Planck's constant, equal to 6.626 x 10^{-34} J s, c is the speed of light in a vacuum, equal to 2.998 x 10^{8} m s^{-1}, and λ is the wavelength of the light. Consider a beam of light being completely reflected from a surface. If each photon striking the surface has momentum $\frac{h}{\lambda}$, and each photon leaves the surface travelling in the opposite direction to the incident direction, then each photon will leave with momentum $-\frac{h}{\lambda}$. Momentum is always conserved, so the total momentum before the collision must equal the total momentum after the collision. Each photon must therefore have transferred $2\frac{h}{\lambda}$ to the surface, which exerts a force on the surface in the direction of incidence [3].

Light entering a dielectric (non-conducting) medium experiences a change in wavelength and velocity that must be accounted for by a change in momentum. The nature of the change in momentum (i.e. positive or negative) is the subject of a long-standing debate known as the Abraham-Minowski controversy. Recent work has suggested that evidence supports the Abraham formulation [4], but the issue has not been fully resolved [5]. The Minowski formulation [5] suggests that the momentum of light inside a dielectric medium should be:

$$p = n\frac{h}{\lambda} \tag{1.4}$$

where n is the refractive index of the dielectric medium. This equation predicts that photons entering a high refractive index material should experience increased momentum. The Abraham formulation [5] predicts that the momentum is given by:

$$p = \frac{h}{\lambda n} \tag{1.5}$$

so that light entering a high refractive index medium would experience reduced momentum. By conservation of momentum, the light must transfer the momentum it has lost or gained to the dielectric medium. Taking Abraham's formulation to be applicable, light therefore exerts a force on the surface of the dielectric medium in the direction of the propagation of light.

An alternative approach to radiation pressure is to consider a field of polarized light incident normally on a reflective (metal) surface. The electromagnetic field induces currents (oscillating charges) in the surface. The charges would be driven parallel to the surface by the electric field, but they are also subject to the incident magnetic field, lying perpendicular to both the electric field and the induced current. The net result is that the charges are driven in the direction of the propagation of the incident light. Radiation pressure is the result of these unbalanced forces at work on the surface [6].

1.5 Optical Trapping

Ashkin first observed laser radiation pressure using polystyrene latex spheres in a glass cell made from microscope slides [7]. A continuous wave laser beam of a few hundred milliwatts of power was focused on the spheres, causing the spheres to move along the cell. When the edge of the beam struck the particle, the particle was drawn into the centre of the beam axis and accelerated along the direction of the beam until it was pushed against the glass cell, where it stayed. Particles were seen to follow the beam if it was moved from

side to side while the particle was moving along the beam. For situations where the radius of the particle is much larger than the wavelength of the light, these observations can be explained by examining the ray optics of the laser beam striking the particle.

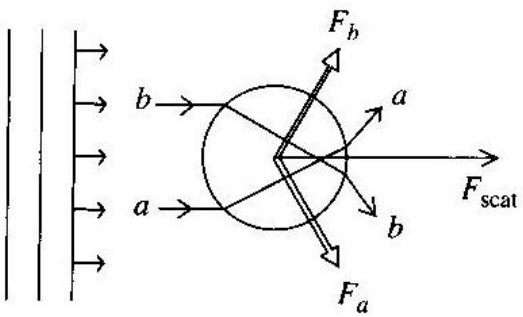

Figure 2: Origin of the scattering force F_{scat} in the direction of an incident plane wave beam. Image from [3].

Figure 2 shows a sphere, large compared to the wavelength of the light, illuminated by a plane wave. Labeled in the figure are two rays, a and b, incident symmetrically about the centre of the sphere. The sphere has a higher refractive index than the surrounding medium, so both rays are refracted by the sphere as shown. Each ray gains momentum in the axial direction and loses some momentum in the transverse direction. Since momentum is conserved, there are net forces F_a and F_b acting on the sphere. The transverse components of these forces cancel each other out, so the vector sum of F_a and F_b, along with other pairs of similar rays, gives a net force F_{scat} in the direction of the incident light.

The profile of a laser beam describes how the light intensity is distributed about its cross section. A Gaussian beam profile suggests that the intensity follows a Gaussian distribution from one edge of the beam to the other, as shown in Figure 3. A sphere placed off axis (off centre) in a Gaussian beam will experience forces similar to those felt by the particle in Figure 2 but we can expect that F_a will be larger than F_b because ray a is more intense than ray b. The vector sum of all the similar pairs of rays gives not only F_{scat} in the direction of the incident light, but also a net transverse force towards the centre of the

beam, which is called the gradient force, F_{grad}. Together these forces account for the observations Ashkin made.

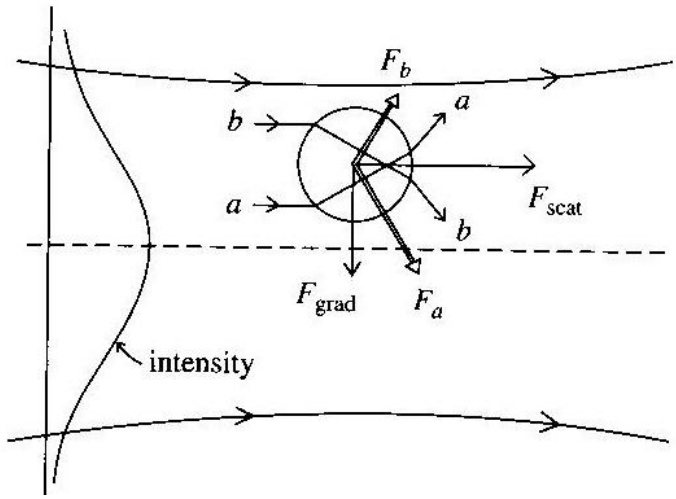

Figure 3: Origin of the transverse gradient force for a particle located off-axis in a mildly focused Gaussian beam. Image from [3].

Spheres that were pushed against the wall of the glass cell by the laser beam were trapped. If the beam was switched off the particle would diffuse away, but it could be recaptured if the beam was switched back on. The next development was the observation of the first three-dimensional 'all-optical' trap [7]. The glass wall was replaced by a second beam, propagating in the opposite direction, which exerted an equal and opposite scattering force (F_{scat}) on the particle to the force exerted by the original beam (see Figure 4). The scattering force is stronger closer to the focus of the beam, so if the particle were to move towards either end of the cell (E'), it would be restored to the centre by the stronger scattering force. Equally, if the particle were to move off axis (E'') it would be returned to the centre by the inward gradient force. Ashkin observed this in action in the form of a bright spot between the two beams, that moved rapidly to the right (in Figure 4) when Beam #2 was blocked off, and returned to the centre when the beam was switched back on. The particle moved rapidly to the left when Beam #1 was blocked off, and again returned to the centre when the beam was restored.

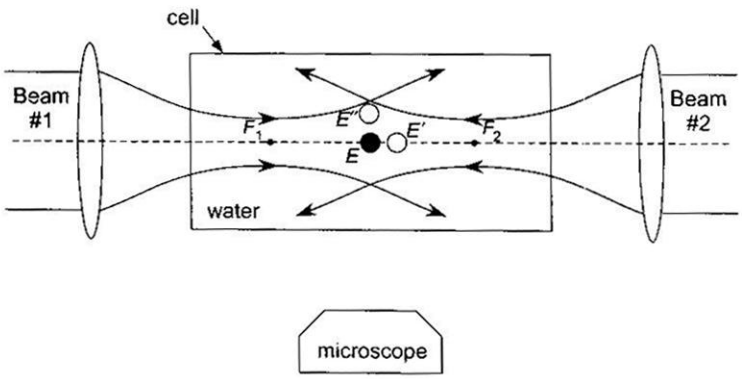

Figure 4: Diagram of the first stable optical trap, with two opposing beams located around the equilibrium point E. Displacement of the particle to E' or E'' results in a restoring force. Image from [3].

1.6 Optical Tweezers [3]

Of particular importance to the current work is Ashkin's discovery of the single-beam optical trap, or optical tweezer, as reported in 1986 [8]. Ashkin's trap uses a single, strongly focused laser beam, with an axial gradient force that dominates the axial stability.

Initial work was done with atoms placed downstream from the focus of a single Gaussian beam. Beyond the focus, there is an axial gradient force pulling the atom back towards the high intensity beam focus. If this force exceeds the forward scattering force, the atom should be pulled back to the focus and come to rest at the point where the two forces balance each other. Ashkin successfully trapped micrometer-sized dielectric spheres in 1986 [8]. A laser beam focused through a high numerical aperture microscope objective comes to a very tight focus. As shown in Figure 5, for sufficiently high beam convergence angles, there is a strong backward gradient force exerted on the sphere. This force holds the sphere in the optical trap or tweezers. The sphere can easily be moved around by moving the beam (or rather by moving the microscope stage relative to the beam focus).

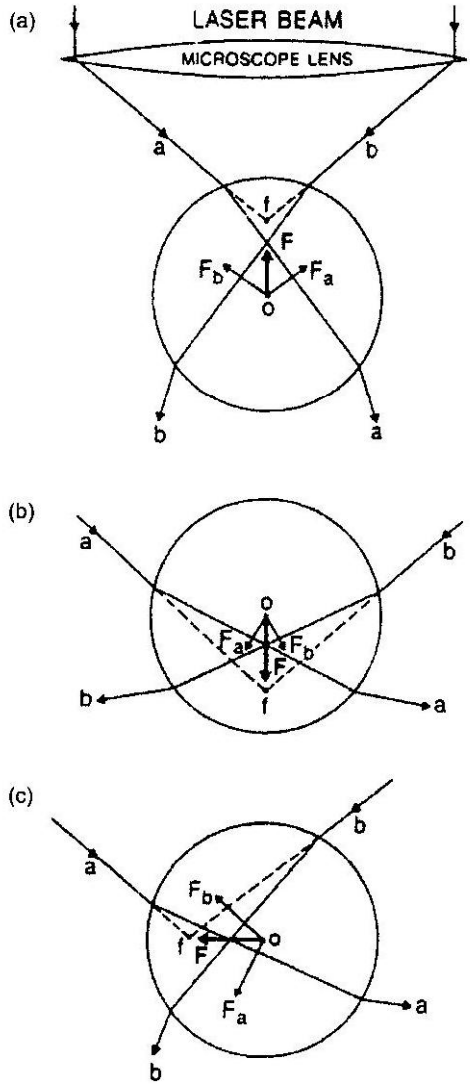

Figure 5: Ray optic explanation of the stability of optical tweezers for spherical particles large compared to the wavelength of light. (a) Sphere located below the beam focus, showing the origin of backwards radiation pressure; (b) sphere located above the beam focus; (c) sphere located to one side of the beam focus. In each case the sphere is drawn back to the focus. Image from [3].

In a typical optical trapping set-up, the laser beam is focused through a microscope objective to form a trap (see Figure 7). The same objective provides a means of imaging trapped particles. A dichroic mirror placed before a CCD camera allows the illumination light to reach the sensor but prevents the laser light from bleaching the image. The laser

beam is expanded to slightly over-fill the back aperture of the objective lens. Filling the back aperture of the objective maximizes the axial intensity gradient of the trap [9].

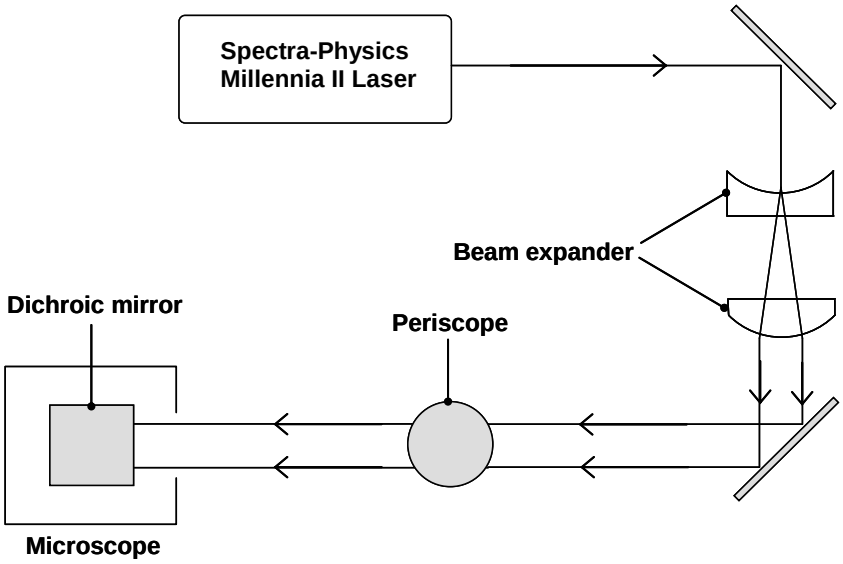

Figure 6: Plan diagram of optics set-up for optical tweezers, showing position of beam expander and periscope.

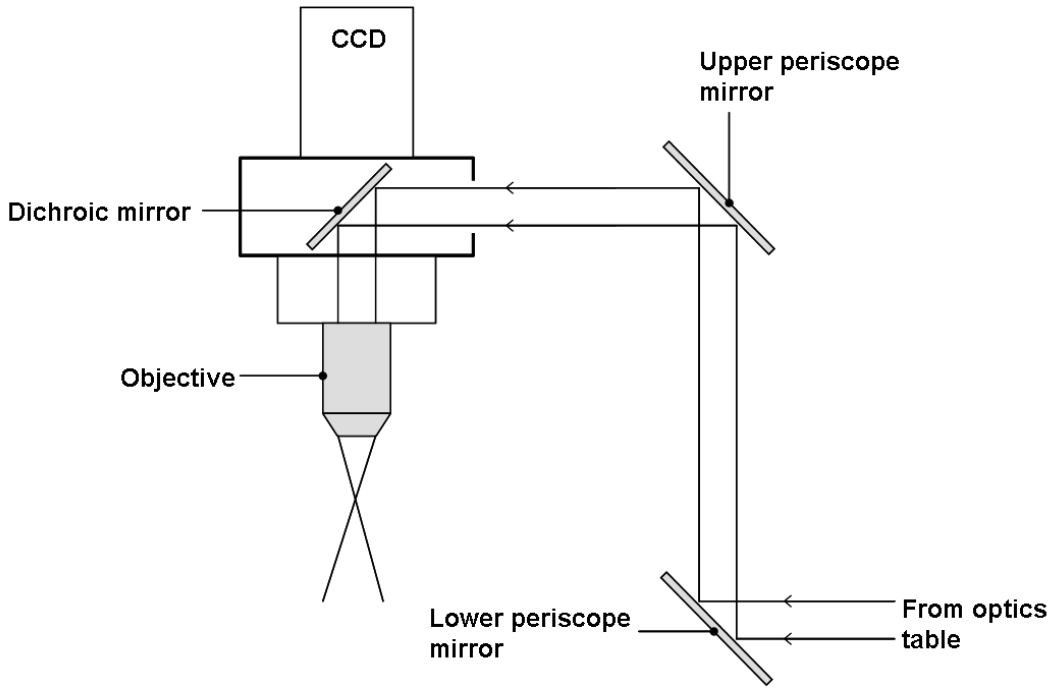

Figure 7: Side-on diagram of optical set up showing periscope and microscope.

1.7 Surface Free Energy [10]

Liquids tend to adopt shapes that minimise their surface area, in order that the maximum number of molecules are in the bulk, and are surrounded by and interact with similar molecules. A sphere is the shape with the smallest surface-to-volume ratio, so droplets tend to be spherical. The force responsible for minimising surface area is known as surface tension.

The work needed to change the surface area, A, of a system, by an infinitesimal amount dA is given by

$$dw = \gamma dA \tag{1.6}$$

where γ is the surface tension of the system. Surface tension has dimensions of energy per area, usually reported as a force per length (N m^{-1}). Surface tension can also be defined as the surface free energy per unit area.

Gibbs free energy is a thermodynamic quantity which, at constant temperature, pressure, number of moles and surface area can be defined as

$$dG_{(T,P,n,A)} = -SdT + VdP + \sum \mu_i dN_i + \gamma dA \tag{1.7}$$

where S is entropy, T is temperature, V is volume, P is pressure, μ_i is the chemical potential of any component in the system, and N_i is the number of moles of any component in the system. Because Equation (1.7) is an exact differential, we can also write

$$\left(\frac{-dS}{dA}\right)_{T,P,n} = \frac{d\gamma}{dT} \tag{1.8}$$

where $\frac{dS}{dA}$ is the surface entropy. Moving a molecule from the bulk of a liquid system to an interface where it is part of an ordered layer reduces the entropy of the system. By Equation (1.8), therefore, the interfacial tension of the system increases with increasing temperature. An interface is the boundary between two immiscible phases, such as oil and water. A surfactant (surface-active agent) is a substance which has the ability to adsorb onto surfaces and interfaces, and reduce the surface free energy or interfacial free energy [11].

As shown in Equation (1.6), interfacial tension is given by interfacial free energy per unit area, or by force per unit length along the interface. From a thermodynamic approach, interfacial tension is the minimum work required to expand an interface by unit area, or to create unit area of new interface [11]. Each of these definitions has the same dimensions.

1.8 Surfactants

Surfactants have a characteristic molecular structure, consisting of a lyophobic group, which repels the solvent, and a lyophilic group which has a strong attraction to the solvent. A molecule with such a structure has the ability to orient itself at an interface such that the lyophobic group points away from the solvent, and the lyophilic group points towards the bulk of the solvent, and is surrounded by solvent molecules. The chemical composition of a surfactant determines its application to a particular system. For example where water is the solvent, the lyophobic (hydrophobic) group could be a hydrocarbon or fluorocarbon chain, and the lyophilic (hydrophilic) group would be ionic or highly polar.

Surfactants can be classified according to their structure. Anionic surfactants (Figure 8) bear a negative charge on the head group of the molecule. Cationic surfactants (Figure 9) have a positive charge, zwitterionic surfactants have both positive and negatively charged groups, and non-ionic surfactants (Figure 10) have no charges on the head group of the molecule. Ionic surfactants always have a counterion associated with the molecule.

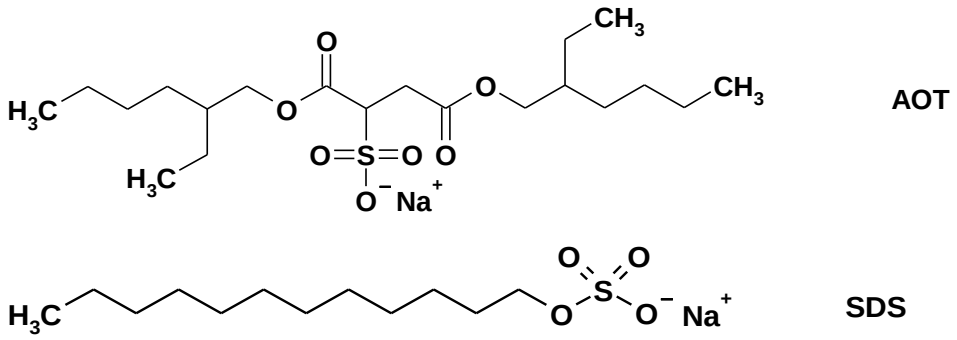

Figure 8: Anionic surfactants: Docusate Sodium Salt (AOT), and Sodium Dodecyl Sulphate (SDS).

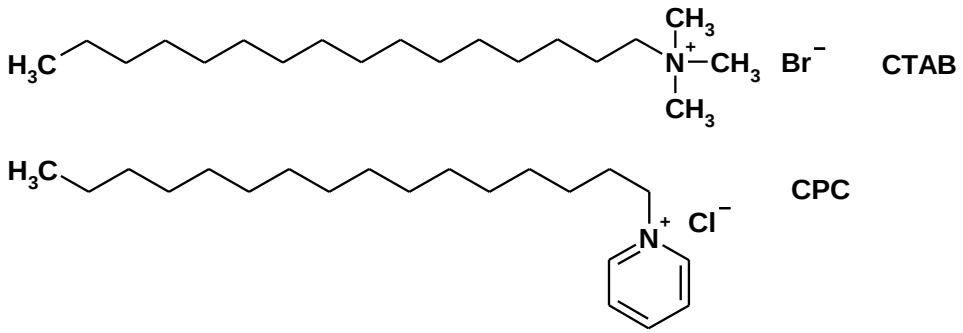

Figure 9: Cationic surfactants: Cetyltrimethylammonium bromide (CTAB), and cetyl pyridinium chloride (CPC).

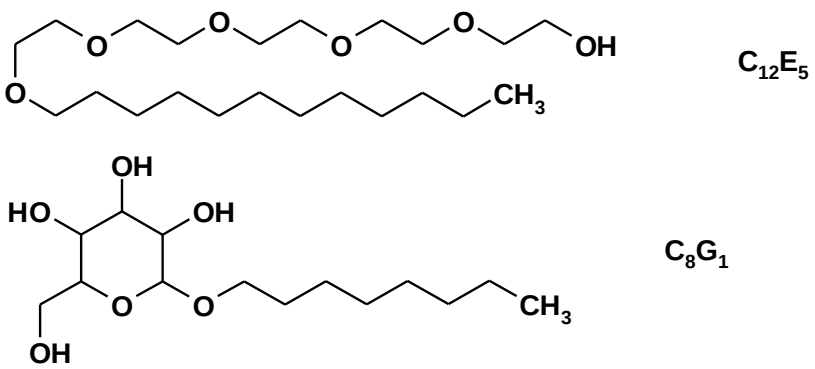

Figure 10: Nonionic surfactants: Pentaethylene glycol monododecyl ether ($C_{12}E_5$), and octyl monoglucoside (C_8G_1).

The interfacial tension, or interfacial free energy of a system, can be regarded as the work required to create a unit area of new interface. In an oil-water system, creating a unit area

of oil-water interface increases the free energy of the system. The new interface consists of water molecules and oil molecules in contact with each other. Without the interface, these molecules would be experiencing favorable interactions with like molecules. For a system stabilised by a surfactant, the surface tension also reflects the movement of surfactant molecules from the bulk solution to the interface. Whilst in aqueous solution, for example, the hydrophobic tail group of a surfactant molecule is subject to unfavourable interactions with surrounding water molecules. Moving the molecule to the interface enables the hydrophilic head group to be hydrated by water molecules, and enables the hydrophobic tail group to reside in the oil phase. The result is a decrease in free energy. In addition, the unfavourable interactions between the oil and water molecules are removed, which further decreases the free energy of the system. A surfactant molecule added to a system of two immiscible liquid phases will therefore adsorb at the interface and reduce the interfacial tension.

Molecules at the surface of a liquid have greater free energies than those in the bulk liquid, because attractive interactions between liquid molecules in the bulk are greater than those between the surface molecules and widely spaced gas molecules. The amount of work required to bring a molecule from the bulk to the surface is equal to the difference in energy between the bulk and the surface. The surface tension is a measure of this work.

1.9 Micelles and Solubilisation

At a particular surfactant concentration, surfactant molecules begin to form colloidal particles (clusters) called micelles. The concentration is known as the critical micelle concentration (CMC). Aggregation of the surfactant molecules into micelles, with the lyophobic groups directed towards the centre of the micelle and the lyophilic groups directed towards the solvent, reduces the free energy of the system by removing unfavourable interactions. Micelles have the ability to solubilise an otherwise immiscible component in the continuous phase.

1.10 Emulsions

An emulsion is a distribution of one liquid phase in another, for example, oil droplets in water. Emulsions are used in cosmetics, paints, food, and textile processing. Emulsions can be classified according to the thermodynamic stability of the dispersion. Macroemulsions are opaque, milky mixtures, and are not thermodynamically stable. Microemulsions are thermodynamically stable dispersions, which exhibit single phase behaviour, and can be optically transparent or translucent. The appearance of the dispersion is an indication of the colloidal size. Emulsions can be stabilised by the presence of an emulsifier, often a surfactant or a mixture of surfactants, which adsorbs at the interface between the two phases. A dispersion formed without a suitable surfactant would normally separate into its two bulk phases very quickly. Stabilisation of the emulsion is achieved because the thermodynamic instability (relative to the two bulk phases) is reduced.

An oil-in-water (o/w) emulsion is a dispersion of a water-immiscible phase, usually called the oil regardless of its nature, in an aqueous phase. The aqueous phase, in this case, is called the continuous phase. A water-in-oil (w/o) or reverse emulsion, is a dispersion of water or an aqueous solution in an oil phase. Oil-in-water emulsions are generally formed with emulsifiers which are more soluble in the aqueous phase than the oil phase, and the reverse is true for water-in-oil emulsions.

1.11 Microemulsions

The confirmation that microemulsions could increase the recovery of petroleum from reservoir stock in the 1980s sparked an increase in interest and research into these systems. Thermodynamics provides a driving force for the formation of microemulsions between the oil and the recovery fluid. The ultralow interfacial tension between the petroleum and the recovery fluid that is necessary to displace the petroleum from the porous rock is a key property of microemulsions.

Macroscopically, microemulsions are homogeneous, but on a microscopic scale they exhibit a range of structures defined by the surfactant monolayer that divides the two

immiscible liquids [12]. There are various systems for labelling microemulsion structures. The description that will be used in this project is as follows. L_1 is the label given to an oil-in-water microemulsion, consisting of microstructures (spherical or otherwise) of oil in a continuous aqueous phase. L_2 refers to a water-in-oil or reverse microemulsion, in which the oil is the continuous phase, containing droplets of water. L_3 describes an isotropic, bicontinuous microemulsion whose structure resembles a sponge; a 3-dimensional continuous bi-layer [13]. Within this bicontinuous mixture of oil and water are fluctuating domains, changing in size and shape, and undergoing coalescence and breakup [14]. Depending on the surfactant concentration, the L_3 phase can exist as a single phase, or as a bicontinuous microemulsion with excess water and oil phases. A microemulsion can also take on a number of liquid crystal structures at low surfactant concentrations [15], including lamellar (L_α) and cubic (I_1) [16].

Microemulsions commonly consist of droplets of oil in water (or the reverse), surrounded by a surfactant monolayer. The structure of the microemulsion is dependent on the spontaneous curvature of the surfactant monolayer, which is equal to $1/r$ where r is the droplet radius. As such, the spontaneous curvature also determines the maximum droplet size [17]. The spontaneous curvature can be determined from the surfactant monolayer film bending energy per unit area, which is a function of the two principle curvatures of the monolayer, and Gaussian bending elastic constants. Curvature is denoted as positive for oil-in-water dispersions, and negative for water-in-oil dispersions. In bicontinuous structures, the spontaneous monolayer curvature is close to zero [17].

Increasing the temperature in a non-ionic surfactant stabilised system causes a decrease in the spontaneous monolayer curvature and growth of microemulsion droplets [18]. The micelles grow as prolate spheroids or cylinders, extending in length along one axis. The transition from spherical to cylindrical oil droplets, and thence to a bicontinuous film or lamellae occurs with decreasing spontaneous monolayer curvature [19]. A spherical shape corresponds to the maximum possible monolayer curvature for a given ratio of surface area to enclosed volume. An L_1 microemulsion has a high, positive monolayer curvature, and the oil phase is not completely solubilised by the surfactant micelles. Spherical micelles

swollen with oil therefore coexist with an excess oil phase [19]. An L_2 microemulsion coexists with an excess water phase, because the curvature of the monolayer is sufficiently negative that not all the water is solubilised by the surfactant micelles.

If the temperature of an aqueous, micellar solution of a polyoxyethylenated (POE) nonionic surfactant (for examples see Figure 10) is increased, the POE chains are dehydrated, i.e. water molecules are dissociated from them because of conformational changes of the POE chain [20]. This increases the hydrophobicity of the surfactant, and increases the solubilisation of non-polar materials in the micelles. The spontaneous monolayer curvature tends towards zero, and the micelles swell into elongated shapes as they solubilise increasing volumes of oil. For POE non-ionic surfactants in the presence of excess oil phase, the volume of the aqueous phase will increase and the volume of the oil phase decrease with increasing temperature. At the same time the oil-water interfacial tension decreases. The spontaneous monolayer curvature passes through zero at a certain temperature. At this temperature, the oil-water interfacial tension is at a minimum. The same effect can be achieved with ionic surfactants by the addition of electrolyte such as NaCl. Similar results are found with the addition of 'cosurfactants' (hydrophilic or lipophilic polar compounds which work in conjunction with surfactants) to certain surfactant systems.

For each of the factors which can be used to alter the hydrophilicity and lipophilicity of the surfactant, there is a value (a certain temperature or concentration of electrolyte) at which the hydrophilic and lipophilic nature of the surfactant is balanced. At this point, the oil-water interfacial tension is at or close to its minimum value, and the emulsion is on the point of inverting. The temperature at which this occurs is called the phase inversion temperature (PIT), and the measure of the hydrophilicity and lipophilicity of the surfactant is called the hydrophile-lipophile balance (HLB).

1.12 Previous Work with Optical Tweezers

Recent work by Ward, Berry *et al.* [21] has sparked interest in the deformability of emulsion droplets with ultra-low interfacial tension using multiple optical tweezers.

According to their work, most small objects in an optical trap do not deform because the radiation pressure of a CW laser is insignificant compared to the Young's modulus of solids or the Laplace pressure within a micron-sized droplet. The Young's modulus is a measure of the stiffness of a material, and indicates how much a material is stressed under a given strain.

Laplace pressure is given by

$$\Delta P = \frac{2\gamma}{r} \tag{1.9}$$

where ΔP is the difference in pressure between the inside and the outside of the droplet, γ the surface tension and r the radius of the droplet. The pressure inside is always greater than the pressure outside the droplet. A low Laplace pressure can be achieved with low surface tension.

In order to achieve droplet deformation, the interfacial tension of the micron-sized emulsion droplets must be comparable with the force of the optical trap, which according to Ward is in the region of 10^{-5} to 10^{-6} N m^{-1}. Oil-water interfacial tensions are in the order of 0.05 Nm^{-1} for alkanes, and therefore need to be significantly reduced for surface deformation to be possible. Ultralow interfacial tensions are achieved close to the microemulsion phase boundary where the interfacial tension vanishes. The system used by Ward *et al.* was heptane, water, salt (0.05 M NaCl) and the surfactant Aerosol OT (1 mM AOT). Altering the temperature of the system to between 20 ºC and 23 ºC enabled an ultralow interfacial tension to be achieved, and large deformations were observed with a laser power of 10^{-2} W [21].

The interfacial tension of the emulsion droplets proved to be low enough that the droplet deformed into an ellipse along the axial direction of the laser beam. Multiple optical traps were used to deform the droplet into various shapes, as shown in Figure 11. The droplet

was held in the optical trap, and the traps moved apart so that the surface of the droplet was pulled out of its spherical shape.

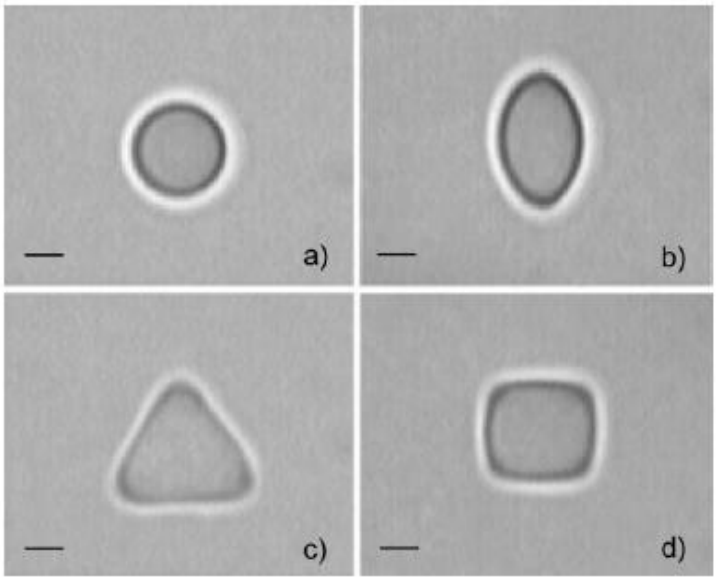

Figure 11: Deformation of an emulsion droplet using multiple optical traps: (a) droplet in a single trap; (b) ellipsoid formed by stretching the droplet with two traps; c) triangle formed using three traps; (d) square formed using four traps. The scale bar represents 2μm. Image from [21].

It has been shown that, for particles larger than the wavelength of the light, the force exerted by an optical trap is independent of the particle radius [22]. However, buoyancy and gravity increase with the cube of the particle radius, and it is forces such as these that an optical trap has to overcome. As a result there is an optimum size of emulsion droplets for optical trapping and deformation. From a practical point of view, droplets in the micrometer range are easy to see with a 100x microscope objective. Previous work with optical tweezers [21] used laser light with a wavelength of 1064 nm. Trapping and deformation were easiest with particles between 1 and 5 μm in diameter. A 532 nm laser will be used in this project, and so 5 μm seems like an ideal droplet size.

1.13 Temperature – Insensitive Microemulsions

There are two reasons for searching for a temperature-insensitive emulsions system to use in this project. The first is that small fluctuations in temperature can have a large effect on the interfacial tensions in a normal microemulsion system. The phase behaviour of a microemulsion depends strongly on the composition of the system in terms of relative amounts of surfactant, co-surfactant and oil/water, and also on the temperature of the system. Ultra-low interfacial tension is achieved in the region of the bicontinuous microemulsion, in which the spontaneous monolayer curvature is close to zero. This can be achieved by altering the temperature of the system. However, for the current work to have applications in industry, it is important for the emulsion droplets to be stable across a range of temperatures. For example, polymerisation reactions in microemulsions and emulsions have had attention in recent years [23]. A polymerisation reaction is exothermic, and will therefore raise the temperature of the medium surrounding the emulsion droplet.

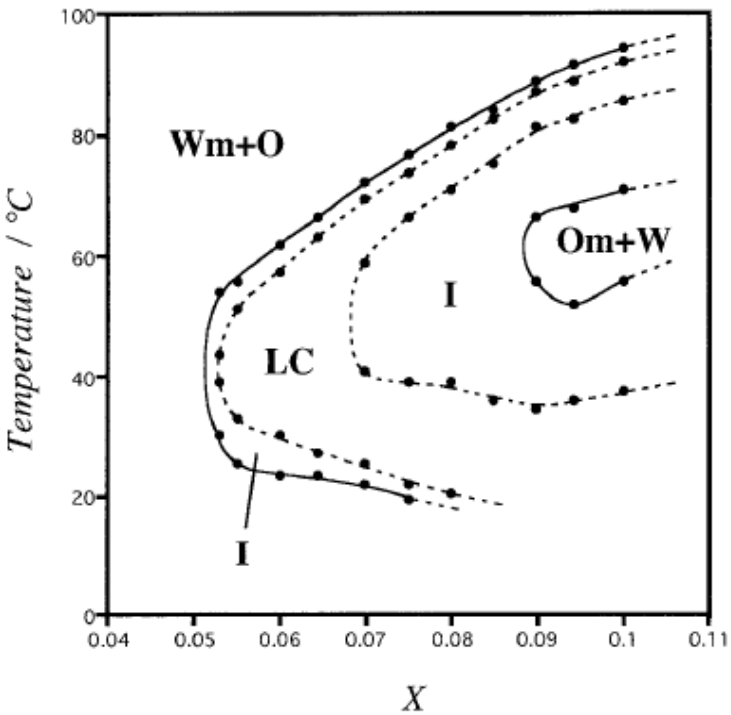

Figure 12: Phase diagram of a 3% (by weight) NaCl/SDS/$C_{12}E_3$/decane system at constant mixing ratio of ionic/non-ionic surfactant (SDS/$C_{12}E_3$ = 33/67). X represents the weight fractions of total surfactant in the system. Wm+O, Om+W, LC and I represent L_1, L_2, liquid crystal and single phase L_3 regions, respectively. Image from [15].

Mixed surfactant systems have received a lot of interest, particularly in the area of temperature-insensitive microemulsions.

Aramaki, Ozawa and Kunieda investigated the effect of temperature on the phase behaviour of mixtures of ionic and non-ionic microemulsions [15]. They reported that microemulsions are formed over a wide range of temperatures in brine/sodium dodecyl sulphate (SDS)/polyoxyethylene dodecyl ether ($C_{12}EO_2$ or $C_{12}EO_3$)/dodecane systems. The authors were able to adjust the HLB of the surfactant system by adding relatively lipophilic polyoxyethylene alkyl ethers as a cosurfactant to the very hydrophilic SDS. Plotting the weight fraction X of total surfactant in the system against temperature gave results as shown in Figure 12. For the system required in this project, an aqueous micellar solution with excess oil (Wm + O) is ideal, approaching the boundary with the single phase microemulsion. It appears from the phase diagram that the system is not completely independent of temperature.

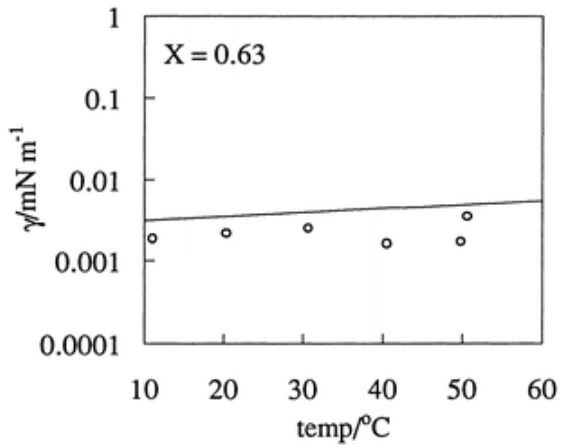

Figure 13: Variation of interfacial tension with temperature for X = 0.63, for a system containing 0.10 M NaCl. X represents the weight fraction of ionic surfactant in total surfactant. Image from [24].

Binks *et al.* investigated the effects of mixing ionic and non-ionic surfactants [24]. AOT and n-dodecyl pentaoxyethylene glycol ether ($C_{12}E_5$) were mixed to produce temperature insensitive microemulsions as shown in Figure 13. The preferred monolayer curvature for a non-ionic surfactant changes from positive at low temperatures to negative at high

temperatures. At an intermediate temperature (the PIT), the preferred monolayer curvature of the surfactant is zero, corresponding to the formation of a bicontinuous microemulsion structure or a lamellar liquid crystalline phase. Ionic surfactant monolayers show the opposite trend with temperature, becoming increasingly positive with increasing temperature. This opposite temperature dependence is used to produce temperature-insensitive microemulsions [24]. It was found that the solubilisation and interfacial tension properties could be further optimised by increasing the concentration of NaCl in the system. The PIT of AOT is sensitive to the concentration of electrolyte in aqueous solution, and low values of the oil-water interfacial tension were achieved for 0.10 M NaCl. Increasing the concentration further lead to the formation of a middle phase (L_3) microemulsion, with natural monolayer curvature and interfacial tension close to zero [24]. It is clear from Figure 13 that the interfacial tension of the system is very nearly independent of temperature.

Work by Pes *et al.* [25] has shown promising results. The authors showed that a middle phase microemulsion was formed in a water/sucrose monododecanoate (SE)/hexanol/decane system, and concluded that the phase behaviour of this system resembles that of a brine/ionicsurfactant/cosurfactant/oil system as seen in the work of Aramaki *et al.* [15]. Hexanol acts as a cosurfactant in this system. Sucrose alkanoates such as sucrose monododecanoate contain a sucrose ring which acts as the hydrophilic part of the molecule. The sucrose ring is more compact than long chain polyoxyethylene type non-ionic surfactants (Figure 10), and is therefore not expected to undergo a large conformational change with increasing temperature. Adding a medium-chain alkyl alcohol such as hexanol compensates for the SE's hydrophilicity, and favours the curvature necessary to form a bicontinuous middle microemulsion phase. Figure 14 shows that an aqueous microemulsion phase with excess oil (Wm + O) can be achieved between 0 ºC and 100 ºC by varying the weight fraction of hexanol in the total surfactant mixture.

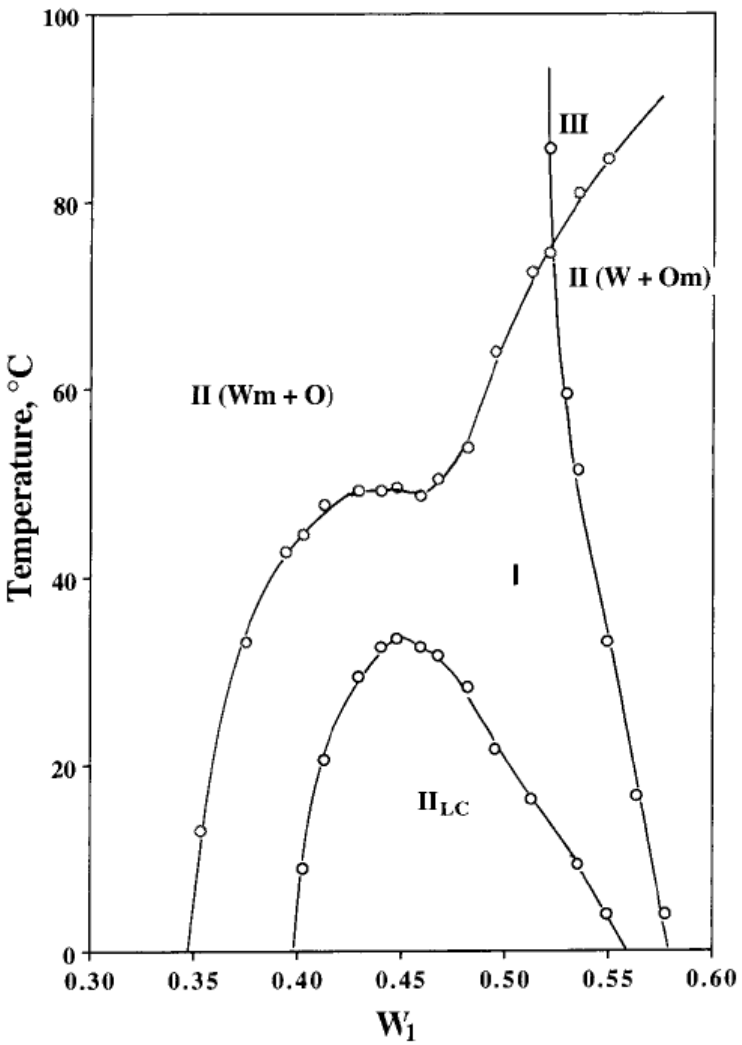

Figure 14: Phase diagram of water/sucrose monododecanoate/hexanol/hexadecane system with increasing temperature. W_1 represents the weight fraction of hexanol in sucrose monododecanoate + hexanol. The weight fraction of total surfactant in the system is fixed at 0.316. II (Wm+O) and II (W + Om) represent L_1 and L_2 microemulsions respectively. III and I represent three- and one-phase L_3 regions respectively, and II_{LC} represents a two-phase liquid crystal region. Image from [25].

A microemulsion has been formulated over a wide temperature range with $C_{12/14}$ alkyl polyglycoside, water and the cosurfactant dioctylcyclohexane glyceryl monooleate (GMO) [26]. The phase diagram for this system is shown in Figure 15. The boundary between the oil-in-water and single phase microemulsion appears to be totally independent of temperature.

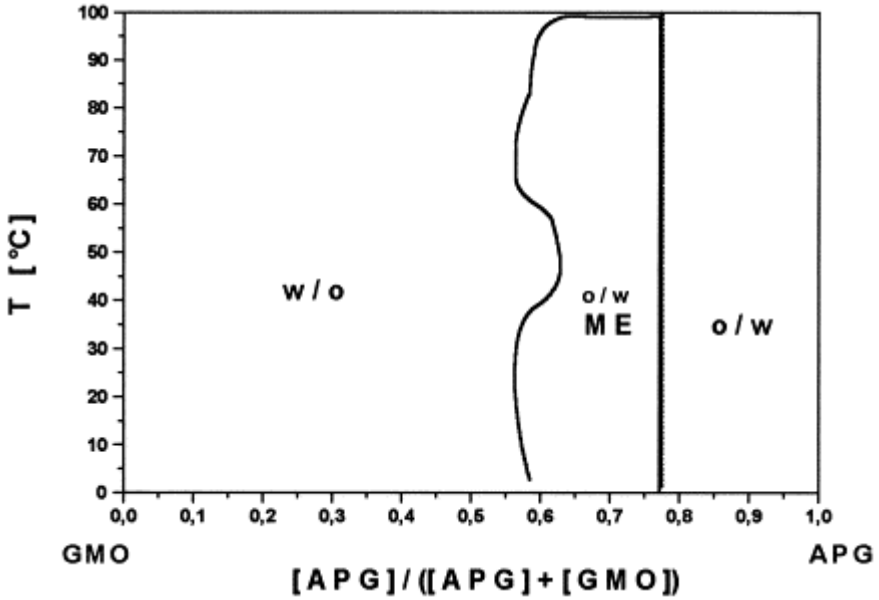

Figure 15: Phase diagram of a 'model emulsion' containing 15% $C_{12/14}$ alkyl polyglycoside and glyceryl monooleate, 42.5% water and 42.5% dioctylcyclohexane. w/o indicates L_2 microemulsion, o/w indicates L_1 microemulsion, and ME indicates single-phase L_3 microemulsion. Image from [26].

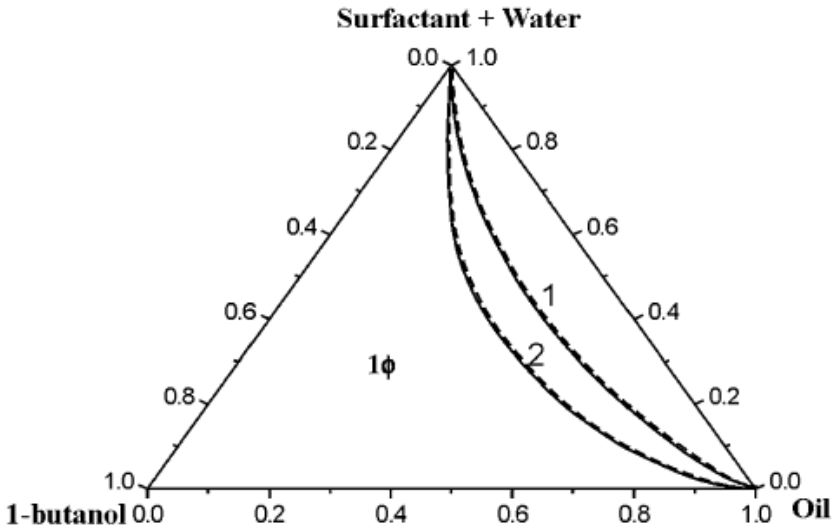

Figure 16: Phase diagram of CTAB/Brij-58/water/1-butanol/oil systems at 293 K (solid line) and 323 K (broken line). Molar ratio of surfactant to water = 1:55.6, and molar ratio of CTAB to Brij-58 = 1:1. Line labelled 1 refers to system with heptane, 2 refers to system with decane. 1φ indicates a single-phase microemulsion. Image from [27].

Mitra *et al.* formed a temperature-insensitive microemulsion with a mixed surfactant system containing CTAB, Brij-58 and butanol [27]. Brij-58 is polyoxyethylene (20) cetyl ether. Once again butanol is used to control the curvature of the interfacial monolayer, so that the microemulsion can be made to exist in any of its three phases by changing the amount of butanol in the system. The phase diagram of the mixed surfactant-stabilised system is shown in Figure 16. Mitra and Paul also investigated an AOT/Brij-35 system [28]. Brij-35 is polyoxyethylene (23) lauryl ether. The role of butanol in this system is the same as in the CTAB/Brij-58 system, and the combination of ionic and non-ionic surfactants is used once again to provide temperature-insensitivity.

1.14 Microfluidics

In order to facilitate the trapping of an emulsion droplet, one aspect of the project is to design and produce a microfluidic device that will generate a monodisperse emulsion. Not having to select a particular emulsion droplet by size, as was the case with previous work [21], will make the trapping process much easier. The optimum droplet diameter for trapping and deformation studies is between 1 and 5 μm.

The emulsion can be generated by shaking by hand the surfactant solution with the oil phase in a small vial, but this produces a polydisperse emulsion. A better alternative is to create a device that will consistently produce droplets of an appropriate size.

Oil-in-water emulsions can be formed by shearing the oil into the aqueous phase. A shear force is one applied tangential to the material (in this case, oil) surface. Oil emerging from an orifice into a flowing aqueous stream will potentially form small droplets, the sizes of which are determined by the geometry of the orifice and the ratio of the relative flow rates.

There are several approaches to obtaining a monodisperse emulsion using microfluidic technology. The first is to create a polydisperse or bidisperse emulsion and sort the droplets according to size. The emulsion could be generated by manually shaking the oil and aqueous solution together, as previously mentioned. Simple geometric considerations can be used to control droplet flow according to the diameter of the droplet. The channels are

designed such that smaller droplets are carried into a side channel by the increased fluid velocity (as a result of the reduced cross-sectional area of the channel). The sorting process has applications in transporting reagents in droplets [29].

Another option is to create a monodisperse emulsion, with droplets larger than those required so that they can be split in a microfluidic device.

A parameter known as the capillary number, Ca, can be defined as

$$Ca = \frac{\eta_c G R}{\sigma} \tag{1.10}$$

where η_c is the viscosity of the continuous phase, G is the shear strain rate, R is the initial droplet radius, and σ is the interfacial tension of the droplet. The capillary number is the ratio of the viscous stresses exerted by the continuous phase, to the restoring force of the interfacial tension. Droplet breakup occurs when the capillary number exceeds the critical capillary number C_{cr} [29], which is the ratio between the viscosities of the continuous and dispersed phase;

$$C_{cr} = \frac{\eta_D}{\eta_C} \qquad \text{(1.11) [30]}$$

Work by Link *et al.* [31] has shown that the critical capillary number for breaking a drop in a T-junction geometry, such as in Figure 17, is

$$C_{cr} = \alpha \varepsilon_0 \left(\frac{1}{\varepsilon_0^{2/3}} - 1 \right) \qquad \text{(1.12) [31]}$$

where α is a dimensionless constant relating to the difference in viscosities of the two fluids, and the channel geometry, and ε_0 is initial droplet extension, which using terms

from Figure 17 is $L_d/\pi W_i$ [29]. From these equations it is possible to calculate appropriate channel geometries to facilitate droplet breakup. If Q_1 and Q_2, the flow in the daughter channels (see Figure 17) are equal, i.e. the flow at the junction is symmetric, the droplets are either randomly distributed into the two daughter channels or break up into two equally sized daughter droplets, according to whether the droplet is breakable by the flow. Under asymmetric flow, unequal sized droplets are formed due to the unequal shear stresses on the droplet [29].

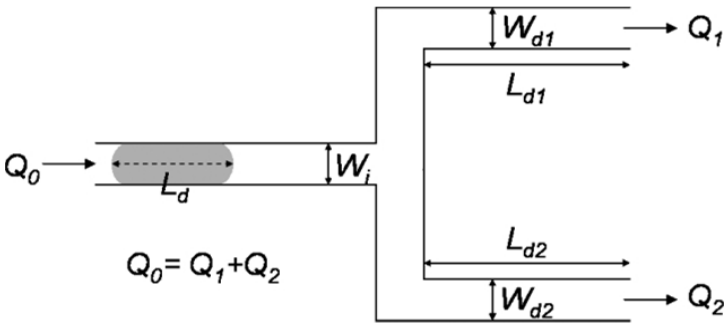

Figure 17: Geometry of microfluidic channels to induce droplet breakup, known as a bifurcating junction [29].

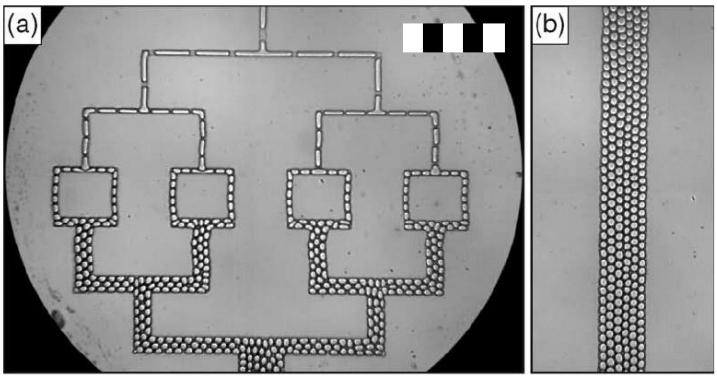

Figure 18: a) Sequential breakup of droplets to produce a monodisperse emulsion; b) Droplets flowing downstream after final T-junction [31]. Scale bar represents 500 µm.

Other designs for droplet breakup have alternative geometries. Droplets entering a T-junction along one of the 'arms' of the T also experience shear forces due to the relative flows of fluids down the channels [32]. More elaborate systems for multiple droplet

breakups have been designed, including a whole series of T-junctions as shown in Figure 18.

The next approach to achieving a monodisperse emulsion is to fabricate a microfluidic device to produce droplets of the exact required size. Several channel geometries are available for such a device. The simplest design is a T-junction, an example of which is shown in Figure 19. This device produces a water-in-oil emulsion but the same principles can be applied to create the oil-in-water emulsion required for this project. Droplet formation occurs at the junction of the two channels containing water and oil surfactant mixture. High shear forces generated at the leading edge of the water flow are responsible for droplet formation [33]. The size of the droplet formed is controlled by the relative pressure or flow rates of the oil and water. Higher water pressures generate larger droplets [33].

The authors cite a simple mathematical model for droplet formation:

$$r = \frac{\sigma}{\eta \dot{\gamma}} \qquad (1.13)\ [34]$$

where r is the final droplet radius, σ is the interfacial tension between the dispersed and continuous phases, η is the viscosity of the continuous phase, and $\dot{\gamma}$ is the shear rate. Shear rate is the rate at which shear force is applied, and is defined as the velocity of the flow divided by the distance between the two surfaces experiencing the force. Shear rate can be estimated as follows;

$$\dot{\gamma} = \frac{2\upsilon}{\gamma_0} \qquad (1.14)$$

where υ is the velocity of the fluid flowing through the gap, and γ_0 is the channel radius at the centre of flow.

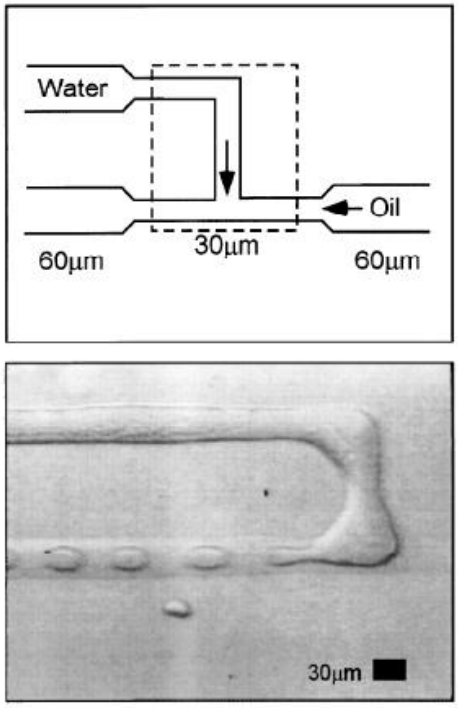

Figure 19: Microfluidic channel geometry of a simple T-junction device [33].

An elaboration on the T-junction geometry is shown in Figure 20, which the authors term a 'step emulsification device' [35]. The dispersed phase enters the main channel at a T-junction, and the main channel flows into a slightly wider and much deeper channel, forming a step. According to the authors the orientation of the dispersed phase inlet relative to the continuous phase, i.e. on the bottom face of the channel rather than entering at the side, produces very different results to those seen in the work by Thorsen *et al.* [33]. The authors observed that emulsification can occur through three mechanisms, depending on the relative flow rates of the dispersed and continuous phases. If the flow rate of the dispersed phase is significantly less than the flow rate of the continuous phase droplet formation occurs at the T-junction, as with the device shown in Figure 19. Droplet formation is induced by the abrupt change in channel geometry. The flow is stable until it reaches the step where it breaks up into smaller emulsion droplets [35]. In this flow regime the device generates extremely monodisperse droplets, with a polydispersity below 1.5% in diameter [35].

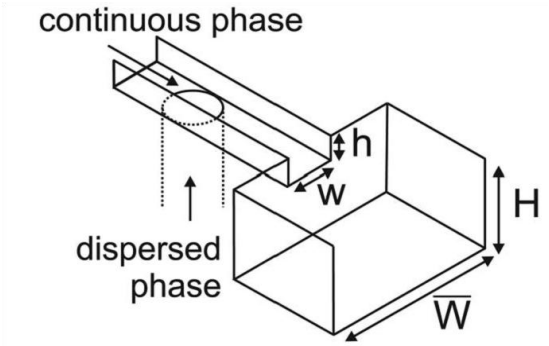

Figure 20: Geometry of step emulsification device [35].

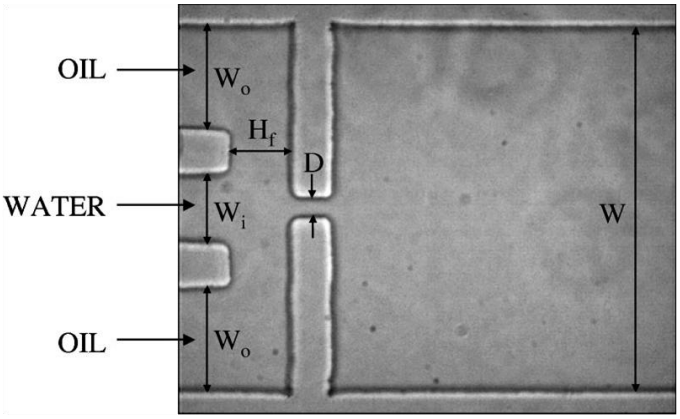

Figure 21: Example of flow focusing geometry in a microfluidic device. Co-flowing water and oil streams are constricted through a small gap of width D (43.5 μm) [36].

An alternative method for creating monodisperse emulsions is to employ 'flow focusing' [36]. An example of such a device is shown in Figure 21. The outer fluid (in this case oil) exerts pressure and viscous stresses that force the inner fluid into a narrow thread, which breaks into droplets inside or downstream of the small gap. As a result of the inner fluid flowing as a narrow thread, droplets with radii much smaller than the inner dimension of the gap can be produced. The advantages of such a design lie in the manufacture of the microfluidic device, because creating very small, smooth channels, as required in the T-junction designs, is a challenge.

1.15 Membrane Emulsification

Traditional methods of emulsion production rely on the dispersion of one phase into another by means of creating turbulent flow, for example by vigorous stirring [37]. For industrial and commercial applications such as food emulsions, the size and size distribution of an emulsion is critical, since its stability is determined largely by the size of the droplets, and the size distribution determines the suitability of the emulsion for its intended use [37]. Producing an emulsion by agitation in a large vessel is energy inefficient because it is difficult to control turbulence in a large reaction vessel, and it cannot normally be generated consistently throughout the vessel. More importantly it is difficult to control the droplet size and size distribution using these methods. Accordingly, much work has been done on finding an energy efficient method of reliably producing monodisperse emulsions for use in the food, cosmetics, pharmaceuticals and chemical industries.

One of the results of this work is the emergence of 'membrane emulsification' [38]. The concept of this relatively new method is simple. A microporous membrane (ceramic, or glass for example) separates the phase to be dispersed from the continuous phase. Pressure is applied to the phase to be dispersed such that it is forced through the pores of the membrane, forming droplets on the surface of the membrane in contact with the continuous phase (Figure 22).

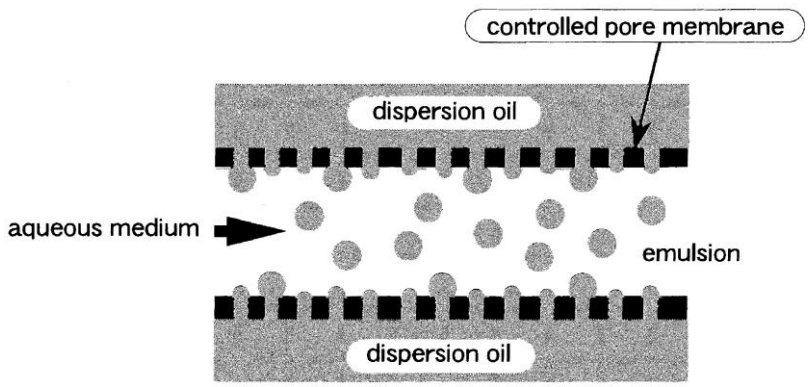

Figure 22: Preparing an oil-in-water emulsion using membrane emulsification. Image from [38b].

The pressure required for emulsification depends on the pore size of the membrane and the oil-water interfacial tension [38b]. There are various methods for detaching the growing droplet from the membrane surface, and these will be discussed shortly. Typical arrangements of apparatus are in the form of a tubular membrane surrounded by continuous phase in a cylindrical vessel (see Figure 23), or a circular membrane disk separating the upper and lower halves of a cylindrical vessel.

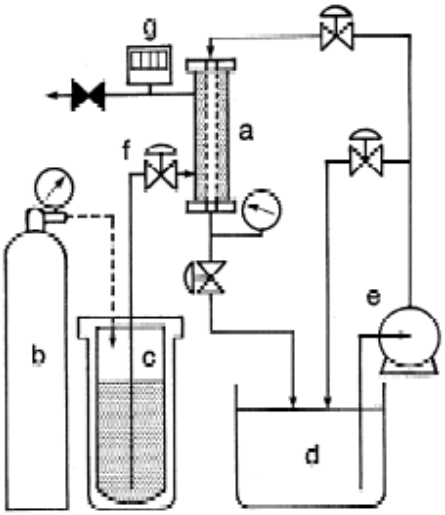

Figure 23: Membrane emulsification apparatus scheme. (a) Membrane module; (b) Pressurising source; (c) reservoir of phase to be dispersed; (d) tank containing continuous phase; (e) pump; (f) valve; (g) pressure gauge. Image from [38b].

As mentioned before, it is common in membrane emulsification to employ a shear force to detach the droplet from the membrane. A shear force is one which acts tangentially or parallel to an object or surface. In the case of membrane emulsification, the shear force (measured in Pa) is provided by the flow of the continuous phase past the membrane surface and past the surface of the growing droplet, sometimes referred to as viscous drag force [39]. Typically the crossflow velocity is between 0.8 and 8 m s^{-1} [40]. The rate of continuous phase mixing (crossflow velocity) should not be so high that it induces droplet breakup in the system [41].

Initial experiments with membrane emulsification involved a material called Shirasu-porous-glass (SPG). Nakashima and co-workers have studied SPG since 1978 and have

found it to be the most suitable material for a low size distribution of pores, and hence a monodisperse emulsion [38b]. A scheme of the preparation of Shirasu porous glass is shown in Figure 24. Shirasu is a volcanic ash found in the southern area of Kyushu Island, Japan. Shirasu, boric acid and calcium carbonate are mixed and heated, and after reaching glass fusion the mixture is formed into a tube or sheet. The heat treatment is annealing, a process by which the glass is slowly cooled to relieve internal stresses. At this point the glass decomposes into calcium- and borate-rich glass and aluminosilicate-rich glass. Treatment with acid leaches out the calcium borate, leaving a porous glass membrane [38b].

An interesting aspect of membrane emulsification using SPG is that the choice of emulsifier is limited to anionic or neutral species. An untreated SPG surface is negatively charged within a pH range of 2 to 8, due to the dissociation of acid silanol groups [41]. In order for the membrane surface to remain hydrophilic and thus assist droplet detachment, the functional groups of the emulsifier must not carry a positive charge. Cationic surfactants such as cetyltrimethyl ammonium bromide (CTAB) bind to the membrane surface, and increase its wettability by the disperse phase.

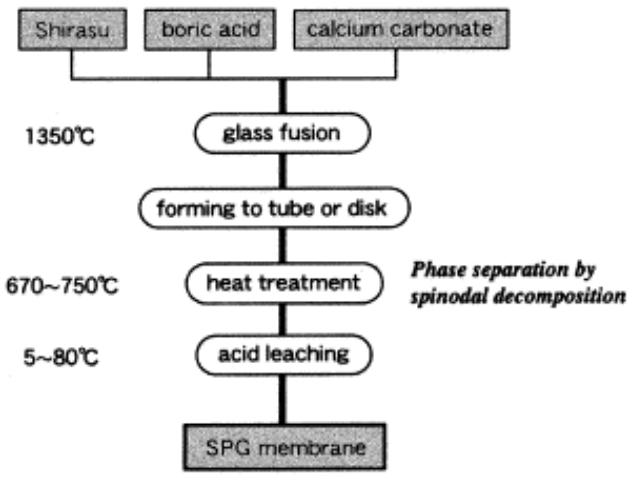

Figure 24: Preparation of Shirasu porous glass (SPG) membrane. Image from [38b].

SPG membranes have been found to produce very monodisperse emulsions [38b]. The degree of monodispersity (or polydispersity) can be measured using the coefficient of

variation CV (relative standard deviation, Equation (1.15)) or the relative span factor (Equation (1.16)).

$$CV = \left(\frac{\sigma}{d_{av}} \right) \times 100 \tag{1.15}$$

where σ is the standard deviation of the droplet diameters, and d_{av} is the number-average mean droplet diameter;

$$Span = \frac{\left(d_{90} - d_{10} \right)}{d_{50}} \tag{1.16}$$

where d_x is the diameter x volume % on a relative cumulative droplet diameter distribution curve [41].

Several key factors influence the size of emulsion droplets formed by a membrane. These are summarised in Table 1. It should be noted that not all the parameters studied in the literature have equal influence on droplet size and size distribution over the operating parameters, and many have coupled effects [42]. Different operating parameters can have a strong influence on the results of these investigations. Egidi *et al.* [45] reported that droplet size may increase or decrease with increasing dispersed phase flux through the membrane, depending on the other operating conditions. They note that there is a 'push-off' force in membrane emulsification, resulting from adjacent droplets exerting a force on each other which encourages droplet detachment. It has been reported that droplets detach sooner at higher disperse phase flux because adjacent droplets push each other off the membrane, resulting in smaller droplets and more uniform droplet size [45]. However Abrahamse *et al.* [46] reported that interference of adjacent droplets led to increased polydispersity.

Transmembrane pressure is defined as

$$\Delta P_{TM} = P_d - P_c \qquad (1.17)\ [47]$$

where P_d and P_c are the disperse and continuous phase pressures, respectively. In order for the oil phase to flow through the membrane, the transmembrane pressure must be greater than the sum of the average continuous phase pressure (1.18), and the capillary pressure (1.19):

$$P_c = \frac{P_{c1} - P_{c2}}{2} \qquad (1.18)\ [42]$$

$$P_{cap} = \frac{4\gamma \cos\theta}{D_P} \qquad (1.19)\ [42]$$

where P_{c1} and P_{c2} are the continuous phase pressures at both ends of the membrane, γ is the oil-water interfacial tension, θ is the contact angle between the dispersed phase and the membrane surface, and D_P is the pore diameter.

Typical values of transmembrane pressure using 0.2, 0.5 and 0.8 µm pore size membranes lie between 20 and 500 kPa. Higher transmembrane pressures are needed for membranes with small pores because of the higher capillary number (see Equation 1.13) [40]. A potential disadvantage of membrane emulsification compared to traditional emulsification methods, is the relatively low maximum disperse phase flux through the membrane (typically 0.01 – 0.1 m h^{-1}) to avoid entering the jetting regime of disperse phase flow, in which droplet formation occurs some distance from the pore opening [41]. For this project, it is not necessary to produce large volumes of emulsion in a short time, so this will not be a hindrance to the suitability of membrane emulsification to the project. A distinct advantage, especially in terms of the requirement of this project, is the high degree of monodispersity that can be achieved with membrane emulsification. Using SPG membranes, relative span factors of 0.26 – 0.45 can be achieved [41]. As noted in Table 1, droplet size is proportional to pore diameter $\left(d_d = kd_P\right)$. The proportionality constant k usually lies in the range 2 to 10 [42].

Table 1: Factors affecting droplet size and size distribution in membrane emulsification.

Factor	Aspect	Effect	References
Membrane	Pore size	Drop size proportional to pore diameter: $d_d = kd_p$.	[39, 48]
		Smaller pores necessitate a higher transmembrane pressure to overcome higher capillary pressure.	[39]
	Porosity	Porosity determines distance between adjacent pores. Higher polydispersity occurs for higher porosity.	[45-46, 49]
	Wetting properties	Membrane should be wetted by continuous phase; oil-in-water emulsions should be produced with a hydrophilic membrane. Increased wettability of membrane surface by dispersed phase leads to larger drops and higher polydispersity.	[37, 39, 43]
Operation	Transmembrane pressure (disperse phase flux [47])	Higher transmembrane pressure produces higher polydispersity.	[43, 45, 47, 48b]
		Higher pressure can produce larger droplets.	[48b, 50]
		Droplet size decreases with increasing shear, although the effect is often small.	[42, 44-47]
		Polydispersity increases with decreasing shear.	[46]
	Emulsifier, interfacial tension	Lower oil-water interfacial tension reduces force holding droplet to membrane, and reduces droplet size.	[39, 42-43, 47]
Chemical System	Oil type	Emulsifying residues left on membrane increase wettability by disperse phase and produce larger droplets.	[43]
		Increased rate of emulsifier adsorption to interfacial boundary (dynamic interfacial tension) decreases droplet size.	[45, 47]
		Low dynamic interfacial tension at droplet detachment point produces smaller droplets.	[43]
		Increased viscosity of disperse phase decreases disperse phase flux, and decreases droplet size.	[39, 48b]

The optimum droplet diameter for this project is 5 µm. As previously mentioned, droplets of this size have been relatively easy to trap in previous work. Table 2 gives a brief summary of the materials and resulting droplet size from the literature studied. It is clear that the nickel membranes with machined pores are unsuitable for this application. It appears that the ceramic and glass membranes will produce an emulsion of a suitable droplet size for this project.

Table 2: Summary of emulsion characteristics.

Author and Reference	**Membrane type**	**Mean pore size**	**Mean droplet size (with a range of transmembrane pressures)**
Schroder and Schubert [47]	Ceramic aluminium oxide (α-Al2O3) membrane tubes	0.8 µm	3 to 11µm
Lepercq-Bost *et al.* [39]	Ceramic aluminium oxide	0.8 µm	1.5 to 2.5 µm
Dragosavic [43]	Nickel membrane containing uniform cylindrical pores	19 µm	100 to 200 µm
Egidi [45]	Nickel disk membrane	20 µm	50 to 300 µm
Vladisavljevic and Schubert [48a]	Shirasu Porous Glass membrane	0.4, 1.4 and 2.5 µm	1.4, 4.6 and 8.5 µm

References

1. Tipler, P. A., *Physics for Scientists and Engineers*. 4th ed.; W H Freeman: New York, 1999; p 1335.
2. Read, E. H., *Electromagnetic Radiation*. John Wiley & Sons: New York, 1980; p 331.
3. Ashkin, A., *Optical Trapping and Manipulation of Neutral Particles Using Lasers: A Reprint Volume with Commentaries*. World Scientific Publishing: Singapore, 2006; p 915.
4. Feigel, A., Quantum Vacuum Contribution to the Momentum of Dielectric Media. *Physical Review Letters* **2004,** *92* (2), 020404-1-4.
5. Padgett, M.; Barnett, S. M.; Loudon, R., The angular momentum of light inside a dielectric. *Journal of Modern Optics* **2003,** *50* (10), 1555-1562.
6. Strong, J., *Concepts of Classical Optics*. 1st ed.; W. H. Freeman: San Francisco, 1958; p 692.
7. Ashkin, A., Acceleration and Trapping of Particles by Radiation Pressure. *Physical Review Letters* **1970,** *24* (4), 156 - 159.
8. Ashkin, A.; Dziedzic, J. M.; Bjorkholm, J. E.; Chu, S., Observation of a single-beam gradient force optical trap for dielectric particles. *Optics Letters* **1986,** *11* (5), 288 - 290.
9. Dufresne, E. R.; Grier, D. G., Optical tweezer arrays and optical substrates created with diffractive optics. *Review of Scientific Instruments* **1998,** *69* (5), 1974-1977.
10. Atkins, P. W., *Physical Chemistry*. 6th ed.; Oxford University Press: Oxford, 1998.
11. Rosen, M. J., *Surfactants and Interfacial Phenomena*. 2nd ed.; Wiley-Interscience: New York, 1989; p 431.
12. Bagger-Jöorgensen, H.; Olsson, U.; Mortensen, K., Microstructure in a Ternary Microemulsion Studied by Small Angle Neutron Scattering. *Langmuir* **1997,** *13*, 1413-1421.
13. Hellweg, T., Phase structures of microemulsions. *Current Opinion in Colloid & Interface Science* **2002,** *7*, 50-56.
14. Klier, J.; Tucker, C. J.; Kalantar, T. H.; Green, D. P., Properties and Applications of Microemulsions. *Advanced Materials* **2000,** *12* (23), 1751-1757.
15. Aramaki, K.; Kazuyo, O.; Kunieda, H., Effect of Temperature on the Phase Behaviour of Ionic-Nonionic Microemulsions. *Journal of Colloid and Interface Science* **1997,** *196*, 74-78.
16. Leaver, M.; Olsson, U.; Wennerström, H.; Strey, R.; Würz, U., Phase Behaviour and Structure in a Non-ionic Surfactant-Oil-Water Mixture. *Journal of the Chemical Society, Faraday Transactions* **1995,** *91* (23), 4269-4274.
17. Sicoli, F.; Langevin, D.; Lee, L. T., Surfactant film bending elasticity in microemulsions: Structure and droplet polydispersity. *Journal of Chemical Physics* **1993,** *99* (6), 4759-4765.
18. Leaver, M.; Furó, I.; Olsson, U., Micellar Growth and Shape Change in an Oil-in-Water Microemulsion. *Langmuir* **1995,** *11*, 1524-1529.

19. Olsson, U.; Schurtenberger, P., Structure, Interactions, and Diffusion in a Ternary Nonionic Microemulsion Near Emulsification Failure. *Langmuir* **1993,** *9*, 3389-3394.
20. Karlstroem, G., A new model for upper and lower critical solution temperatures in poly(ethylene oxide) solutions. *Journal of Physical Chemistry* **1985,** *89* (23), 4962-4964.
21. Ward, A. D.; Berry, M. G.; Mellor, C. D.; Bain, C. D., Optical sculpture: controlled deformation of emulsion droplets with ultralow interfacial tensions using optical tweezers. *Chemical Communications* **2006,** (43), 4515-4517.
22. Ashkin, A., Forces of a single-beam gradient laser trap on a dielectric sphere in the ray optics regime. *Biophysical Journal* **1992,** *61*, 569-582.
23. Schwuger, M.-J.; Stickdorn, K.; Schomaecker, R., Microemulsions in Technical Processes. *Chemical Reviews* **1995,** *95* (4), 849-864.
24. Binks, B. P.; Fletcher, P. D. I.; Taylor, D. J. F., Temperature Insensitive Microemulsions. *Langmuir* **1997,** *13*, 7030-7038.
25. Pes, M. A.; Aramaki, K.; Nakamura, N.; Kunieda, H., Temperature-Insensitive Microemulsions in a Sucrose Monoalkanoate System. *Journal of Colloid and Interface Science* **1996,** *178*, 666-672.
26. von Rybinski, W.; Guckenbiehl, T. H., Influence of co-surfactants on microemulsions with alkyl polyglucosides. *Colloids and Surfaces A: Physicochemical and Engineering Aspects* **1998,** *142*, 333-342.
27. Mitra, R. K.; Paul, B. K.; Moulik, S. P., Phase behaviour, interfacial composition and thermodynamic properties of mixed surfactant (CTAB and Brij-58) derived w/o microemulsions with 1-butanol and 1-pentanol as cosurfactants and n-heptane and n-decane as oils. *Journal of Colloid and Interface Science* **2006,** *300*, 755-764.
28. Mitra, R. K.; Paul, B. K., Physicochemical investigations of microemulsification of eucalyptus oil and water using mixed surfactants (AOT + Brij-35) and butanol. *Journal of Colloid and Interface Science* **2005,** *283*, 565-577.
29. Tan, Y. C.; Fisher, J. S.; Lee, A. I.; Cristini, V.; Lee, A. P., Design of microfluidic channel geometries for the control of droplet volume, chemical concentration, and sorting. *Lab on a Chip* **2004,** *4* (4), 292-298.
30. Briscoe, B. J.; Lawrence, C. J.; Mietus, W. G. P., A review of immiscible fluid mixing. *Advances in Colloid and Interface Science* **1999,** *81*, 1-17.
31. Link, D. R.; Anna, S. L.; Weitz, D. A.; Stone, H. A., Geometrically mediated breakup of drops in microfluidic devices. *Physical Review Letters* **2004,** *92* (5), 054503-1-4.
32. Menetrier-Deremble, L.; Tabeling, P., Droplet breakup in microfluidic junctions of arbitrary angles. *Physical Review E* **2006,** *74* (3), 035303-1-4.
33. Thorsen, T.; Roberts, R. W.; Arnold, F. H.; Quake, S. R., Dynamic pattern formation in a vesicle-generating microfluidic device. *Physical Review Letters* **2001,** *86* (18), 4163-4166.
34. Taylor, G. I., The Formation of Emulsions in Definable Fields of Flow. *Proceedings of the Royal Society of London A* **1934,** *146*, 501-523.
35. Priest, C.; Herminghaus, S.; Seemann, R., Generation of monodisperse gel emulsions in a microfluidic device. *Applied Physics Letters* **2006,** *88* (2), 024106-1-3.

36. Anna, S. L.; Bontoux, N.; Stone, H. A., Formation of dispersions using "flow focusing" in microchannels. *Applied Physics Letters* **2003,** *82* (3), 364-366.
37. Peng, S. J.; Williams, R. A., Controlled Production of Emulsions using a Crossflow Membrane, Part 1: Droplet Formation from a Single Pore. *Trans IChemE* **1998,** *76* (A), 894-901.
38. (a) Nakashima, T.; Shimizu, M.; Kukizaki, M., Membrane emulsification by microporous glass. *Key Engineering Materials* **1991,** *61-62*, 513-516; (b) Nakashima, T.; Shimizu, M.; Kukizaki, M., Particle control of emulsion by membrane emulsification and its applications. *Advanced Drug Delivery Reviews* **2000,** *45* (1), 47-56.
39. Lepercq-Bost, E.; Giorgi, M.-L.; Isambert, A.; Arnaud, C., Use of the capillary number for the prediction of droplet size in membrane emulsification. *Journal of Membrane Science* **2008,** *314*, 76-89.
40. Joscelyne, S. M.; Tragardh, G., Membrane emulsification - a literature review. *Journal of Membrane Science* **2000,** *169*, 107-117.
41. Vladisavljevic, G. T.; Williams, R. A., Recent developments in manufacturing emulsions and particulate products using membranes. *Advances in Colloid and Interface Science* **2005,** *113*, 1-20.
42. Rayner, M.; Tragardh, G., Membrane emulsification modelling: how can we get from characterization to design? *Desalination* **2002,** *145*, 165-172.
43. Dragosavac, M. M.; Sovilj, M. N.; Kosvintsev, S. R.; Holdich, R. G.; Vladisavljevic, G. T., Controlled production of oil-in-water emulsions containing unrefined pumpkin seed oil using stirred cell membrane emulsification. *Journal of Membrane Science* **2008,** *322*, 178-188.
44. Rayner, M.; Tragardh, G.; Tragardh, C.; Dejmek, P., Using the Surface Evolver to model droplet formation processes in membrane emulsification. *Journal of Colloid and Interface Science* **2004,** *279*, 175-185.
45. Egidi, E.; Gasparini, G.; Holdich, R. G., Membrane emulsification using membranes of regular pore spacing: Droplet size and uniformity in the presence of surface shear. *Journal of Membrane Science* **2008,** *323*, 414-420.
46. Abrahamse, A. J.; van Lierop, R.; van der Sman, R. G. M.; van der Padt, A.; Boom, R. M., Analysis of droplet formation and interactions during cross-flow membrane emulsification. *Journal of Membrane Science* **2002,** *204* (1-2), 125-137.
47. Schroder, V.; Schubert, H., Production of emulsions using microporous, ceramic membranes. *Colloids and Surfaces A: Physicochemical and Engineering Aspects* **1999,** *152*, 103-109.
48. (a) Vladisavljevic, G. T.; Schubert, H., Preparation and analysis of oil-in-water emulsions with a narrow droplet size distribution using Shirasu-porous-glass (SPG) membranes (vol 144, pg 167, 2002). *Desalination* **2002,** *144*, 167-172; (b) Yuan, Q.; Hou, R.; Aryanti, N.; Williams, R.; Biggs, S.; Lawson, S.; Silgram, H.; Sarkar, M.; Birch, R., Manufacture of controlled emulsions and particulates using membrane emulsfication. *Desalination* **2008,** *224*, 215-220.
49. (a) Vladisavljevic, G. T.; Kobayashi, I.; Nakajima, M.; Williams, R.; Shimizu, M.; Nakashima, T., Shirasu Porous Glass membrane emulsification: Characterisation of membrane structure by high-resolution X-ray microtomography and microscopic observation of droplet formation in real time. *Journal of Membrane Science* **2007,** *302* (1-2), 243-253; (b) Zhu, J.; Barrow, D., Analysis of droplet size during

crossflow membrane emulsification using stationary and vibrating micromachined silicon nitride membranes. *Journal of Membrane Science* **2005,** *261*, 136-144.

50. Schroder, V.; Behrend, O.; Schubert, H., Effect of Dynamic Interfacial Tension on the Emulsification Process Using Microporous, Ceramic Membranes. *Journal of Colloid and Interface Science* **1998,** *202*, 334-340.

2 Microfluidics

2.1 Introduction

Microfluidics is the study and technology of fluids confined to channels having a cross-sectional diameter of between 10 and 100 μm [1], and has applications in chemistry, biotechnology, clinical medicine and microtechnology amongst many other areas. The advantages of miniaturisation are many and varied, and include manufacture cost reduction, reduced consumption of reagents, and portability. As mentioned by Cooper *et al.* in their key review [1] there are some studies and applications which are impossible in larger-scale devices. The production of very small-scale emulsions is one such application.

2.2 Design of microfluidic device

As described in the introduction to this thesis, there are three options for creating a monodisperse emulsion using microfluidics. The first is to create a polydisperse emulsion (such as would be produced by manually shaking oil and surfactant solution in a small vessel) or bidisperse emulsion (e.g. through jet break-up) and use a sorting device to select the droplets of the required size. This can be achieved by optical sorting (for example using optical tweezers) or by arranging microfluidic channels such that large and small drops are separated by means of the flow and the channel size. The second option is to create a monodisperse emulsion using flow-focusing or T-junction device to consistently produce droplets of the same size. The third option is to create a monodisperse emulsion of large droplets (which is simpler and more reliable than creating small droplets) and to divide them into small droplets using microchannels and microfluidic flow. It seemed that the simplest channel geometries and patterns would be required for the second of these options.

2.2.1 Geometry and dimensions

A conceptually simple and mechanically achievable design was chosen for the microfluidic device for this project. Of the various channel geometries and arrangements, and shear

production (such as flow focussing, splitting droplets etc) the T-junction design used by Thorsen *et al.* [2] was considered to be the easiest to reproduce.

The smallest emulsion droplets produced by Thorsen *et al.* were ca. 10 µm in diameter, which is slightly larger than the ideal size for optical trapping and deformation. The dimensions for the channels were chosen to be similar to those used in the paper by Thorsen *et al.*, with the idea that if this device was successful further work would be done towards reducing the size of the droplets produced. The channels were designed to have a square cross section, so that they would be 30 µm deep.

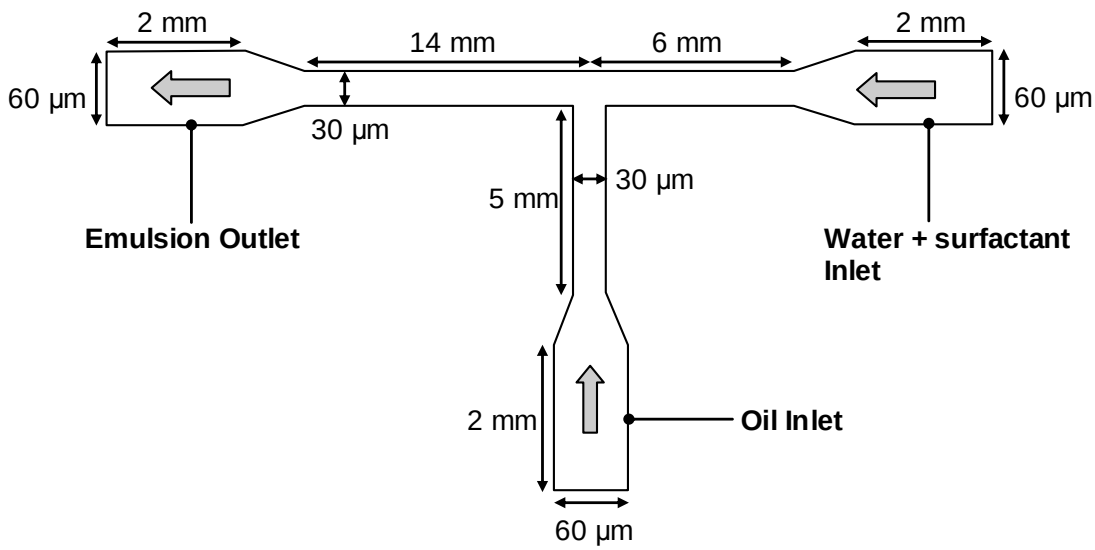

Figure 1: Microchannel pattern showing layout and dimensions. Grey arrows indicate direction of flow.

Emulsions are formed by using shear forces to create droplets of one liquid in a second immiscible liquid [2]. Microfluidic devices facilitate emulsion formation by providing the shear force and manipulating contact between the liquids. The T-junction device reported by Thorsen *et al.* relied upon the instability created at the boundary between continuous and disperse phases to create small droplets. They report that this boundary is not static, and that the motion of one fluid can direct the other. Droplet formation is a result of the balance of surface tension and shear forces. A droplet of one liquid at rest in another liquid of the same density assumes a spherical shape. Shear forces applied to the droplet by the

surrounding liquid, such as at the junction between two channels, deform the droplet from its spherical shape. Surface tension tends to keep the droplet spherical, but there will be a shear force at which the droplet breaks up, or in the case of the microfluidic device, at which a droplet breaks off from the bulk disperse phase.

Thorsen *et al.* [2] reported that the droplet size and frequency of droplet production can be precisely controlled by changing the relative pressure of the continuous and disperse phases. If the oil pressure (continuous phase) was greater than the water pressure (disperse phase), monodisperse reverse micelles were formed. Despite the microfluidic device having been designed to produce water-in-oil emulsions, by switching the two liquids round it is reasonable to assume that a similar device could be used to produce an oil-in-water emulsion, as required for this project.

2.2.2 Materials

Thorsen *et al.* produced their microfluidic device from a polymer of urethane diacrylate. However many other authors [3 - 9] chose polydimethyl siloxane (PDMS) as the material for their microchannels. There are many properties of PDMS that make it a suitable material from which to fabricate a microfluidic device. PDMS is classed as an elastomer, being an elastic and rubbery polymer above its glass transition temperature. The glass transition temperature is the temperature at which a polymer becomes glassy and brittle on cooling, or soft and elastic on heating. PDMS has a glass transition temperature of less than -127 ºC [10] which means that at room temperature the polymer is a soft, deformable rubber-like substance.

The PDMS for soft lithography applications is supplied in the form of a base and a curing agent [11]. Silicon hydride groups in the curing agent react with vinyl groups in the base to form a cross-linked polymer [11]. The process of moulding the polymer into channels involves spreading the liquid mixture of base and curing agent (pre-polymer) onto a silicon mould, and then removing the polymer once it has set (see Method). This is easy with a flexible, rubber-like polymer such as PDMS. Because the PDMS is easily removed, it leaves the silicon mould undamaged and facilitates reproduction of the device without

repeating the initial photolithography steps involved in the microfabrication process. The liquid PDMS pre-polymer moulds around the structures of the silicon mould and replicates the pattern with high accuracy (tens of nanometres) [1].

PDMS is optically transparent, which facilitates imaging the device using a microscope. The channels formed in the PDMS are sealed by bonding the PDMS to a flat surface, such as glass or silicon. Bonding the PDMS to a glass surface is simple. Van der Waals interactions provide a reversible seal strong enough to resist pressures of up to but not greater than ca. 30 kPa [1]. Alternatively the PDMS can be permanently bonded to glass by exposure of the PDMS and glass to an air plasma. It is believed that this oxidises methyl groups on the surface of the PDMS to silanol (Si-OH), which facilitate the bonding of the PDMS to the second surface [12].

Despite the obvious benefits of using PDMS to fabricate the device, there are several drawbacks. PDMS is hydrophobic and requires surface treatment to make it suitable for applications involving aqueous phases. It is important that the walls of the channels are wet fully by the aqueous continuous phase, in order that steady, laminar flow can be achieved, and to prevent the oil emulsion droplets adhering to the sides of the channels. Fortunately, surface treatment of PDMS is simple (see Method) [1].

PDMS is a silicone-based polymer, which means that the main repeating unit contains Si-O bonds. The structure is shown in Figure 2.

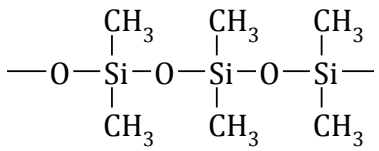

Figure 2: Molecular structure of PDMS [13].

Although PDMS is considered to be chemically inert, its structure makes it susceptible to swelling by a number of alkanes and other organic solvents including heptane, toluene, acetone and ethanol. This property of PDMS holds potential problems for use in a

microfluidic device that incorporates oils such as heptane. The emulsion system chosen for the testing of the microfluidic device was heptane, water, AOT and salt. We decided that if major problems occurred during the use of heptane with the device, a second device would be produced from PMMA. We hoped that because heptane was the dispersed phase, it would only be in direct contact with the PDMS walls in the oil inlet channel.

2.2.3 Fluid Flow

There are two options for driving the fluid flow along the microfluidic channels. The most precise method is to incorporate reservoirs of both fluids into the design, and to apply pressure to these reservoirs using compressed gas. A simpler approach is to use syringes and syringe pumps. A syringe pump is a simple device which applies a continuous force to the plunger of the syringe, according to the flow rate programmed into the pump. Providing the syringe dimensions are accurately measured and inputted into the pump, the volumetric flow rate in the channels (volume per unit time) will be the same as that programmed into the pump. This is an advantage since flow rates are often quoted in microfluidic literature, and relative flow rate is a key parameter governing droplet production. Another advantage of using syringe pumps is that they can be integrated into the system with relative ease. The connection between the microfluidic device and the syringes can be achieved with silicone tubing.

2.3 Microfabrication

The following section is based on information gathered from Franssila, in *Introduction to Micro Fabrication*, Wiley, Chichester, 2004 [14].

Microfabrication is the area of engineering concerned with the production of devices composed of micrometre scale structures and elements. Electronic components, channels for fluid flow, and mechanical devices can all be engineered on a micrometre scale, and integrated into systems.

Microfabrication must take place under very clean conditions. Micrometre scale structures and devices can be blocked by relatively large particles of dust. Fabrication takes place in a cleanroom, a workspace in which temperature, humidity, vibrations and lighting are carefully controlled. The introduction of dust into the work area is carefully minimised by special outer clothing and shoes.

The most common substrate for microfabrication (i.e. the base on which the components of a system are assembled) is silicon. Silicon is an ideal material for a substrate due to a number of important and useful properties. Being as strong as steel, it can withstand mechanical processes in microfabrication. Silicon is available in a variety of shapes and sizes, but the most widely used is the silicon wafer – a thin, smooth, flat plate of silicon which is compatible with machinery developed for microfabrication. In general, thin films of materials with specific properties are deposited onto the silicon substrate.

2.3.1 Spin coating and photoresists

Various methods are available for depositing a thin film onto the substrate, but the method with relevance to this project is spin-coating. Spin-coating is suitable for applying thin layers of photoresists and spin-on glasses, and for thick polymer layers. Viscosity, solvent evaporation rate, and spin speed determine the thickness and nature of the film deposited.

A photoresist is a mixture of chemicals whose solubility is affected by exposure to light. Photoresists are mixtures of a base resin, a photoactive compound, and a solvent. The resin determines mechanical properties such as elasticity. The photoactive compound determines the solubility of the mixture following exposure to light. The solvent controls the viscosity of the mixture, and provides a means of applying very thin layers of the mixture to a substrate. A positive photoresist is one which becomes more soluble on exposure to UV light. A negative photoresist becomes less soluble on exposure to UV light.

The thickness of the layer applied can be adjusted to an extent by the spin speed, but there are limitations with each resist formula, and thick layers are achieved using a more viscous resist (i.e. one with more solid content per volume of solvent). Various defects are

associated with spin-coating a wafer, such as pinholes caused by particulates or moisture on the wafer. Such defects increase in frequency with a decrease in film thickness, but a thinner film provides better resolution (ability to distinguish between small structures). The thickness of the film is therefore a compromise between performance and the size of the structures required.

The substrate is placed on a rotating stage, and secured by a vacuum. The stage is inside a container with a hinged lid through which the photoresist can be pipetted. The lid is closed and locked, and the photoresist is dispensed onto the substrate when the substrate is static or at low rotation (ca. 300 rpm). The solvent begins to evaporate from the resist immediately it is deposited, so rapid acceleration to ca. 5000 rpm is required to spread the resist across the substrate before differences in viscosity result in an uneven film being deposited. The film is partially dried through evaporation by a final spinning stage at 5000 rpm. Following spin coating, the substrate is baked on a hot plate to complete the deposition of the film. The depth of the resist layer partially determines the depth of structures and features that will appear on the wafer following exposure through a photomask.

2.4 Photolithography

2.4.1 Photomask Fabrication

Pattern generation on a thin film serves a variety of purposes in microfabrication. In this project, it was necessary to form the microchannel pattern on the substrate. The initial step in creating and transcribing a pattern onto the device is photomask fabrication (see Figure 3). A magnified version of the pattern is laser-printed onto an overhead transparency. A glass plate covered with photographic emulsion (a photoplate) is loaded into a box with a sliding shutter. The large transparency, with the pattern of the microchannels printed in black, is laid over a large, flat white light source and the photographic plate is loaded above the transparency. The shutter is opened and the resist is exposed to the light source, then the shutter is closed again. The glass plate is removed from the box in a dark room, and the mask is developed, fixed, and rinsed. For details of these processes see Method. The

contrast on the emulsion mask is not high enough for good exposure of a thick layer of photoresist, so the pattern must be written on a metal mask.

A second glass plate is covered with a thin layer of chromium, then spin coated with positive resist. The first mask and the chromium plate are aligned, and the chromium is exposed to UV light through the photomask. The areas of resist which have been exposed become more soluble, and those areas are dissolved. The chromium underneath is etched, then the remaining resist is stripped away to reveal the pattern written in chromium (see Figure 3).

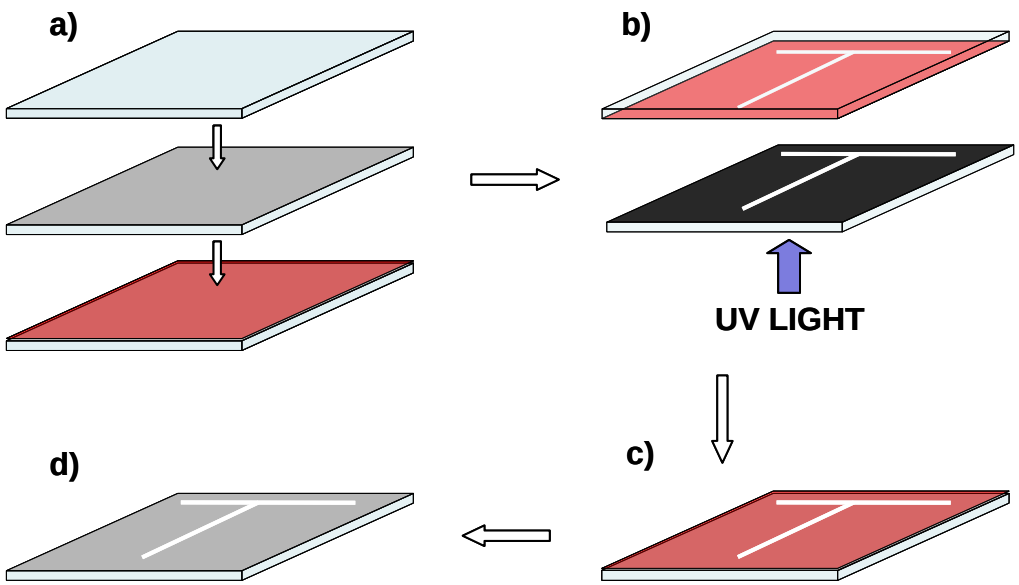

Figure 3: Fabrication of chromium photomask: a) Glass plate coated with chromium, then spin coated with positive photoresist; b) Glass plate exposed to light through first photomask (chromium not shown for clarity); c) Soluble resist dissolved, and chromium etched to form microchannel pattern; d) Remaining resist stripped away, revealing pattern in chromium.

2.4.2 Pattern Generation

Photolithography is conceptually similar to photography. The mask (which is equivalent to the photographic negative) is aligned with the substrate wafer, which has been coated in

photoresist. There are several options for aligning the substrate and mask. The simplest of these, used in this project, is known as contact lithography. The photomask is placed directly on top of the resist-coated wafer, and the wafer is exposed to UV light through the mask. Where the chromium is deposited, no light passes through the mask, and so the pattern is transferred to the resist (see Figure 4 and Figure 5).

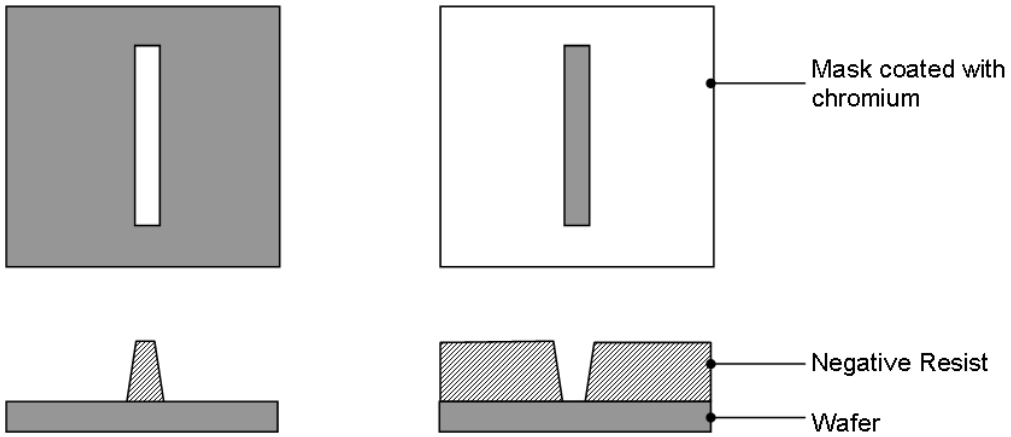

Figure 4: Pattern shapes and negative resist profiles. Left: line; right: trench. Dark grey areas indicate position of chromium on mask. Patterned areas indicate resist that remains after development of wafer [14].

When the wafer is developed, i.e. the soluble resist is etched away using chemicals, the negative resist which has not been exposed to light dissolves in preference to the areas of resist which have been exposed. A line drawn in chromium on the photomask will produce a trench in the resist. A trench (i.e. a line gap in the chromium on the mask) will produce a line in the resist. Due to the variation of the intensity of UV light through the mask, vertical resist walls, at 90º to the substrate, are difficult to achieve. Rather, the walls of a structure such as a trench or a line will slope towards the wafer and towards the top of the resist respectively. Very small features on the mask, such as a series of narrow, straight lines, are difficult to resolve on the resist, and there are limitations to the minimum size of structures. Useful shapes and proper resist profiles are produced for larger structures and spaces. Figure 4 shows basic line and trench/channel shapes and their negative resist profiles. With a positive resist, a line of chromium on the mask will produce a line in the resist, and a trench on the mask will produce a trench on the resist.

Once the pattern has been formed on the resist, the underlying material (e.g. the silicon wafer) can be etched to form the desired structure. If a line of resist is present on the substrate, the resist will protect the silicon during the etching process. Other material surrounding the line will be dissolved, leaving a line of resist covering a line of the underlying material. The resist then needs to be removed to reveal the final structure in the desired material. Wet etching involves leaving the substrate in sulphuric acid or some other substance that will dissolve the resist and underlying substrate, but not the other areas of the wafer. The length of time the wafer is left to etch determines the depth of the structures that will be produced on the wafer. The etching process leaves rounded profiles and undercuts the resist, so that the final structures will be a slightly different size and shape to the original mask. These variations are taken into consideration when designing patterns and process times.

2.4.3 Soft Lithography

For the production of a microfluidic channel, there are two approaches. The first is to etch channels into the silicon wafer, as described above, and complete the channel with a glass plate or similar, bonded to the wafer. The second approach is to use the layer of photoresist on the wafer as a mould, and apply a layer of a polymer over the resist so that the pattern is imprinted in the polymer, which can then be removed and bonded to a glass plate. The second approach was used in the fabrication of the device for this project. The process of moulding a polymer using an etched wafer is known as soft lithography, and is frequently employed in the field of microfluidics. To make a channel in PDMS, a pattern of raised lines is required in the mould. Negative photoresist is applied to the silicon wafer and exposed through a dark field mask, such that the areas of resist surrounding the channel pattern are dissolved, leaving a raised impression of the microchannels. The polymer is then poured on top of the mould. An elastomer such as PDMS can be peeled away once cured, as shown in Figure 5.

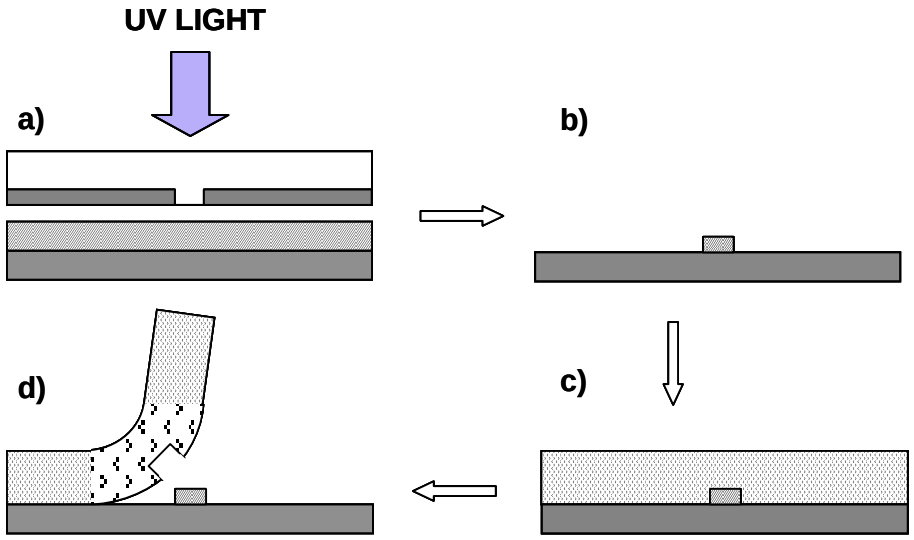

Figure 5: Soft lithography: a) Photomask (top) and spin-coated silicon wafer (bottom) are aligned and wafer is exposed to UV light through mask; b) Negative resist is stripped, leaving raised profile of channel pattern; c) PDMS is poured onto silicon mould and cured; d) Once cured, PDMS is peeled away with imprint of channel pattern on underside.

2.5 Method

The device was designed and fabricated in the Micro-Electro-Mechanical Systems (MEMS) department of the School of Engineering at Durham University. My thanks go to Alice Delcourt-Lancon for her hard work on the design and fabrication of the device, and on the subsequent improvements to the design. The following section gives details of the actual method used in the fabrication of the microfluidic device.

2.5.1 Production of photomask

The pattern of microchannels was drawn using CorelDRAW 11. The dimensions used were 10 times larger than the required dimensions, so that the image would be reduced to the right size on the photomask. The design was printed onto an acetate sheet, and placed on a light box (white light source). A glass plate covered with silver halide photographic emulsion (photoplate) was exposed to white light through the acetate sheet for six minutes. The image reduced using a Sinar plate camera. The photoplate was developed in AGFA Millimask G282c Reversal & High Speed Developer. Fixing was done with AGFA G333c Rapid Fixer. The plate was immersed in each liquid for 2 minutes, and was rinsed in water

between development and fixing, and then rinsed again at the end. The plate was cleaned in water in an ultrasonic bath for 1 minute, and then allowed to dry.

The pattern was transferred to a chromium photoplate using Microposit S1813 positive photoresist. S1813 was spin coated onto the chromium-covered plate at 3700 rpm for 1 minute, before being baked on a vacuum hotplate for 4 minutes at 95 ºC. The two masks were aligned and exposed to UV light for 3 seconds using an EVG620 double sided mask aligner.

The positive photoresist was made more soluble by exposure to light, and was dissolved with Microposit 351B developer (aqueous sodium hydroxide) diluted by half with deionised water. The plate was rinsed several times with deionised water, and then the exposed chromium was etched with a solution of ceric ammonium nitrate, containing 10 g of ammonium ceric nitrate, 1 ml nitric acid and 49 ml water. The remaining resist was stripped from the glass plate using Microposit Remover 1112A (Ethyleneglycol n-butyl ether), and the plate was cleaned and dried. The photomask produced was a negative of the original acetate print, and as most of the area remained covered in chromium, it was a dark field mask.

2.5.2 Production of silicon mould

Prior to spin coating with the resist, the substrate was cleaned and dried to ensure that the resist was successfully applied. The substrate was cleaned in water an ultrasonic bath, and rinsed with deinonised water, before being baked at 200 ºC on a hotplate to dehydrate the surface.

Micro Chem Nano SU-8 Negative Tone photoresist (glycidyl-ether-bisphenol-A novolac) was used to create the raised channel pattern on the silicon wafer [15]. SU-8 is suitable for producing high aspect ratio structures with near vertical side walls, and film thicknesses from 1 to 200 μm. When the resist is exposed to near UV light (350-400 nm) a strong acid is produced in the resist. The resist is baked following exposure, and the acid initiates epoxy cross-linking, rendering the exposed areas insoluble. The recommended sequence of

processes is as follows: Spin coat onto substrate, soft bake the resist, expose to UV light through photomask, post exposure bake, develop, rinse and dry.

2.5.3 Spin-coating

The desired channel depth was 30 μm, so the SU-8 layer would also have to be 30 μm thick. Several versions of SU-8 are available, with different viscosities according to the thickness of the film required. SU-8 10 is suitable for a 30 μm layer. The silicon wafer was loaded into a spin coater from Laurell Technologies. Approximately 2 ml of SU-8 10 was dispensed onto the wafer whilst static, and the spin coater was accelerated to 500 rpm at 100 rpm/second. The spin coater was ramped to the final spin speed of 1000 rpm at an acceleration of 300 rpm/second, and held at 1000 rpm for 30 seconds.

2.5.4 Exposure and Baking

The resist-coated wafer was pre-baked for 3 minutes at 65 ºC, and 'soft baked' for 7 minutes at 95 ºC. The resist was exposed to UV light through a photomask for 10 seconds using the EVG620 double sided mask aligner. A post-exposure bake must be performed to cross-link the exposed portions of the film [15]. A two-step bake is recommended by the suppliers to avoid cracking of the film. The wafer was baked at 65 ºC for 1 minute, and then at 95 ºC for 3 minutes. The wafer was left on the hotplate after the final bake to avoid rapid cooling.

2.5.5 Developing

The wafer was immersed in EC Solvent Developer (2-methoxy-1-methylethylacetate) to remove the unexposed SU-8. The wafer was rinsed in deonised water, and left to dry.

2.5.6 Preparation of PDMS

The base and curing agent supplied by Dow Corning for microfluidic applications consist of silicone-hydride substituted monomers containing a platinum cross-linking agent, and methyl-vinyl based silicones respectively. When the two are mixed an addition reaction

occurs, resulting in the cross-linked polymer [13]. The reaction occurs at room temperature, so the two components were mixed together in a beaker shortly before being poured onto the silicon mould. The base and curing agent were mixed in a volumetric ratio of 10 units of base to 1 unit of curing agent.

Air bubbles are incorporated into the viscous polymer liquid when the base and curing agent are mixed together. In order to avoid air bubbles in the finished device, the mixture was degassed by placing the beaker in a vacuum for ten minutes.

2.5.7 Fabricating Connections

The device was connected to the syringes using 2 mm internal diameter silicone tubing. The tubing was connected to the channels by making small holes in the PDMS. This was done at the moulding stage. Short lengths of tubing were positioned and glued onto the wafer and the PDMS was moulded around them. The holes were created with tubing of a smaller outer diameter than the tubing we intended to use with the syringes, in order that the PDMS would seal tightly around the tubing.

2.5.8 Moulding and Curing PDMS

The PDMS pre-polymer was poured onto the substrate and cured for 20 minutes at 120 ºC in an oven. After curing and cooling, it was carefully peeled away from the mould.

2.5.9 Surface Treatment and Assembly

Adhesion of the PDMS to a glass plate, and rendering the PDMS hydrophilic were achieved using plasma activation. The PDMS and glass plate were exposed to 60% of oxygen for 40 seconds, at a pressure of 40 Pa and a temperature of 20 ºC. The PDMS remains hydrophilic for ca. 30 minutes on exposure to air, but contact with a polar liquid such as water protects the surface [1]. The PDMS was placed channel-side down on the glass slide, and pressed down to create a permanent seal. Silicone tubing with an inner diameter of 3 mm was inserted into the inlet holes.

2.6 Testing of first device, results and improvements

I chose to test the device using the heptane/AOT/water/NaCl system that had been used successfully to produce emulsions in previous work [16]. This choice was based on the premise that this system was likely to be used in later parts of the project, despite the risk of causing swelling of the PDMS with heptane. The equipment used in preparing the surfactant solution, and in dispensing both the heptane and surfactant solution (syringes, beakers and pipettes) were immersed in a 1% solution Borer Chemie 15PF Cleaner (hereafter called Deconex) and cleaned in an ultrasonic bath for 15 minutes. The equipment was rinsed in deionised water and dried with clean air, or left to dry. AOT and heptane were supplied by Sigma Aldrich, with a minimum purity of 99%. Sodium chloride (minimum purity 99.5%) was supplied by Sigma. All the chemicals were used as received. A Metler-Toledo AG135 balance was used. A small sheet of Whatman Pergamyn paper was placed on the balance, and dry chemicals were weighed out onto the paper to within 3 decimal places of the desired weight. The chemicals were transferred to a clean, dry volumetric flask from the paper, and the volumetric flask was filled to the requisite volume with MilliQ water. The solution was sonicated in a Langford Sonomatic ultrasonic bath until the dry chemicals had dissolved, and then left to equilibrate to room temperature.

The surfactant solution (1 mM AOT, 0.05 M NaCl, deionised water) was pumped slowly along the silicone tubing and into the microchannel using the syringe pump, until the flow reached approximately half way along the inlet channel. The same was done with the heptane.

The set-up for using and viewing the device is shown in Figure 6 (only the surfactant solution syringe is shown). A 20x Newport microscope objective with a working distance of 17 mm was used to view the channels.

The fluids in the device reported by Thorsen *et al.* [2] were pressurised with compressed air, so the fluid flow operating parameters are given in pressures relative to atmospheric pressure, rather than volumetric flow rates. Fluid dynamic considerations were unlikely to yield accurate values of the pressures in the microchannels due to the large surface effects

present in such a small-scale device, so I decided to find the right relative flow rates by a process of trial and improvement.

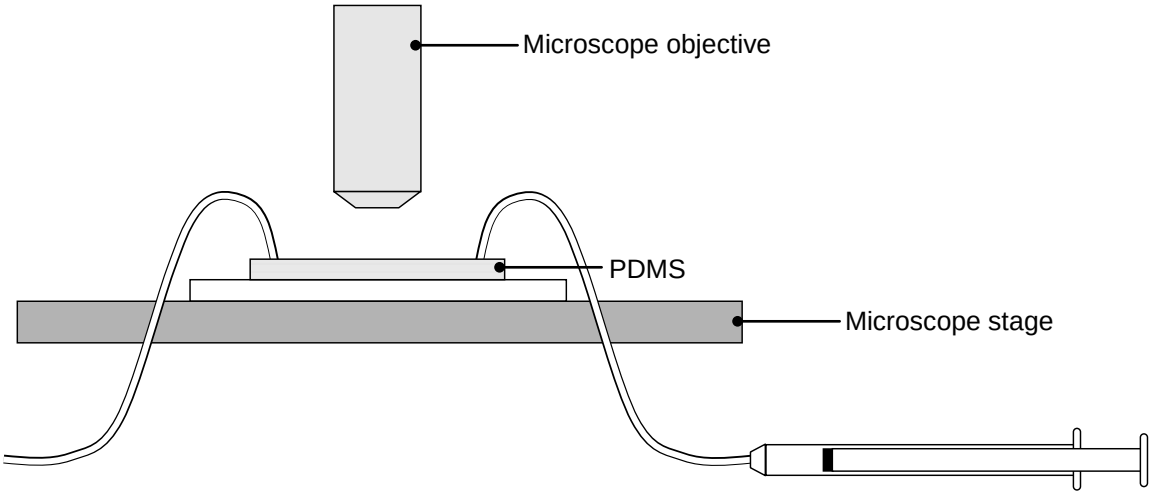

Figure 6: Set-up for testing and viewing microfluidic device.

None of the attempts to produce emulsion droplets were successful with the microfluidic device. Several factors made precise control of the fluid flow difficult to achieve. The first of these was that there was a significant delay between changing the flow rate at the syringe pump, and the flow rate in the channels changing.

Even though the PDMS had been treated to render it hydrophilic, swelling caused by contact with oil in the oil inlet channel was still evident. The constrictions caused by the swelling of the PDMS caused very unsteady flow, and lead to the blockage of the channels on a number of occasions. Small pieces of what I assumed to be PDMS were moved along the channel by the liquid flow, and proceeded to cause blockages at other points in the channel (Figure 7c). As previously mentioned, the PDMS remains hydrophilic for ca. 30 minutes, unless protected by a polar liquid. Figure 7b shows an air bubble in the channel following wetting with the surfactant solution. It appears that the PDMS is not hydrophilic, as the surface is not completely wetted by the solution. Figure 7d shows what appeared to be the PDMS delaminating from the surface of the glass plate. This occurred on two occasions only, and after both occasions the PDMS seemed to re-adhere itself to the glass surface. This did not seem to have any adverse affects on the flow of the heptane.

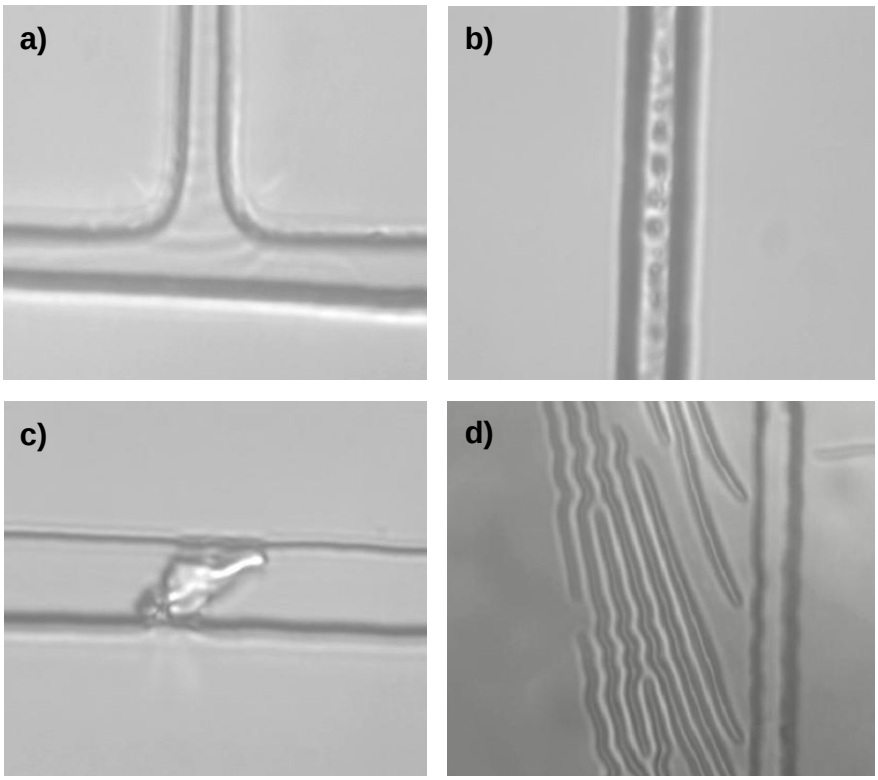

Figure 7: a) Shape of T-junction showing rounded corners and varying widths of channels; b) Air bubble in channel showing water not wetting channel walls; c) Piece of PDMS in channel; d) PDMS delaminated from glass plate.

We were able to measure the channel depth by observing the PDMS 'upside down' with a microscope. By focussing on the bottom surface of the PDMS where the channels were imprinted, and then focussing down to the top channel wall, we ascertained that the channels were 16 μm deep. The intended depth was 30 μm. The difference was unlikely to be due to the thickness of the SU-8 film. Rather, it is likely that the SU-8 was not exposed long enough to ensure a good resist profile.

2.6.1 Connectivity

The method of moulding the PDMS around a piece of the tubing to be used with the syringe pumps proved to be unsatisfactory at the pressures required to drive the fluid flow. Our initial solution to this was to use Dow Corning 732 Multi-purpose sealant. This product is a silicone-based acetoxy adhesive/sealant that cures on exposure to moisture in the air. The tubing was placed in the holes, and sealed in place with a generous amount of

the sealant. This provided a temporary solution to the problem, but after an hour of using the device, the seal broke. The device is viewed through a microscope, and it was necessary to move the stage in order to view the various sections of the channels. This caused the microscope objective to push against the tubing and in some instances to push the tubing out of the holes in the PDMS (see Figure 6). The silicone sealant was not sufficiently strong to prevent the tubing being pushed out of the holes, so another solution was required.

2.7 Design of second device

A brief search of the literature revealed that the best approach was to make the holes in the PDMS much smaller than the tubing, ensuring a strong seal [17]. When the second device was fabricated, we did not mould the PDMS around the tubing, but made holes with a needle in the PDMS once it had cured. In order to ensure that the holes were made in the right place in the PDMS, the second device was designed with reservoirs at the surfactant solution and oil inlets (see Figure 8).

As well as creating a tighter seal for the tubing, tubing with a much smaller inner diameter (0.05 mm) was used. This would decrease the pressure at the junction between the tubing and the microchannels, and was the same diameter of tubing used by Thorsen [2]. Two more sections of tubing, with increasing inner diameter, connected the syringe to the small diameter tubing. At each connection a small rubber O-ring was placed around the joint to hold the sections of tube together, and prevent leaking or disconnection.

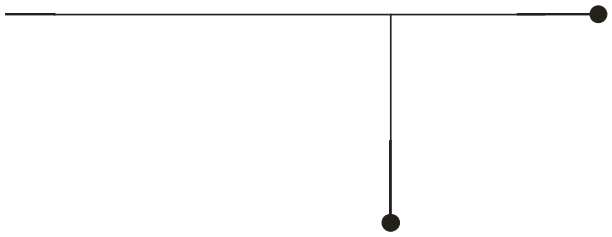

Figure 8: Design of second microfluidic device, produced in CorelDraw. Reservoirs at oil and water/surfactant inlets are shown as black circles.

As previously mentioned, the channels were only 16 µm deep in the first device. To rectify this problem, we exposed the SU-8 for the second device for 30 seconds, rather than the previous 10 seconds, in order to ensure that the UV light penetrated the resist right through the film.

2.8 Testing of second device, results and improvements

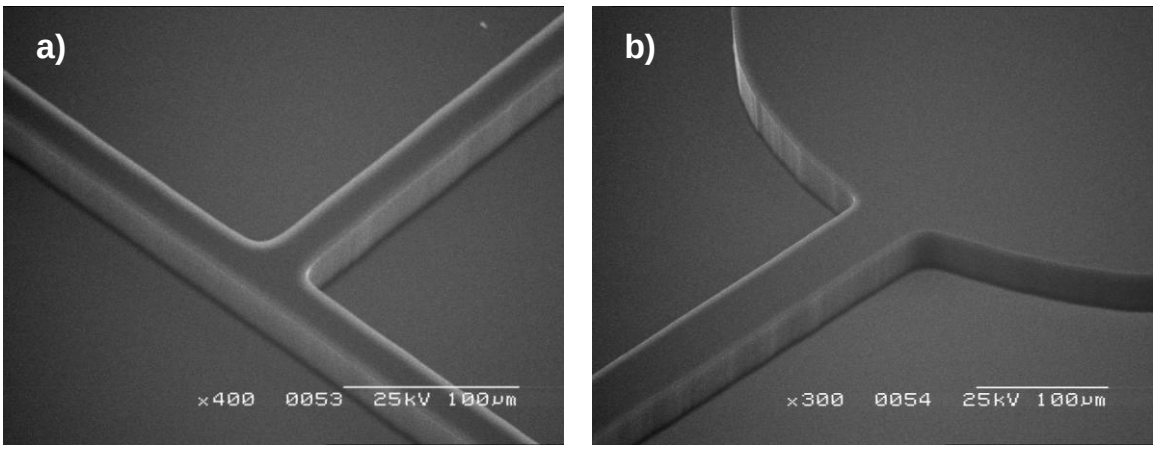

Figure 9: a) Scanning Electron Microscope image of T-junction in SU-8; b) SEM image of reservoir and inlet in SU-8.

The structure of the channels in the second device was very good (see Figure 9); the channel walls were smooth and the junction corners were rounded as suggested by Thorsen *et al.* [2]. A channel depth of 30 μm was achieved in the second device.

2.8.1 Connectivity

The technique of making a hole for the tubing with a needle was more successful than moulding the PDMS around the tubing, or using silicone sealant. It was difficult to push the tubing into the hole, but once the tubing had been forced in, a good seal was made. A disadvantage of using this method is that small pieces of PDMS inevitably fall into the hole that has been made, and potentially block the channel entrance. I noticed while testing this device that a higher volumetric flow rate (and therefore higher pressure) was required to start the surfactant solution (continuous phase) flowing down the channel. I assume that this was because of small pieces of PDMS blocking the channel that were cleared on application of pressure.

Eventually the connections between the sections of tubing failed. It seemed that leaking or disconnection occurred because of the pressure exerted on one liquid by the other. Each attempt to make the two liquids co-flow, or to produce an emulsion, failed because of the connections falling apart or leaking whenever the two liquids were at the appropriate relative flow rates to begin making emulsion droplets.

Ultimately it was the time constraint on this project that prevented me from continuing work on the microfluidic device, although there were several other factors involved.

There was a significant delay between a new flow rate being applied at the syringe pump, and a change in flow rate occurring in the channels. This may be because of the expansion of the silicone tubing with an increase in pressure. It was thus very difficult to precisely control the flow of the fluid in the channels, and I was only able on two occasions to make

the fluids co-flow down the outlet channel. I did not succeed in creating any emulsion droplets with either of the devices.

2.9 Future Work and Improvements to Design

2.9.1 Connectivity

The problem of connectivity between the microfluidic device and tools of a much larger scale, i.e. syringes, pumps, reservoirs etc, is a much-discussed issue in the field of microfluidics [11, 17 - 19]. In this project, the main issue was that the pressure at the junction between the tubing and the channel was large enough to force the tube out of the hole cut for it in the PDMS. The hole was significantly smaller than the outer diameter of the tubing, and before the device was connected to the syringes, there seemed to be a strong connection between the tube and the PDMS, but as previously mentioned the connection failed several times during the testing of the device. The use of tubing with much smaller inner diameter is a potential solution to this problem, but one which creates problems at other points in the system. In order to connect the small diameter tubing to the syringe, a series of tubes with increasing diameter must be joined together, or a connector must be used between the syringe and the tubing. Each connection is a weak point in the system, and has the potential to leak or to detach.

Mohanty and Beebe [17] suggest a simple method of fabricating PDMS connectors consisting of a small block of PDMS with a hole right through the centre, and double-sided adhesive film. A blunt needle is used to create the hole, and the core that is left in the PDMS is removed by peeling away the adhesive from the underside of the PDMS. Investigations into this design would be useful in future work.

An alternative design has been suggested by Saarela *et al.* [18]. Pieces of tubing are used to fabricate holes in small blocks of PDMS, much in the same way that the holes were created for our first microfluidic device. The connector chip is self-sealing but presumably both surfaces could be treated with air plasma, and bonded together irreversibly. The connector

can withstand a pressure of 220 kPa with additional compression provided by a small clamp.

2.9.2 Materials

Further attempts at creating a microfluidic device for the production of monodisperse oil-in-water emulsions would necessarily require some investigation and reconsideration of material properties, such as the suitability of PDMS, PMMA and other potential polymers.

Since PDMS has been shown to swell considerably in contact with alkanes and other organic solvents, it is clear that it is not an ideal candidate for moulding microchannels for the formation of oil-in-water emulsions. Since surface to volume ratios are large at the microfluidic scale (e.g. for channel dimensions of 30 μm x 10 μm) and swelling that occurs in the channels has a large effect on the size and shape of the channel, and significantly affects the flow of the liquid. A steady flow seems to be essential for successfully creating emulsion droplets, and for maintaining a fixed pressure in the channels. Hydrophilic PDMS has shown similar results in other work [13].

An alternative polymer is polymethyl methacrylate (PMMA). The glass transition temperature of PMMA is 105 ºC [10]. Below this temperature (i.e. at room temperature) the polymer is hard and glassy, which means removing the polymer from the mould requires more mechanical stress and is likely to damage both the mould and the wafer. An alternative fabrication method, involving etching the channels directly into the polymer, would be required to make the device from PMMA.

A potentially useful material is a dicyclopentadiene-dicyclooctadiene copolymer [13]. A 40 % DCPD (dicyclopentadiene) 60 % DCOD (dicyclooctadiene) mixture produced a copolymer with elastomeric properties, which showed good adhesion to glass. The curing process for this material is less reliable than the process for PDMS, but the extra effort would perhaps be worth the benefits gained from using a material that is impervious to alkanes.

Another potential material is the polymer of urethane diacrylate [13]. Ebecryl 270 (UCB Chemicals) is slightly harder than silicone polymers (such as PDMS) but retains elastomeric properties that make it suitable for moulding and cutting. The bond between the polyurethane and glass is much stronger than that between PDMS and glass. Being slightly harder than PDMS, the urethane diacrylate polymer may hold tubing more tightly, and may go some way to solving the problem of leaking and disconnection at tubing-polymer interfaces. The polymer does not swell with alkanes, but being hydrophilic, does take up water. The choice of material, therefore, would be a compromise between swelling with oil and swelling with water.

2.9.3 Fabrication

Soft lithography was considered to be the best approach to this project, because it had been successfully employed by Thorsen *et al.* [2] and replicated by other authors. However, considering the difficulties of choosing a suitable polymer for soft lithography, it would be worth investigating the possibilities of fabricating a microchannel structure through substrate etching. Substrates are available in a wide variety of materials, including quartz, glass, fused silica, and plastics. Substrates for microfluidics must be smooth, inert, mechanically strong, and must be susceptible to etching in order that the channels can be cut into the substrate.

2.10 Design of a microfluidic device with Epigem

Epigem is a company specializing in polymer-based microengineering. A visit to Epigem during this project provided us with valuable information and advice regarding the development of a microfluidic device suitable for this project. Despite PDMS having been used successfully by several authors [1-3, 6, 11], we were advised by Epigem that it was not a suitable material for this application. The fact that PDMS swells on contact with heptane and alkanes in general proved to be more of a problem than we had hoped. In addition, the thermoplastic nature of PDMS does not make it suitable for forming small structures, such as the 10 μm (or less) channel width that would be required to produce 5 μm droplets. In fact it would be a challenge to produce any device that would form

emulsion droplets as small as 5 μm. We decided that a good alternative to producing the emulsion droplets with a microfluidic device was to design a device to control the flow of droplets, and to provide a small reservoir in which trapping experiments could be undertaken. The requirements were that the flow rate of emulsion droplets in the channels should be low enough that the optical trap would be able to pull a droplet from the flow, and that once a droplet had been trapped, there would be an area outside the flow where it could be observed and deformed. We have called this area the viewing cell (see Figure 10). The fluid flow in the viewing cell should be slower than elsewhere in the device, and so the channel was designed to be wider at this point (see Figure 10). In addition, it was suggested that the formation of emulsion droplets in a surfactant solution may be difficult, and that forming the droplets either in the absence of surfactant, or in the case of the AOT system previously used, without added NaCl. To be able to deform the droplets, the oil-water interfacial tension would have to be lowered by addition of surfactant or salt after the droplets had been formed. The microfluidic device was therefore designed to have inlet and outlet channels to remove most of the initial aqueous phase and replace it with one that would exhibit low interfacial tension with the oil droplets (see Figure 10).

The channels would be fabricated by etching the pattern in PMMA. The reservoir or viewing cell would be constructed separately to the main channel section, and connected to the top of the channels via compression ferrules. The 100x microscope objective that is used to form the optical trap is designed to be used with a certain thickness of cover glass, and the working distance is 2 mm. For this reason the top of the viewing cell would be a microscope cover glass, to enable the trapping experiments to be carried out. In recognition of the difficulty of connecting microfluidic channels to syringes, pumps and other elements, Epigem make use of Cheminert fittings. These fittings provide fluid connections between the channels and the tubing that connects the device to the pumps and syringes. The connections to the syringes would be facilitated with Cheminert fittings, to suit tubing with an inner diameter of 0.13 mm.

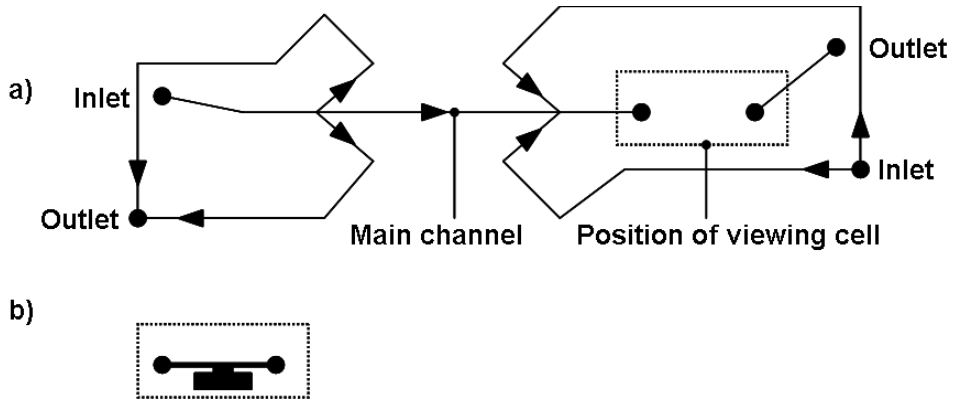

Figure 10: a) Plan view diagram of microfluidic device. Black arrows indicate direction of flow. Black circles indicate inlets or outlets, connected with tubing via Cheminert connectors. The main channel is 30 µm wide, and the whole device is 100 mm in length. b) Shape of channels in viewing cell, showing reservoir for trapping, and wide channel to slow fluid flow rate. This design is the work of Phil Summersgill, of Epigem.

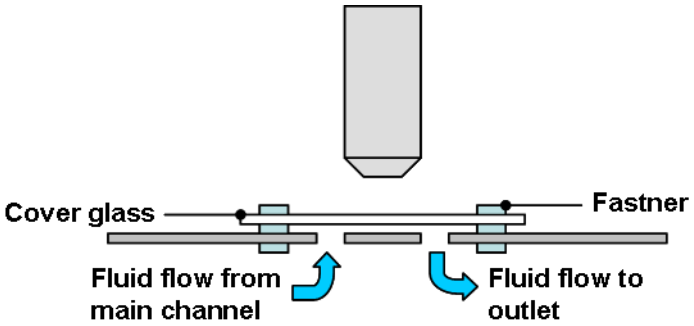

Figure 11: Side-on view of viewing cell, showing fluid connections.

My thanks go to Dr Tim Ryan and Phil Summersgill for their help and advice on designing a microfluidic device for this project. The device has not yet been fabricated, and as a result I have been unable to test it. However the design is a useful tool for illustrating the specifications for a microfluidic device suitable for use in this project.

References

1. Cooper McDonald, J., et al., *Fabrication of microfluidic systems in poly(dimethylsiloxane).* Electrophoresis, 2000. **21**: p. 27-40.
2. Thorsen, T., et al., *Dynamic pattern formation in a vesicle-generating microfluidic device.* Physical Review Letters, 2001. **86**(18): p. 4163-4166.
3. Tan, Y.C., et al., *Design of microfluidic channel geometries for the control of droplet volume, chemical concentration, and sorting.* Lab on a Chip, 2004. **4**(4): p. 292-298.
4. Tan, Y.C., V. Cristini, and A.P. Lee, *Monodispersed microfluidic droplet generation by shear focusing microfluidic device.* Sensors and Actuators B-Chemical, 2006. **114**(1): p. 350-356.
5. Malloggi, F., et al., *Electrowetting-controlled droplet generation in a microfluidic flow-focusing device.* Journal of Physics-Condensed Matter, 2007. **19**(46): p. -.
6. Menetrier-Deremble, L. and P. Tabeling, *Droplet breakup in microfluidic junctions of arbitrary angles.* Physical Review E, 2006. **74**(3): p. 035303-1-4.
7. Link, D.R., et al., *Geometrically mediated breakup of drops in microfluidic devices.* Physical Review Letters, 2004. **92**(5): p. 054503-1-4.
8. Chen, C.T. and G.B. Lee, *Formation of microdroplets in liquids utilizing active pneumatic choppers on a microfluidic chip.* Journal of Microelectromechanical Systems, 2006. **15**(6): p. 1492-1498.
9. Lee, C.H., S.K. Hsiung, and G.B. Lee, *A tunable microflow focusing device utilizing controllable moving walls and its applications for formation of micro-droplets in liquids.* Journal of Micromechanics and Microengineering, 2007. **17**(6): p. 1121-1129.
10. Goosey, M.T., *Plastics for Electronics*. 1985, London; New York: Elsevier Applied Science Publishers. 180.
11. Cooper McDonald, J. and G.M. Whitesides, *Poly(dimethylsiloxane) as a Material for Fabricating Microfluidic Devices.* Accounts of Chemical Research, 2002. **35**(7): p. 491-497.
12. Owen, M.J. and P.J. Smith, *Plasma Treatment of Polydimethylsiloxane.* Journal of Adhesion Science and Technology, 1994. **8**: p. 1063-1075.
13. Thorsen, T., *Microfluidic Technologies for High-Throughput Screening Applications*, in *California Institute of Technology*. 2003: Pasadena. p. 166.
14. Franssila, S., *Introduction to Micro Fabrication*. 1st ed. 2004, Chichester: John Wiley & Sons Ltd. 402.
15. MicroChem. *Nano (TM) SU-8 Negative Tone Photoresist Formulations 2-25*. Available from: http://www.microchem.com/products/pdf/SU8_2-25.pdf.
16. Ward, A.D., et al., *Optical sculpture: controlled deformation of emulsion droplets with ultralow interfacial tensions using optical tweezers.* Chemical Communications, 2006(43): p. 4515-4517.
17. Mohanty, S. and D.J. Beebe. *Chips & Tips: PDMS connectors for macro to microfluidic interfacing*. 2006; Available from: http://www.rsc.org/Publishing/Journals/lc/PDMS_connector.asp.

18. Saarela, V., et al., *Re-usable multi-inlet PDMS fluidic connector.* Sensors and Actuators B-Chemical, 2006. **114**: p. 552-557.
19. Christensen, A.M., D.A. Chang-Yen, and B.K. Gale, *Characterization of interconnects used in PDMS microfluidic systems.* Journal of Micromechanics and Microengineering, 2005. **15**: p. 928-934.

3 Membrane Emulsification

3.1 Droplet Formation and Detachment

The mechanism of droplet formation and detachment is an important factor in membrane emulsification. It determines operating parameters such as transmembrane pressure and crossflow velocity, and therefore the design of the emulsification unit. It also influences the choice of membrane. The polydispersity of an emulsion produced by membrane emulsification can be accounted for by examining the droplet formation mechanism. Two possible mechanisms are described here.

3.1.1 Force Balance Model

The force balance model describes droplet formation and detachment through a number of forces acting on a droplet, as illustrated in Figure 1. The interfacial tension force, F_γ, is the key retaining force during droplet formation, and represents the tendency for the droplet to adhere to the pore opening in preference to increasing its interfacial area with the continuous phase. The drag force, F_D, is created by the flow of the continuous phase across the membrane surface, and acts to detach the droplet. The buoyancy force, F_B, is shown to act perpendicular to the membrane in this representation, but acts in an upwards direction regardless of the orientation of the membrane. F_I is an inertial or linear momentum force associated with a mass of fluid flowing out from the pore opening [1]. It has been shown that for micron scale droplets the inertia (F_I) and buoyancy (F_B) forces are 9 and 6 orders of magnitude smaller respectively than the interfacial tension (F_γ) and drag (F_D) forces and can therefore be neglected in a force balance model [2].

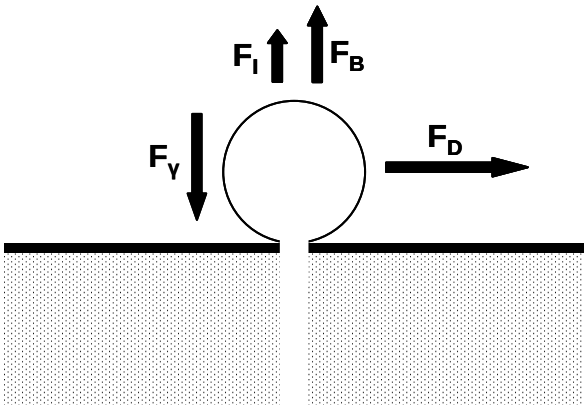

Figure 1: Forces acting on a droplet [1].

The force balance argument presented above is just one approach to the problem of droplet formation at a pore. Many authors have used this approach in their work [1-4]. However, there is evidence to suggest that the mechanism of droplet formation and detachment varies with the operating conditions [5-8]. Rayner *et al.* [9] have reviewed droplet formation mechanisms and suggested that the force balance model does not properly predict droplet size. According to the force balance model, the point of detachment should occur when the sum of the forces equals zero. However, the droplet sizes predicted by this model are generally not supported by experimental results [9].

3.1.2 Spontaneous Transformation Based Model

Sugiura *et al.* [10] have presented a spontaneous droplet formation mechanism based on the effects of interfacial tension. In a microchannel emulsification (MC emulsification) device, the disperse phase is pressurised through small channels which terminate in a terrace. Beyond the terrace is a well. When the disperse phase reaches the end of the terrace, it flows down into the well and is transformed into droplets. The curvature of an interface produces a pressure difference between the inside and outside of a droplet called Laplace pressure, which can be defined by the Young-Laplace equation:

$$\Delta P = \gamma_{OW}\left(\frac{1}{R_1}+\frac{1}{R_2}\right) \tag{3.1}$$

where ΔP is the pressure difference across the interface, γ_{OW} is the interfacial tension between the disperse and continuous phases, and R_1 and R_2 are the two principal radii of curvature of the interface. Due to the difference in principle radii of curvature the Laplace pressure is larger on the terrace than in the well, causing the disperse phase to flow into the well. This is the shearing mechanism for MC emulsification. The authors note that this mechanism is different to that for droplet formation from a circular nozzle, which requires external shearing forces [1]. The disk-like shape formed by the droplet on the terrace is unstable with respect to interfacial free energy because of its large interfacial area compared to the final spherical shape.

Further work with MC emulsification [11] showed that at a critical disperse phase flow velocity, the mechanism of droplet formation and detachment changed from the interfacial-driven spontaneous transformation model, to a continuous flow model. Below the critical value the droplet diameters were almost constant. The droplet diameter increased above the critical velocity, and polydisperse emulsions were formed. Experimental results showed that the critical point at which the state of flow changed was determined by the Capillary number, which can be defined as

$$Ca = \frac{\text{viscous forces}}{\text{interfacial forces}} = \frac{\eta U}{\gamma} \tag{3.2}$$

where η is the viscosity of the disperse phase, U is the velocity, and γ is the interfacial tension between the disperse phase and the continuous phase. The state of flow is determined by Ca and therefore by the balance between viscous and interfacial forces. This change from one flow state to another with increasing disperse phase flux was also observed for an SPG (Shirasu porous glass) membrane [8], suggesting that the mechanism can also be applied to ceramic membrane emulsification providing that the pore openings are not circular.

However, there is evidence that the force balance model is also applicable to droplet formation at an SPG membrane in the absence of shear [12]. This recent work has shown that a decrease in surfactant concentration causes an increase in droplet size, which

suggests that interfacial tension is acting as a retaining force rather than a detaching force. The authors noticed a transition from a 'size-stable zone' spontaneous transformation model) to a 'continuous outflow zone' [13] in which the force balance model seems to be applicable.

Monodisperse emulsion droplets were spontaneously formed by oblong through-holes in a silicon microchip [14]. Kobayashi *et al.* investigated droplet formation from circular and oblong straight-through microchannels, finding that droplets formed at a circular pore would grow to a large diameter (100 μm compared to a pore diameter of 10 μm) without an applied shear force. Droplet diameter decreased with increasing wall shear stress, and increased with increasing disperse phase pressure, indicating that droplet detachment was reliant on the drag forces exerted by the continuous phase. Droplets formed at an oblong slot appeared to detach spontaneously as a result of interfacial tension forces. The average droplet diameter and coefficient of variation (measure of droplet size distribution) were independent of the continuous phase velocity in the range measured, and changed little over a range of disperse phase pressures. A monodisperse emulsion was produced even without the continuous phase flow. As previously described a non-spherical droplet (e.g. an elongated droplet at an oblong slot) has a greater surface area than a sphere of equivalent volume, and the interfacial tension acts to make the droplet spherical. This interfacial tension force is responsible for droplet detachment in this mechanism. The authors later reported that the aspect ratio of the oblong slot was a key parameter in droplet formation [15]. Disperse phase passing through a low aspect ratio slot tends to flow continuously, and is sheared off by the continuous phase much as a droplet forming at a circular pore would be. The disperse phase passing through a high aspect ratio slot was transformed spontaneously into uniform sized droplets, and once again the size and coefficients of variation were independent of the continuous phase velocity. These results confirm that the mechanism of droplet detachment relies upon a deformation of the growing droplet from its ideal spherical shape, and that the key detaching force is interfacial tension.

The spontaneous transformation based model has implications for the effect of different surfactants on droplet formation. Since droplet detachment is driven by interfacial tension at low disperse phase flow rates (i.e. when interfacial tension dominates other forces), a

low interfacial tension between the disperse and continuous phases will result in larger droplets, and will shift the critical capillary number and disperse flow rates to lower values. The opposite is true for the force balance model. Vladisavljevic *et al.* have shown that, for asymmetric microchannels, increasing the concentration of surfactant in the continuous phase up to the CMC, and thereby reducing the interfacial tension, causes an increase in droplet size [16]. Since this is the opposite result to that obtained by van der Graaf *et al.* [17], using a single circular pore and cross-flow, it seems likely that the two different mechanisms operate for different pore geometries and operating conditions. As previously mentioned, a circular pore requires a cross flow to detach droplets, whereas the geometry of a rectangular pore, as demonstrated by Kobayashi [15] causes spontaneous droplet detachment without a cross flow.

3.1.3 Push-off Force

Several authors have observed and reported a ‘push-off’ force acting between droplets that can lead to increased polydispersity [5-6, 18]. Droplets forming at adjacent pores will push each other off the membrane if they grow large enough for their surfaces to touch, meaning that the pore size does not dictate droplet size. This puts restrictions on the ideal distance between pores, the ideal porosity of the membrane and the number of active pores. The number of active pores increases with increasing transmembrane pressure [6-7, 19] and so the chance that two adjacent pores will be active also increases.

3.2 Choice of Membrane

A key parameter in the design of a membrane emulsifier is the choice of membrane. A literature study revealed that the droplet size tends to be a multiple of pore size, with the proportionality constant being between 2 and 10 depending on operating conditions and the chemical system used [6]. A monodisperse emulsion can only be produced if the membrane pore size distribution is narrow [20]. Ceramic micro- and mesoporous membranes, Shirasu Porous Glass (SPG), and microengineered membranes (e.g. silicon plates) are the three most common types of membrane employed in membrane emulsification.

Shirasu porous glass membranes are said to produce a more monodisperse emulsion than ceramic alumina membranes, and to be competitive with microchannel plates under the same operating conditions [19]. Many authors have quoted the narrow pore size (± 15 %) distribution of Shirasu porous glass membranes as an advantage over ceramic membranes [21-22]. Vladisavljevic *et al.* used SPG membranes to produce emulsions with spans ranging from 0.30 to 0.45. The relative span of droplet size distribution was calculated from the experimental data using the equation $span = (d_{90} - d_{10})/d_{50}$ where d_x is the droplet diameter corresponding to x vol. % on a cumulative droplet volume curve [23]. In a separate paper, also investigating SPG membranes, Vladisavljevic reported a range of spans from 0.29 to 0.68 [24]. Dragosavic *et al.* have reported span values between 0.35 and 0.60 for a microengineered flat disk membrane in a stirred cell [18]. Joscelyne and Tragardh [25] reported spans between 0.87 and 1.64 for emulsification with a ceramic membrane. Williams *et al.* [26] achieved a span of 0.82 with an alumina ceramic membrane.

In a comparative study of SPG and ceramic membranes [27] Vladisavljevic *et al.* reported span values of 0.51 – 0.59 for the ceramic membrane, and 0.26 – 0.45 for the SPG membrane under the same operating conditions. They concluded that a narrower droplet size distribution could be achieved with the SPG membrane. As previously mentioned, in order to produce a monodisperse emulsion there must be no steric hindrance between neighbouring droplets. Because of the lower porosity of the ceramic membrane, the chance of neighbouring droplets exerting a ‘push-off’ force on each other, or coalescing on the membrane, was lower than for the SPG membrane with higher porosity [27].

Microengineering technology offers the possibility of creating a membrane with pores which are identical in size and shape [20]. Several authors have made use of such membranes in their work [5, 7, 16, 18, 20, 28]. Although microengineered membranes have been reported to be more successful in producing monodisperse emulsions [16, 20, 28-29], the ease with which an SPG or ceramic membrane could be acquired meant that the choice of membrane material was between these two. A comparison of SPG and ceramic membranes showed that the main disadvantage of SPG membranes was their affinity for

cationic surfactants [30-31]. In order to ensure that the emulsifier could be used with a range of chemical systems, a ceramic membrane was chosen.

Many authors [3, 6, 18, 32-33] use a tubular membrane, with the cross flow surrounding the outer surface of the membrane, but it was decided a simpler design could be achieved by using a circular disk membrane such as those supplied by Sterlitech Corporation. There are many examples in the literature [5, 7, 16, 23, 34] of similar membranes being used for emulsification. The disperse phase is introduced on one side of the membrane, and the continuous phase flows across the other side. The choice of pore size was determined by the size of emulsion droplets desired. Ceramic membranes are available in pore sizes ranging from 0.14 μm to 1.40 μm in the microfiltration range. Given that droplet size tends to be 2 to 10 times larger than pore size, the 0.8 μm membrane was chosen, with the intention of producing droplet approximately 5 μm in diameter.

3.3 Structure of Ceramic Membranes

Ceramic membranes normally have an asymmetrical structure composed of at least two, usually three, different porosity levels. A mesoporous intermediate layer (containing pores between 2 and 50 nm in diameter) is often applied in order to reduce the surface roughness before applying the outer, active layer. The macroporous support ensures the mechanical resistance of the membrane. Ceramic membranes are made of oxides of titanium, aluminium and zirconium.

3.4 Design and Construction

There are various approaches to producing the cross-flow of the continuous phase across the membrane. The simplest is to use a syringe pump or pressurised reservoir to pump the fluid through the emulsifying unit. An alternative is to rotate the membrane within the unit, thus ensuring that no droplet break-up occurs in the emulsion due to shear forces acting because of the pumping system [32, 35]. In other examples the membrane is kept stationary but the continuous phase is stirred to generate shear forces [5, 18, 34]. In this experiment both the continuous and disperse phases were driven using syringe Harvard Apparatus 11 Plus syringe pumps.

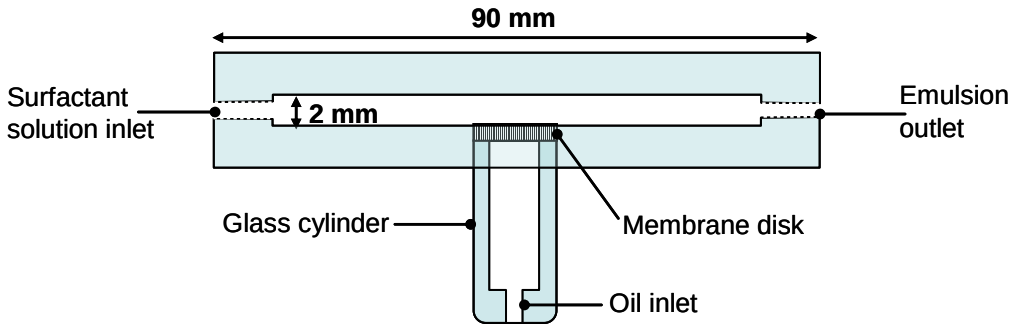

Figure 2: Cross-section of assembled emulsifier.

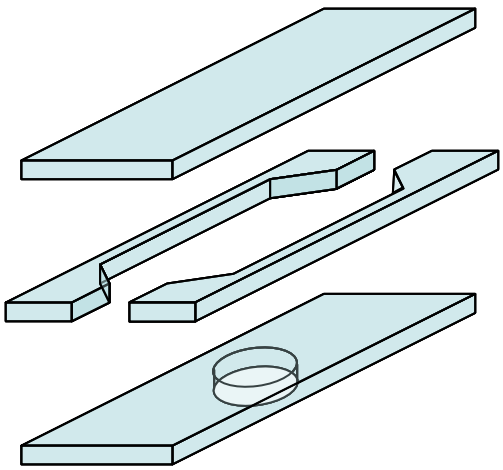

Figure 3: Construction of channel.

The emulsifier unit was designed such that the surface of the membrane would be flush with the bottom face of the channel, thus ensuring good contact with the continuous phase flow. To maximise cross flow velocity in the channel, and to minimise the amount of surfactant solution used to produce an emulsion, the channel was designed to be shallow (see Figure 2). The channel was constructed from three glass slides, so that the emulsification process could be observed with a microscope and camera. The top face of the channel is a plain glass slide. The bottom face is a glass slide with a hole cut out to fit the membrane disk into. The channel itself and the inlet and outlets are formed by a third glass slide, cut into two pieces, as shown in Figure 3.

The membranes were supplied as 2.5 mm thick disks, with a diameter of 47 mm. This was too large for the intended design so smaller disks, 10 mm in diameter, were cut out of the large ones. The glass slides were fused together using heat treatment. The small glass cylinder which would contain the oil, and the membrane, were fixed in place with UV-curable glue. The inlet and outlet holes were designed to take 3 mm outer diameter Teflon tubing. The tubing was attached to the syringes using Kinesis connectors.

3.5 Calculation of Shear Stress

According to the literature the shear stress provided by the continuous phase is a key operating parameter in membrane emulsification, influencing droplet size and polydispersity. The maximum flow rate available with the syringe pumps in use is 39.5 ml min^{-1}. The dimensions of the rectangular section of the cross flow channel are 2 mm x 18 mm x 45 mm.

The Reynolds number is a dimensionless number which characterises the state of fluid flow as either laminar or turbulent:

$$\mathrm{Re} = \frac{QL}{\nu A} \tag{3.3}$$

where Q is the volumetric flow rate (0.67 x 10^{-6} m^3 s^{-1}), L is a characteristic length of the system, ν is the kinematic viscosity of the fluid (1.0 x 10^{-6} m^2 s^{-1}), and A is the cross-sectional area of the pipe through which the fluid flows (3.6 x 10^{-5} m^2). The kinematic viscosity of the surfactant solution is taken to be the same as that of water. L is typically taken as the hydraulic diameter of the pipe, which for a rectangular cross section is found by dividing four times the cross sectional area by the wetted perimeter:

$$D_H = \frac{4A}{P} \tag{3.4}$$

The hydraulic diameter of the cross flow channel is therefore 3.6 x 10^{-3} m. At the maximum flow rate achievable (40 ml min^{-1}), the Reynolds number of flow in the cross

flow channel is $\mathrm{Re}=\frac{(0.67\mathrm{x}10^{-6}\mathrm{m}^3\mathrm{s}^{-1})(3.6\mathrm{x}10^{-3}\mathrm{m})}{(1.0\mathrm{x}10^{-6}\mathrm{m}^2\mathrm{s}^{-1})(3.6\mathrm{x}10^{-5}\mathrm{m}^2)}=67$ (1 d. p.). Flow through pipes at a Reynolds number less than 2000 may be regarded as laminar, and flow for a Reynolds number greater than 4000 may be taken as turbulent. It is clear that a very slow laminar flow is operating in the cross flow channel.

The wall shear stress for turbulent flow in a pipe can be calculated as follows:

$$f=\frac{\tau_0}{\frac{1}{2}\rho u^2} \qquad (3.5)[36]$$

where f is a coefficient known as the friction factor, depending on the roughness of the pipe surface, τ_0 is the mean stress at the wall of the pipe, ρ is the density of the fluid (1000 kg m^{-3}) and u is the mean fluid velocity (0.019 m s^{-1} for a flow rate of 40 ml min^{-1}). This equation applies to turbulent flow in pipes, so it's use for laminar flow is an approximation only. For laminar flow, the friction factor is given by

$$f=\frac{16}{\mathrm{Re}} \qquad (3.6)[36]$$

which for a Reynolds number of 67 gives a friction factor of 0.24.

Rearranging Equation (3.5) gives

$$\tau_0=\frac{1}{2}f\rho u^2 \qquad (3.7)$$

which gives a maximum wall shear stress of 0.043 Pa. Even though this value is very approximate, it indicates that only very low shear stresses are achievable with the current apparatus. Schroder and Schubert [33] used an 0.8 μm ceramic membrane to produce droplets between 5 and 10 μm in diameter. At a wall shear stress of 20 Pa the droplet size was approximately 6 μm. Smaller droplets can be achieved with a low shear stress if the transmembrane pressure is also reduced. Lower transmembrane pressure tends to reduce the span of droplet sizes produced [37] but low shear stresses give a higher span of droplet sizes [6-7, 37]. The effects of these two operating parameters are coupled, however, and

reducing the transmembrane pressure also reduces the influence of wall shear stress on the span, so it may be possible to produce a reasonably monodisperse emulsion at low transmembrane pressure and low shear stress.

3.6 Method

3.6.1 Surfactant Solution

Emulsions were prepared with a 1 mM AOT/0.05 M NaCl solution, prepared as described in Microfluidics. The temperature in the laboratory where the surfactant solutions were prepared was 19 ºC.

3.6.2 Disperse Phase

The disperse phase was heptane (minimum purity 99%), which was used as received from Sigma Aldrich.

3.6.3 Cleaning

The syringes, connectors and Teflon tubing were cleaned by sonicating in 1 % Deconex solution for 15 minutes. They were rinsed 20 times with MilliQ water, and dried in clean air. It has been reported that thorough cleaning of ceramic membranes improves their performance in membrane emulsification [37]. Increased wetting of the membrane by the disperse phase and absorption of surfactant molecules onto the membrane can increase the size and size distribution of the droplets produced. Before being glued into the emulsifier, the small membrane disks were cleaned according to the manufacturer's instructions, as follows. The membranes were heated to 85º C in a 15 g L^{-1} solution of sodium hydroxide for 30 minutes. The membrane was rinsed with MilliQ water, and then sonicated in water for 15 mintues, and then again in a new beaker of water. At this point the pH was neutral. The membrane was then heated at 50º C in a 5 ml L^{-1} solution of nitric acid for 15 minutes. The membrane was rinsed and sonicated in MilliQ water until the pH returned to neutral, and then dried in an oven overnight.

Once the membrane was fixed into the emulsifier, it was necessary to clean the unit as a whole to remove any contaminants from the construction of the channel. The emulsifier

was placed in a large Teflon beaker full of 1% Deconex solution, and sonicated for 15 minutes. However, the glue fixing the membrane and glass cylinder to the channel was broken down by the detergent solution and the sonication, and the emulsifier fell apart. Once it had been glued back together, it was not cleaned again before use. Further cleaning of the emulsifier involved simply flushing both the channel and the membrane with acetone, followed by rinsing MilliQ water. This did not affect the glue.

3.7 Experiments

Initial experiments, using two 5 ml Hamilton GasTight syringes, showed that a much larger syringe would be required to provide the necessary volume of surfactant solution and oil to the membrane emulsifier, so both syringes were swapped for 50 ml Hamilton GasTight syringes. However the minimum flow rate achievable with a 50 ml proved to be too fast, so once the oil reservoir had been filled using the 50 ml syringe, the tubing was swapped onto a 5 ml syringe (minimum flow rate 0.015 ml $hour^{-1}$). Figure 4 shows the set-up of the membrane emulsifier, positioned so that droplet formation could be observed on the top of the membrane. The microscope objective was a Newport Precision Objective Lens with magnification of 20x and a working distance of 17.0 mm. The temperature in the laser bay where the emulsification experiments took place was 24 ºC.

Prolonged contact of the UV glue with heptane (more than 2 hours) caused the glue to fail, so it was necessary to limit the amount of time the oil inlet was filled with oil, and to wash the emulsifier with acetone followed by MilliQ water immediately after use to remove the heptane. The emulsifier was left in direct sunlight for an hour to allow the glue to re-cure.

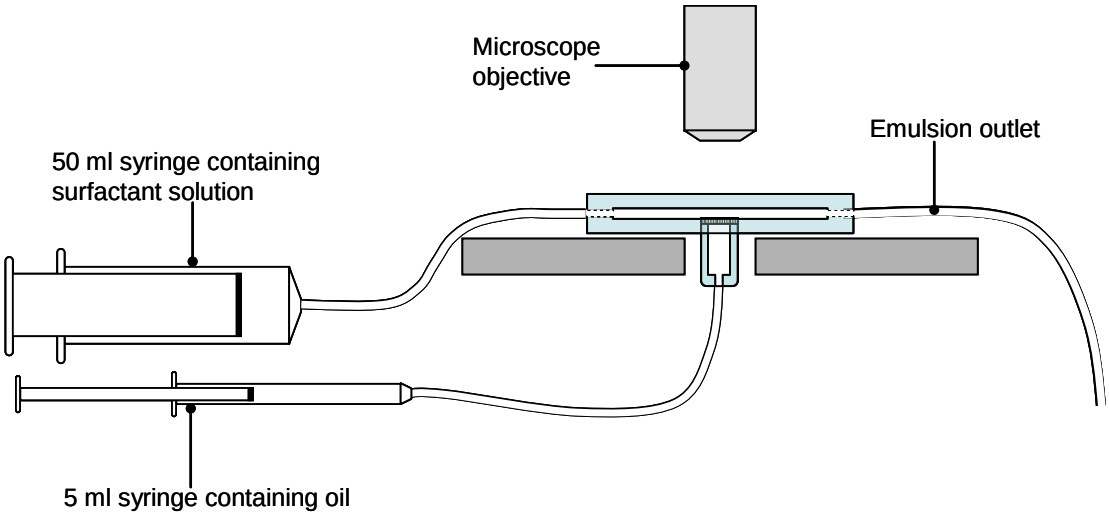

Figure 4: Set-up of membrane emulsifier experiments.

In order to find a good starting point for the experiments with transmembrane pressure and continuous phase flow rate, a wide range of syringe pump flow rates were tried for both the disperse and continuous phases. The oil flow rate was set at its minimum value of 0.0145 ml hour^{-1}, at which the oil was pushed very slowly through the membrane. The continuous phase flow rate was then increased in 5 ml min^{-1} steps from its minimum value of 0.0017 ml min^{-1}. The minimum flow rate required to detach droplets from the membrane was 15.0 ml min^{-1}. The maximum continuous phase flow rate achievable was 39.5 ml min^{-1}. In order to test the effect of the transmembrane pressure (oil flow rate) on the size and size distribution of emulsion droplet produced, the continuous phase flow rate was set at 27.5 ml min^{-1}, which is the middle value between 15 and 39.5 ml min^{-1}. Darcy's Law states that an increase in pressure across a porous medium will result in an increase of fluid flow through the medium. It is reasonable, therefore, to assess the effects of transmembrane pressure by studying the effects of oil flow rate. The oil flow rate was increased from its minimum value of 0.0145 ml hour^{-1} in 0.5 ml hour^{-1} steps, until the oil flow rate was deemed to be too high to produce emulsion droplets of the required size and monodispersity. Once an optimum oil flow rate had been found, the effect of the shear stress (continuous phase flow rate) on the emulsion was investigated. The continuous phase flow rate was increased from 27.5 ml min^{-1} to its maximum value of 39.5 ml min^{-1}.

3.8 Results

Although it was not possible to produce good quality still images from the videos taken of the membrane emulsifier in action, the videos were a useful tool for characterising droplet formation and size at different operating conditions.

Droplets appeared to be nearly spherical in shape during formation, suggesting that the spontaneous transformation based model is not applicable to droplet formation at a ceramic membrane. However, there seems to be a critical size at which a droplet forming at a particular pore will detach. Droplet detachment was observed in the absence of a cross flow, but the droplets inflated to a large size before detaching. A 'push-off' force was active between droplets forming at adjacent pores, when the droplets grew large enough to make contact with each other. It is possible that the deformation of adjacent droplets from the ideal spherical shape may have induced detachment, as in the spontaneous transformation based model of droplet formation. The alternative mechanism is that the force exerted by one droplet on another combined with the force contributed by the cross flow to push the droplet off the membrane. The distance between adjacent active pores was estimated to between 10 and 20 μm, based on the size of droplets detached from the membrane by the push-off force.

3.8.1 Effect of Transmembrane Pressure

The data presented below should be treated with caution. The droplet sizes were estimated using a 100 μm stage micrometer, imaged using the same objective that was used to observe the membrane. The droplet formation rates were estimated by counting the number of droplets forming at a pore in a given time. Due to the dimensions of the cross flow channel, the velocity of the continuous phase was not equal across all parts of the membrane. The central third of the membrane disk experienced a much higher cross flow velocity than the outer parts of the disk, although it was not possible within the scope of this experiment to quantify the difference in velocity. Droplets forming in the fast flow were smaller, and droplet formation time was shorter (see Figure 6 and Figure 7). Droplets forming outside the fast flow, toward the edges of the membrane, were much larger, and spent more time attached to the membrane.

Figure 5 shows the effect of transmembrane pressure (plotted as oil flow rate) on mean droplet formation rate (number of droplets formed per second). The data is skewed by the proportion of each video representative of regions of high and low cross flow velocity. For example, the outlying point at an oil flow rate of 5.015 ml hour^{-1} is caused by the data for that oil flow rate being representative of high cross flow velocity only. Until the droplet formation times were analysed, it was difficult to tell whether each video was representative of the membrane as a whole. When the point is included, the gradient is 0.09 with a standard error of 0.05. When the point is not included, the gradient is reduced to 0.06, and the standard error is reduced to 0.02. Similarly, there are data points missing for oil flow rates of 3.015 ml hour^{-1}, 3.515 ml hour^{-1} and 4.515 ml hour^{-1}. The quality of these videos was not high enough to enable the droplet formation to be studied. Overall, the data shows increasing droplet formation rate with increasing transmembrane pressure.

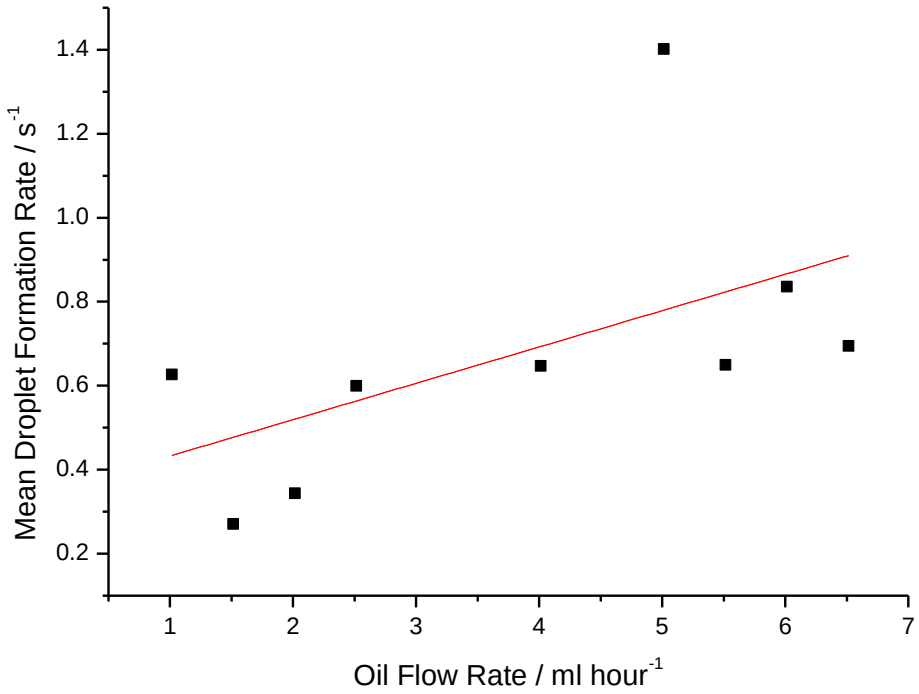

Figure 5: Effect of transmembrane pressure on droplet formation rate.

Figure 6 indicates that the influence of oil flow rate on droplet formation rate is similar for regions of high and low cross flow velocity.

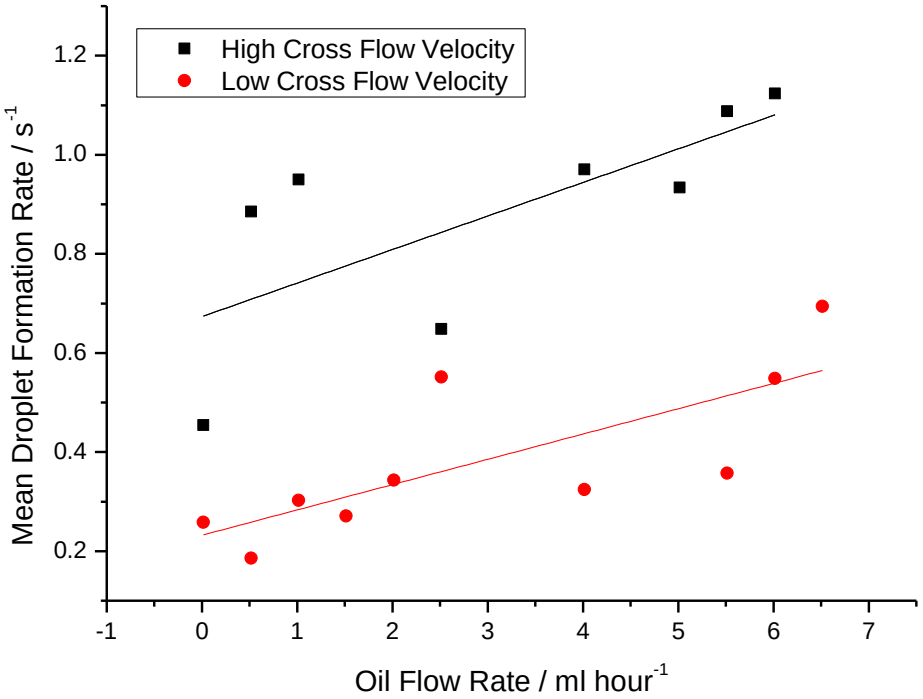

Figure 6: Effect of oil flow rate on mean droplet formation rate for regions of high and low cross flow velocity.

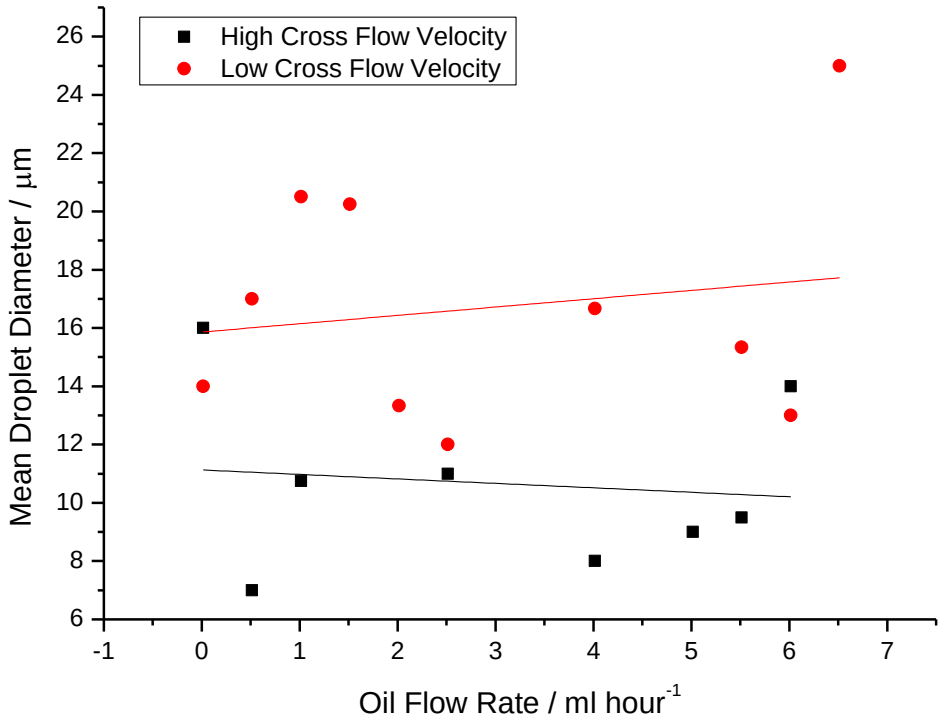

Figure 7: Effect of oil flow rate on mean droplet diameter for regions of high and low cross flow velocity.

Figure 7 demonstrates that there is no clear relationship between oil flow rate and mean droplet diameter, for regions of high and low cross flow velocity. However, increasing the oil flow rate (transmembrane pressure) significantly increased the droplet formation rate in the region of low cross flow velocity (Figure 6), because the chief droplet detachment force was the push-off force between adjacent droplets. The size of the droplet is determined by the distance between adjacent active pores, rather than the oil or cross flow rate. The droplet formation time was determined by the oil flow rate, because a higher oil flow rate inflates the droplet quicker. These results are in agreement of those reported by Egidi [5] and Abrahamse [7] who both suggested that under conditions where the droplets are growing large enough to come into contact with each other, the main detaching force is the push-off force between the droplets, not the cross flow.

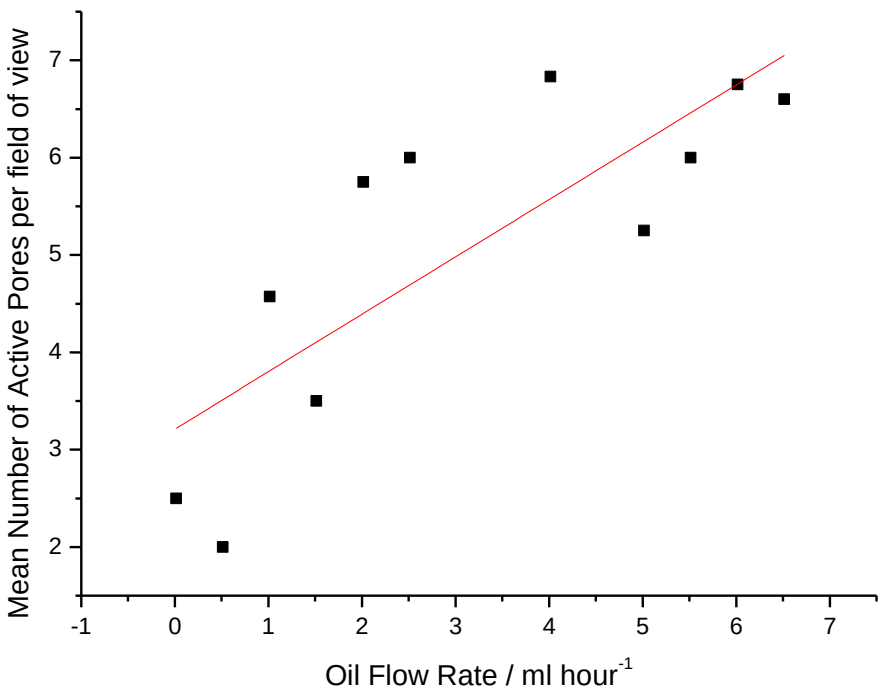

Figure 8: Effect of transmembrane pressure (shown as oil flow rate) on number of active pores.

Although the data is very scattered (with a slope of 0.59 and associated standard error of 0.14) it is clear from Figure 8 that the number of active pores increases with increasing transmembrane pressure (shown as oil flow rate).

The size of droplets produced from a single pore appeared to be constant for a given set of operating conditions (cross flow velocity and oil flow rate), but the size of droplets produced at different pores under the same operating conditions showed a large variation, suggesting that the membrane pores were not all the same size. Table 3 gives examples of droplet sizes and formation rates from adjacent pores. It can be assumed that adjacent pores experience the same cross flow rate.

Table 3: Details of droplet formation at adjacent pores, for different oil flow rates. Data from adjacent pores is outlined with a bold border. Data is presented only for the oil flow rates for which it was possible to compare adjacent pores.

Oil Flow Rate / ml hour^{-1}	Droplet diameter / µm	Droplet formation rate / s^{-1}
0.015	7	0.179
	19	0.458
1.015	8	0.746
	11	1.075
	10	1.052
1.515	26	0.295
	16	0.310
2.515	14	0.752
	8	0.652
4.015	9	0.657
	8	1.116
5.015	5	0.925
	6	0.757
5.515	12	1.115
	7	1.061
5.515	13	0.403
	16	0.401

The experiments ended at 6.5145 ml hour^{-1} because, even in the region of highest cross flow, the droplet diameters were between 10 and 20 μm, and adjacent droplets were pushing each other off the membrane. The optimum oil flow rate was found to be between 4.0145 and 5.0145 ml hour^{-1}. These values are a compromise between achieving the right droplet size and a useful droplet formation time, i.e. number of droplets produced in a period of time. The emulsions produced throughout the range of oil flow rates studied appeared to be very polydisperse, although it was not possible to quantify the droplet size distribution within the scope of this experiment.

3.8.2 Effect of Cross Flow Velocity

Having chosen an optimum oil flow rate of 4.015 – 5.015 ml hour^{-1}, the next stage of experiments was to find an optimum cross flow rate to give droplets of the desired size and polydispersity. Since the cross flow rate of 27.5 mil min^{-1} gave larger droplets than desired (most being in the region of 10 μm or larger), the cross flow rate was increased to its maximum value of 39.5 mil min^{-1}. Increasing the wall shear stress or cross flow velocity has the potential to reduce droplet size in all methods of membrane emulsification [1, 5-6, 18-19, 27, 33-34] although beyond a certain value the wall shear stress has little or no influence on the droplet size for a given transmembrane pressure [18, 27, 33, 37]. However Abrahamse *et al.* [7] found that for cross flow velocities ranging between 0.011 and 0.039 m s^{-1} the rate did not significantly affect droplet size. The optimum flow rate in this project was 3×10^{-5} m s^{-1}.

It is clear from the data presented in Table 4 that the cross flow rate had no noticeable effect on the droplet diameter, for regions of high and low cross flow velocity. These results are similar to those obtained by Abrahamse *et al.* [7]. I propose that a much higher cross flow rate would be required to have a significant effect on droplet size. Droplet formation rate seemed to increase with an increase in cross flow rate, but a much wider range of values would be needed to make a good assessment of the influence of cross flow rate on droplet formation time. Even under the highest cross flow rate of 39.5 ml min^{-1}, droplets outside the fastest region of flow were subject to a push-off force from adjacent droplets, and some very large droplets were produced (between 15 and 20 μm).

Table 4: Effect of cross flow rate on droplet diameter and droplet formation rate for regions of high and low cross flow velocity. Greyed cells indicate the absence of data for those particular conditions. Oil flow rate = 5.015 ml hour^{-1}.

Cross flow rate / ml min^{-1}		Mean Droplet diameter / µm	Mean Droplet formation rate / s^{-1}
27.5	High	9	0.97
	Low		
30.0	High	12	1.08
	Low	11.5	0.66
35.0	High	7.75	1.73
	Low	16	0.87
39.5	High		
	Low	18	0.69

3.9 Discussion and Conclusions

3.9.1 Droplet Formation and Detachment

A droplet forming at a pore seems to reach a critical size before it is detached from the membrane, either by the cross flow or by interfacial tension forces. This critical size varies between pores. Peng and Williams [1] present a theoretical approach to droplet formation and detachment in which droplet growth and droplet detachment are considered as two separate stages. Using the force balance model, Peng and Williams suggest that the droplet growth period ends when the forces at the contact edge between the droplet and the pore are balanced. The two main forces acting on the droplet are the interfacial tension force and the force exerted by the cross flow. The force exerted on the droplet by the cross flow increases with increasing droplet radius and increasing cross flow velocity [1]. The interfacial tension force is a function of interfacial tension and pore radius, and so does not change as the droplet grows. The droplet reaches a critical diameter, at which it is detached from the membrane. The force exerted on the droplet by the cross flow is given by:

$$F = 3\pi f k_x \rho V_w^{\,2} R_d^{\,2} \tag{3.8}$$

where f is the friction factor calculated above (Equation (3.6)), k_x is a wall correction factor quoted in [1] as 1.7, V_w is the cross flow velocity (0.019 m s^{-1}), and R_d is the droplet radius. The interfacial tension force can be calculated by:

$$F = 2\pi\gamma R_p \tag{3.9}$$

where γ is the interfacial tension and R_p is the pore radius. The droplet begins to detach from the membrane when the component of the interfacial tension force parallel to the membrane is balanced by the force exerted on the droplet by the cross flow. Thus increasing interfacial tension should increase the droplet size, since the force exerted on the droplet will only be large enough to detach it when the droplet has reached a larger diameter. In addition, increasing the pore size also increases the droplet size, as reported in many examples in the literature. Increasing the velocity of the cross flow should reduce the droplet size. This was not observed in the current experiments, perhaps because the wall shear stress was so low. It is also possible that the cross flow velocity did not influence droplet diameter because droplet detachment was driven by interfacial tension.

Peng and Williams [1] note that the droplet continues to grow after the growth stage, before it is fully detached from the membrane. The final droplet size is dependent on both the growth size and the oil flow rate through the membrane, so increasing transmembrane pressure increases the final droplet size. I observed that the droplet size increased with increasing transmembrane pressure, but only for those areas that were not affected by droplet-droplet interactions.

Applying the force balance approach to droplet formation and detachment explains the increase in droplet formation rate (equivalent to a decrease in droplet formation time) with increasing cross flow velocity. The force exerted on the droplet by the cross flow increases with velocity, which by Equations (3.8) and (3.9) reduces the droplet radius at detachment. A smaller droplet takes less time to inflate, so more droplets will be produced in a given time.

In the force balance model, the effect of lowering interfacial tension would be to encourage droplet detachment from the pore. Interfacial tension acts as a retaining force, keeping the droplet attached to the edge of the pore. If the oil-water interfacial tension is lowered enough with suitable surfactants, this retaining force will be weakened. The energy difference between the droplet being attached and detached will be reduced, and the droplets will be detached sooner from the pore, leading to smaller droplets. The work of Lepercq-Bost *et al.* [6] has confirmed this. The same authors reported an increase in droplet size with increasing transmembrane pressure. As the disperse phase flux increases, the droplet grows faster at the pore, and the surfactant has less time to adsorb to the interface to lower the interfacial tension. The droplet therefore has more time to grow before the interfacial tension is lowered enough for the droplet to detach [6]. Van der Graaf *et al.* [17] have shown that using a high concentration of surfactant reduces droplet size, and that a lower concentration leads to larger droplets. They also report that droplet formation time decreases at high disperse phase pressure, while droplet diameter increases, as was observed in this experiment.

Given that there was little influence on the droplet size and droplet size distribution in the range of cross flow rates studied, it is possible that a spontaneous transformation based (STB) mechanism of droplet detachment was in place. The work of Kobayashi [14] indicated that droplet size and size distribution for droplets formed at a non-circular pore were not affected by the cross flow in the range measured. However, the polydisperse nature of the emulsions produced in this experiment, and the observation that droplets inflated to a large size in the absence of shear flow, suggests that the STB mechanism was not in place. The droplets appeared to be spherical during formation, with deformation from the ideal shape only occurring just before droplet detachment. It is unlikely, therefore, that droplet formation and detachment was entirely interfacial tension driven.

3.9.2 Activation of Pores

The minimum transmembrane pressure required to push oil through the membrane can be found as follows:

$$P_C = \frac{4\gamma \cos\theta}{d_P} \tag{3.10}$$

where P_C is the critical pressure (minimum pressure required to make the oil permeate the membrane), γ is the interfacial tension between the oil and continuous phase, θ is the contact angle between the oil and the wall of the pore, and d_P is the pore diameter. The critical pressure therefore decreases with increasing pore size, indicating that the oil will flow more readily through larger pores for a given transmembrane pressure. I observed that increasing the oil flow rate from 0.0145 to 4.015 ml hour^{-1} increased the number of small droplets being produced. There are other examples of similar results [27, 37]. At a transmembrane pressure close to the critical pressure, only the largest pores will be active. As the transmembrane pressure is increased, smaller pores become active, and more small droplets are produced. Beyond a certain pressure, the droplets produced at all pores will become larger, and the average size will then increase with increasing transmembrane pressure.

Several authors have reported that the higher the transmembrane pressure, the higher the influence of wall shear stress on droplet diameter [27, 37]. The reason for this could be that different droplet formation mechanisms are in action at different transmembrane pressures, as suggested by Yasuno *et al.* [8] and Lepercq-Bost *et al.* [6]. The membrane emulsifier in this project was operated at low oil flow rates, which equates to low transmembrane pressure. This could account for the negligible effect of wall shear stress on droplet diameter.

3.9.3 Droplet Size

The droplets produced in this experiment were larger than expected, the ratio of droplet to pore size being between 6 and 25. It is possible that the relatively low interfacial tension of the chemical system at the ambient temperature (approximately 5 x 10^{-4} mM m^{-1} at 25 ºC) was the cause of the large droplets. As mentioned at the beginning of this chapter, the spontaneous transformation based model predicts that larger droplets will be formed at lower interfacial tension, since interfacial tension is a detaching rather than a retaining

force. The force balance model predicts that smaller droplets will be formed at lower interfacial tension. Abrahamse *et al.* also found that droplet to pore size ratios were higher than expected under the operating conditions studied in their experiments [7]. They do not quote the interfacial tension in their work, but attribute the droplet sizes to low shear stress. It is not possible without further study to say whether the large droplet sizes were caused by low interfacial tension or low wall shear stress. It would be worthwhile investigating this question in future work.

3.9.4 Droplet Size Distribution

It is possible that not being able to clean the membrane properly before use was responsible for the polydispersity of the emulsions produced. Both wetting of the membrane by the oil, and adsorption of surfactant molecules onto the membrane surface, increase the wettability of the membrane by the oil phase, and can potentially increase droplet size and size distribution [37]. Lepercq-Bost *et al.* suggest that the increased polydispersity with increased transmembrane pressure could be the result of increased steric hindrance, or increased wetting of the membrane by the disperse phase [6].

Abrahamse *et al.* produced a polydisperse emulsion with very low wall shear stress, but attributed the polydispersity to droplet-droplet interactions [7]. These interactions account for the polydispersity of droplets produced in the region of low cross flow velocity, but not for droplets produced in high cross flow velocity, which were not subject to the push-off force. The authors also note that the number of active pores increased with increasing transmembrane pressure, as was observed in this project. Lepercq-Bost *et al.* reported that the lower the interfacial tension, the less influence the wall shear stress has on the droplet diameter [6]. They also report that the higher the wall shear stress, the narrower the droplet size distribution. Vladisavljevic and Schubert reported that more uniform droplets are formed at higher shear stresses, due to the reduced likelihood of droplet-droplet interactions [37]. The very low wall shear stresses used in this experiment could account for the high polydispersity of the emulsions produced.

Abrahamse *et al.* [7] have reported that a uniform membrane only produces a monodisperse emulsion under the right conditions. Using a microengineered membrane

with uniform pore sizes, they showed that a single pore may produce droplets of a uniform size, but the average droplet diameter may vary between pores. Based on these results, it is reasonable to assume that the pores in the ceramic membranes used in this project were of a uniform size, and that the wide range of droplet sizes was a result of the operating parameters.

3.10 Improvements to Design and Future Work

It would be interesting to investigate higher cross flow velocities. I propose that higher velocities than those achievable given the maximum flow rate of the syringe pump and the dimensions of the cross flow channel are required to have a significant effect on droplet diameter. To this end, reservoirs of oil and continuous phase should be pressurized and controlled with gas in order that the transmembrane pressure can be measured and varied, and that a higher wall shear stress can be achieved at the membrane.
Using glue to hold the membrane in place in the channel means that the membrane cannot be thoroughly cleaned, potentially increasing the polydispersity of the emulsions produced. Future designs should ensure that the emulsifying unit can be cleaned as a whole unit either by sonicating in Deconex solution or by cleaning as suggested by Sterlitech.

Given that the push-off force was observed throughout the range of conditions studied, and that it has been reported to increase the polydispersity of the emulsion produced [7], it would be wise to manufacture a membrane with widely spaced pores, so that droplet-droplet interactions would not influence droplet size and detachment.

To investigate whether the spontaneous transformation based model or force balance model is most applicable to membrane emulsification with a microporous ceramic membrane, it would be useful to observe whether droplet detachment occurs without a cross flow, and whether the resulting emulsion is any more monodisperse than those produced in this experiment. Investigating a wide range of operating conditions (oil flow rate and cross flow rate) would also provide some insight into whether the droplet formation and detachment mechanism changed at a critical transmembrane pressure or wall shear stress.

3.11 Premix Membrane Emulsification

Since I was not able to produce a monodisperse emulsion with the ceramic membrane, I have investigated premix membrane emulsification using an Avanti Mini-Extruder. Designed for the preparation of lipid vesicles, the extruder supports a polycarbonate track-etch membrane.

The Mini-Extruder consists of a stainless steel outer casing in two parts, which are screwed together once the extruder is assembled. The membrane is supported by two Teflon 'internal membrane supports'. The supports are bored to allow the flow of fluid to the membrane, and threaded to facilitate connection to the syringes. The extruder is designed to be used with Hamilton Gastight syringes. To minimize both the time it took to produce an emulsion, and the volume of surfactant and oil used to test the extruder, two 500 μL syringes were used in this experiment.

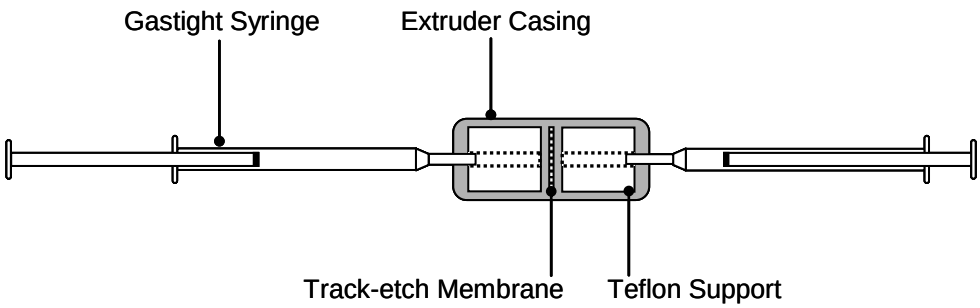

Figure 9: Schematic of Mini-Extruder. Syringes are operated using syringe pumps.

Track-etch membranes are produced by the irradiation of a thin film with either fragments from the fission of heavy nuclei, or with ion beams from accelerators. The 'track' left by the particle is etched using chemicals to produce a well-defined pore, the size and shape of which can be precisely controlled by the chemical system and operating conditions [38]. Track-etch membranes are characterized by having a very narrow pore size distribution. This is important in emulsification because the size of emulsion droplets produced is a function of the shape and size of the membrane pores. Whatman polycarbonate Nuclepore membranes were used in this project.

An AOT/ NaCl solution was chosen, along with heptane, for the preparation of emulsions using the extruder. All initial work in this project has been undertaken using this system because it is well characterized [39], and has been shown previously to be suitable for optical trapping and deformation [40].

3.12 Droplet Formation and Break-up

In premix membrane emulsification, a crude emulsion is passed through a microporous membrane so that large drops are broken into smaller drops (see Figure 10). This is precisely the process that was used in this project to form emulsions using the Avanti Mini-Extruder. It is reasonable to approach the problem of droplet formation from the point of view of premix membrane emulsification.

When a droplet experiences a shear stress the shape it adopts is a result of the balance between viscous forces and interfacial forces. Viscous forces tend to deform and break the droplet, interfacial forces tend to retain or recover the spherical shape [41]. The relationship between viscous and interfacial forces is expressed by the capillary number, Ca, which can be given by

$$Ca = \tau_m R / \sigma \tag{3.11}$$

where τ_m is the shear stress in the continuous phase, R is the droplet radius in the absence of shear, and σ is the interfacial tension between the droplet and the continuous phase. A large capillary number indicates the dominance of interfacial tension, and suggests that the droplet remains spherical under shear stress, and does not break up. A small capillary number indicates that shear stresses dominate, and that the droplet will deform and break up. Droplet break-up occurs if Ca exceeds a critical number Ca_{crit}. Under these conditions the droplet does not reach a steady state, but continues to deform and eventually breaks up into smaller droplets [41]. Since the interfacial tension in the current chemical system remains constant for a given temperature, the properties governing droplet break-up in the extruder are the shear stress and droplet radius.

At transmembrane pressures (flow rates across the membrane) lower than a critical value, droplets larger than the pore size are unable to pass through the membrane, and no droplet break-up occurs. At transmembrane pressures above the critical value, all droplets, irrespective of their size, pass through the membrane.

As previously mentioned, droplet break up occurs when applied shear stress overcomes the tendency of interfacial tension to retain the droplet's spherical shape. The droplet deforms into an elongated sphere or distorted cylinder, the surface area-to-volume ratio of which is greater than that of a sphere. It is therefore more energetically favourable for the deformed droplet to break into two or more smaller droplets, which will recover their spherical shape in the absence of shear.

Droplet break-up in premix emulsification occurs inside the membrane pores. At small shear stresses inside the pores, the final droplet size will be larger than the pore size [42]. Large droplets are deformed as they enter the pores, and are further deformed due to friction between the droplet and the pore walls (see Figure 10) [42]. The large droplets break up, and the resulting droplets leave the pores, where they regain their spherical shape. At higher shear stresses, the droplets are more disrupted inside the pores, leading to smaller final droplets. A higher transmembrane pressure leads to greater flux through the membrane, which in turn leads to higher shear stresses in the pores. A higher transmembrane pressure (or in the case of the extruder a faster flow rate) therefore leads to smaller droplets. This is in contrast to normal membrane emulsification, in which higher transmembrane pressures lead to larger droplets [18, 33].

The mechanism of droplet break-up in the pores suggests that the polydispersity of the emulsion should decrease with an increasing number of passes through the membrane. This was found to be the case, with the biggest change in droplet size distribution occurring between one and ten passes through the membrane. Since the droplet break-up mechanism is determined by the transmembrane pressure, the optimum number of passes through the membrane will be different at different pressures [42]. Droplets which are smaller than the pores will pass through without being broken up, so there will be a minimum size that can be reached for a given pore size. At this size, the emulsion should be nearly monodisperse.

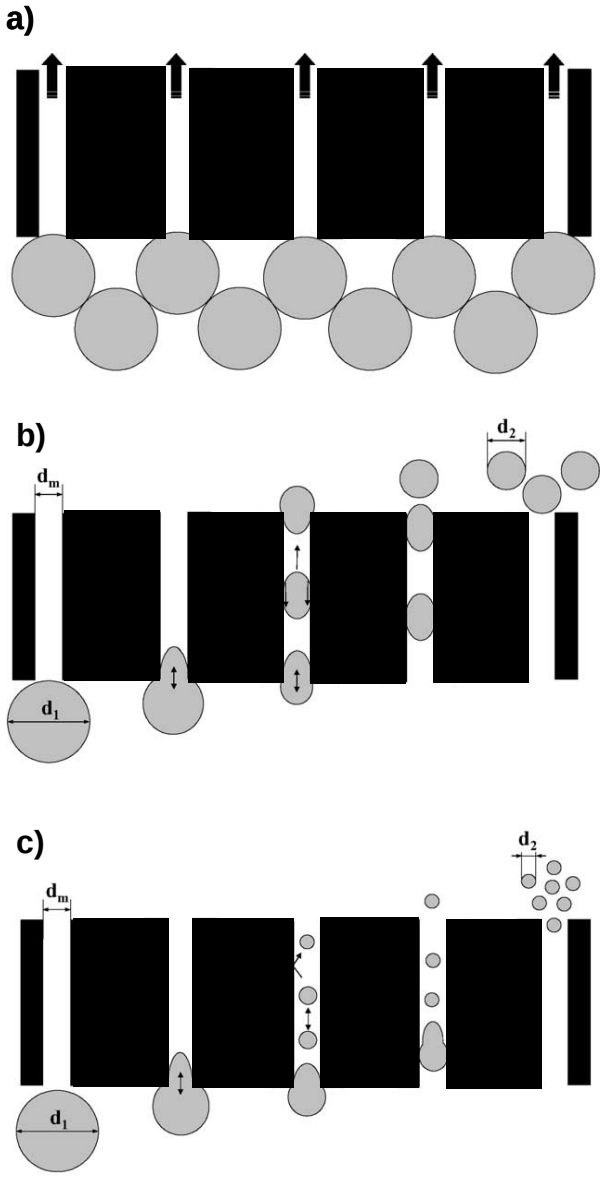

Figure 10: Droplet break-up in premix membrane emulsification: a) Retention of large droplets by membrane below a critical transmembrane pressure; b) Break-up at low shear stresses ($d_m < d_2 < d_1$); c) Intensive break-up at high shear stresses ($d_2 < d_m < d_1$). Image from [42].

At lower pressures, where the droplets being produced are bigger than the pores, it seems likely that more passes will be required to break the droplets into smaller droplets. At high transmembrane pressures, the diameter of the droplets produced is smaller than that of the

pore, so fewer passes through the membrane will be needed to achieve the minimum droplet size.

Vladisavljevic *et al.* have shown that increasing the number of passes at high pressure increases the span of droplet size distribution, and also that the lowest span is achieved for lower transmembrane pressures [42]. Their results also confirm that smaller droplets are produced at high transmembrane pressures. Since the largest pore size available in this experiment was 2 μm, the best results should have been achieved at lower transmembrane pressures. The membrane used by Vladisavljevic *et al.* was a Shirasou Porous Glass membrane, with an average pore size of 10.7 μm. The most monodisperse emulsion they produced was with their lowest transmembrane pressure (100 kPa), after 3 passes through the membrane. The droplets produced under these conditions had an average diameter of approximately 9 μm, which is just smaller than the membrane pore size. It is reasonable to assume that a monodisperse emulsion produced with the 2 μm track-etch membrane in the extruder would have had a maximum droplet size of between 1 and 2 μm, which is much too small for trapping and deformation. A 5 μm membrane would be more promising, and would be worth investigating in any future work.

3.13 Method

3.13.1 Cleaning and Assembly

A 1mM AOT/ 0.05mM NaCl solution was prepared as described in ‘Microfluidics’. All the extruder parts and the gastight syringes were cleaned by sonicating in a 1% Deconex solution for 15 minutes. The parts were rinsed ten times in MilliQ water to remove any trace of surfactant molecules. There was no need to dry the parts. They were stored in a clean beaker until the extruder was assembled. The extruder was assembled according to the manufacturer’s instructions [43], and tested for leaks with MilliQ water.

3.13.2 Extrusion

Prior to initial use, the extruder was checked for leaks by rinsing through with MilliQ water, and then cleaned by rinsing with the AOT/NaCl solution. One syringe was filled with the surfactant solution, and the plunger was pressed to force the solution through the

extruder into the other syringe. The solution was discarded, and repeated. This process had the dual purpose of cleaning the extruder, and reducing the 'dead volume' (empty space) in the extruder and connections. The extruder had a tendency to leak fluid from the stainless steel joint unless it was very tightly connected, and from the syringe connectors. It was necessary to tighten each of these connectors until the extruder stopped leaking.

Any droplets of heptane remaining in the extruder between experiments could potentially be incorporated into the next emulsion produced, which would affect the results of each experiment. Between uses, therefore, the extruder was cleaned of heptane by rinsing with surfactant solution as described above. This was repeated until the waste solution appeared clear, indicating that most of the heptane had been removed from the membrane and extruder parts.

The emulsions were prepared in a similar way to that suggested by the manufacturer for the preparation of lipid vesicles [43]. Instead of pushing the syringe plungers by hand, a Harvard Apparatus syringe pump was used. This enabled investigation into the effect of flow rate on the droplet size and size distribution of the emulsion produced. The diameter of the syringe was entered into the pump in order that the flow rate could also be entered. 450 µl of surfactant solution was drawn into a syringe, followed by 50 µl of heptane into the same syringe. The extruder was assembled with the plunger of the empty syringe fully depressed. The full syringe was placed in the syringe pump, and the pump was set to run. Once one syringe had been emptied into the extruder, and had filled the other syringe, the process was repeated again by turning the extruder around and fixing the now full syringe into the syringe pump.

3.14 Examination of Emulsions

Once the emulsion had been prepared, it was examined under a microscope using a 100x oil immersion objective and a haemocytometer cell which prevented the sample from drying out due to the heat from the microscope lamp. Three drops of the emulsion were placed on the haemocytometer from the syringe, and the sample was covered with a clean cover glass. A 100 µm graticule was used to assess the size of emulsion droplets produced.

According to information provided by the manufacturer, the size distribution or polydispersity of the vesicles produced with the extruder is a function of the number of passes through the membrane. The manufacturers recommend that the solution is passed through the extruder a minimum of eleven times [43]. In order to verify this, the solution was examined at different stages in the extrusion process.

3.15 Results

In agreement with the findings of Vladisljevic *et al.* [42], there was a critical flow rate at which droplets of heptane were pushed through the membrane and broken up. By increasing the flow rate from 10 ml per hour up to the maximum flow rate of 23.7 ml per hour, it was possible to identify a region in which emulsification occurred. 10 ml per hour was too slow to push the heptane through the membrane without waiting for a build-up of pressure. 20 ml per hour was chosen as a suitable flow rate at which to conduct the initial experiments as it was sufficient to cause droplet formation and break up.

3.15.1 100 nm Membrane

After one pass through the membrane very little of the heptane had been emulsified and the few droplets that were seen in the sample were very large (between 5 and 15 μm in diameter). After ten passes through the membrane, there were many more emulsion droplets in the sample. Many of the droplets were 2 μm or less in diameter, but there were several larger droplets seen (see Figure 11a). After 20 passes through the membrane, the average size of emulsion droplets appeared to be larger. There were more droplets larger than 2 μm in diameter. Several droplets were approximately 4 μm in diameter, but there were too few to be of use in the trapping experiments (see Figure 11b). It appeared that the polydispersity of the emulsion certainly decreased after ten passes through the membrane, but the emulsion was still quite polydisperse.

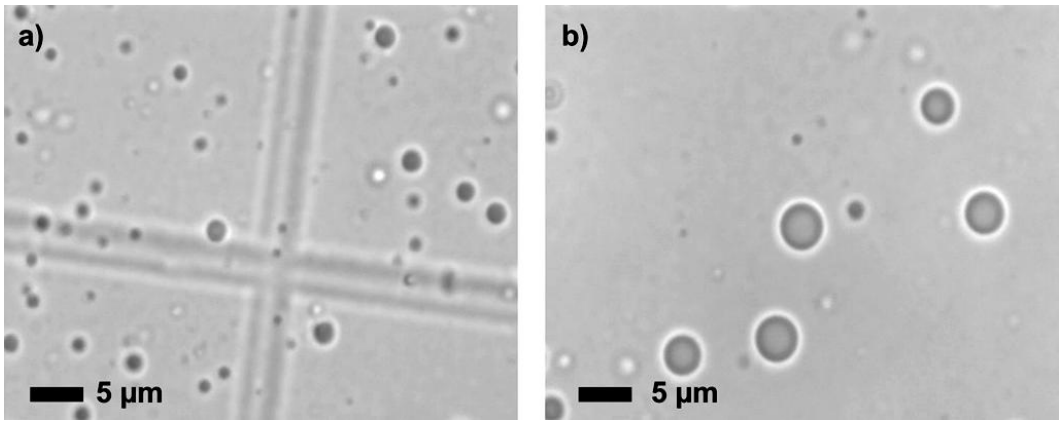

Figure 11: a) Emulsion produced after twenty passes through the 100 nm membrane at 20 ml per hour. The grid pattern in the image is part of the counting chamber in the glass slide; b) Emulsion droplets after twenty passes through the membrane. These droplets were larger than average.

It was expected that the average size of the emulsion droplets produced would be in the order of the membrane pore size, i.e. 100 nm. However, the resolution of the 100x objective, with a numerical aperture of 1.25, is in the region of 200 nm, so any 100 nm droplets would not be seen in the sample. It is possible that 100 nm droplets were present in the sample, but the fact that there were many emulsion droplets much larger than 100 nm in the sample suggests that the average size of the emulsion droplets exceeded 100 nm, and that the droplet break-up mechanism was different to that described above. Possible reasons for this will be discussed later.

3.15.2 2 µm Membrane

The temperature in the laboratory was between 23 and 25 ºC during the time of the experiments with the 2 µm membrane. The AOT/NaCl system in use has well-documented temperature sensitive phase behaviour. It is known that a region of ultra-low interfacial tension exists for this system at around 26 ºC [39]. The temperature in the laboratory caused problems with the formation of droplets, since the size of the emulsion droplets produced was apparently being determined by the interfacial tension between the heptane and the water, rather than the mechanical action of the extruder.

As with the 100 nm membrane, one pass through the extruder produced very few droplets, these being between 5 and 10 μm in diameter (see Figure 12a). As well as these large droplets, some other structures were seen in the sample (Figure 12b) that were believed to be a result of the ultra-low interfacial tension region the system had reached at the ambient temperature. Normal emulsion droplets are spherical in shape as a result of the interfacial tension between the disperse and continuous phases. Several emulsion droplets appeared to have very low interfacial tension (Figure 12c), and did not consist simply of a droplet of heptane in the surfactant solution. The shape of these droplets fluctuated continuously during the time the sample was examined. The interface between the droplet and the surfactant solution was not smooth, and the interior of the droplet appeared to consist of a bicontinuous phase, characteristic of the microemulsion regime. In addition to these low interfacial tension droplets, larger areas of what appeared to be bicontinuous microemulsion were also seen (Figure 12b). It was difficult to bring these areas into focus because of the nature of the boundary between the microemulsion and the surrounding surfactant solution. It should be noted that microemulsions are normally formed at a water-to-oil ratio of 1:1, and that such systems exhibit large bicontinuous regions. In this system, a small droplet of oil was used in approximately 5 mL of surfactant solution, so large areas of bicontinuous microemulsion would not be expected. These unusual structures were seen after one, five and twenty passes through the membrane, and after thorough cleaning of the equipment and preparation of a new surfactant solution. They were clearly a result of the chemical system and ambient temperature rather than the number of passes through the membrane or any contamination of the sample. The emulsion produced after twenty passes through the membrane contained many droplets around 2 to 3 μm in diameter. Some droplets were closer to 5 μm in diameter, but there were not enough of these for the emulsion to be useful in the trapping experiments. As with the 100 nm membrane, the emulsion was quite polydisperse (see Figure 12d).

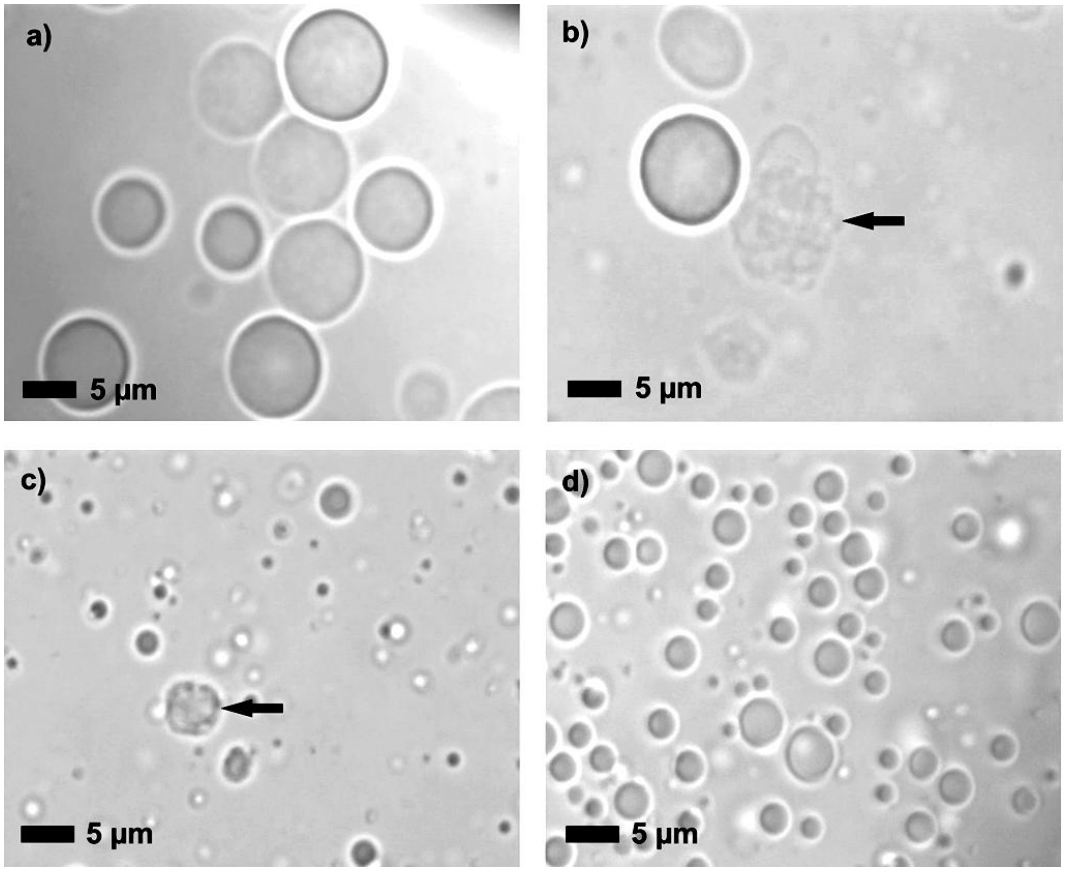

Figure 12: a) Large droplets produced after one pass through 2 µm membrane; b) Example of structures seen in the sample after one pass through 2 µm membrane. Arrow indicates possible bicontinuous domain, next to a 'normal' emulsion droplet; c) Arrow indicates an emulsion droplet with very low interfacial tension. The surface of the droplet is not smooth and the droplet did not maintain a spherical shape. The interior of the droplet was not a continuous density; d) Example of emulsion produced after twenty passes through the 2 µm membrane.

3.15.3 5 µm Membrane

Due to time constraints, it was not possible to acquire a 5 µm Track-Etch membrane with the correct diameter to fit into the extruder. In order to test the viability of producing 5 µm droplets with a 5 µm membrane, small disks were cut out of a larger membrane which was available in the laboratory. The membrane was an acrylic copolymer membrane on a nylon support, and would not offer the same accuracy of pore size and shape as the Track-Etch membranes, would give a good idea of the success of a 5 µm membrane.

Despite considerable effort to prevent the extruder from leaking, any pressure applied to the syringe resulted in the solution leaking out of the stainless steel casing rather than being pushed through the membrane. A possible explanation of this is that the membrane did not make a good seal with the Teflon supports, due to its rough surface.

3.16 0.03M NaCl/1mM AOT Solution

According to Aveyard *et al.* [39] reducing the NaCl concentration from 0.05M to 0.03M changes the temperature at which the interfacial minimum occurs from approximately 25 ºC to less than 20 ºC. By avoiding this region of ultra-low interfacial tension, it was hoped that the formation of droplets with the extruder would be more consistent and that the structures seen in Figure 12b and Figure 12c would be absent. As well as testing the effect of lower salt concentration, the effect of speed on the resulting emulsion was also investigated. If the droplet break-up mechanism was the same as that described by Vladisljevic [42] a higher flow rate would produce smaller droplets.

The 0.03M NaCl/1mM AOT solution was prepared as described in Microfluidics. The extruder was rinsed through twice with the surfactant solution, as described above. The initial experiments with the extruder had confirmed that increasing the number of passes through the membrane decreased the polydispersity of the emulsion, so the emulsions prepared with the 0.03M NaCl solution were passed twenty times through the membrane.

Figure 13 shows the results of the first experiment. The emulsion was passed through the membrane using a syringe pump, at a flow rate of 20 ml per hour. It is evident that a very polydisperse emulsion was produced, with droplet diameters ranging from less than 1 μm to more than 20 μm. No areas of very low interfacial tension were seen in the emulsion produced with the 0.03M NaCl/1mM AOT solution. This confirms that the reduction in salt concentration shifted the region of ultra-low interfacial tension to a lower temperature, i.e. below room temperature.

The images in Figure 13 are all taken from the same sample. The distribution of droplet sizes throughout the sample is due to the geometry of the haemocytometer used to view the

sample. The haemocytometer consists of a glass slide, at the centre of which is a ring-shaped well approximately 10mm in diameter. The purpose of using such a slide in these experiments is to prevent the sample drying out under the heat from the microscope lamp. The centre of the ring is raised, so that when a cover slip is applied to the slide, the centre of the ring is the shallowest part of the cell. Around the outside of the ring, there is slightly more room between the cover slip and the glass slide. The ring itself is the deepest part of the haemocytometer.

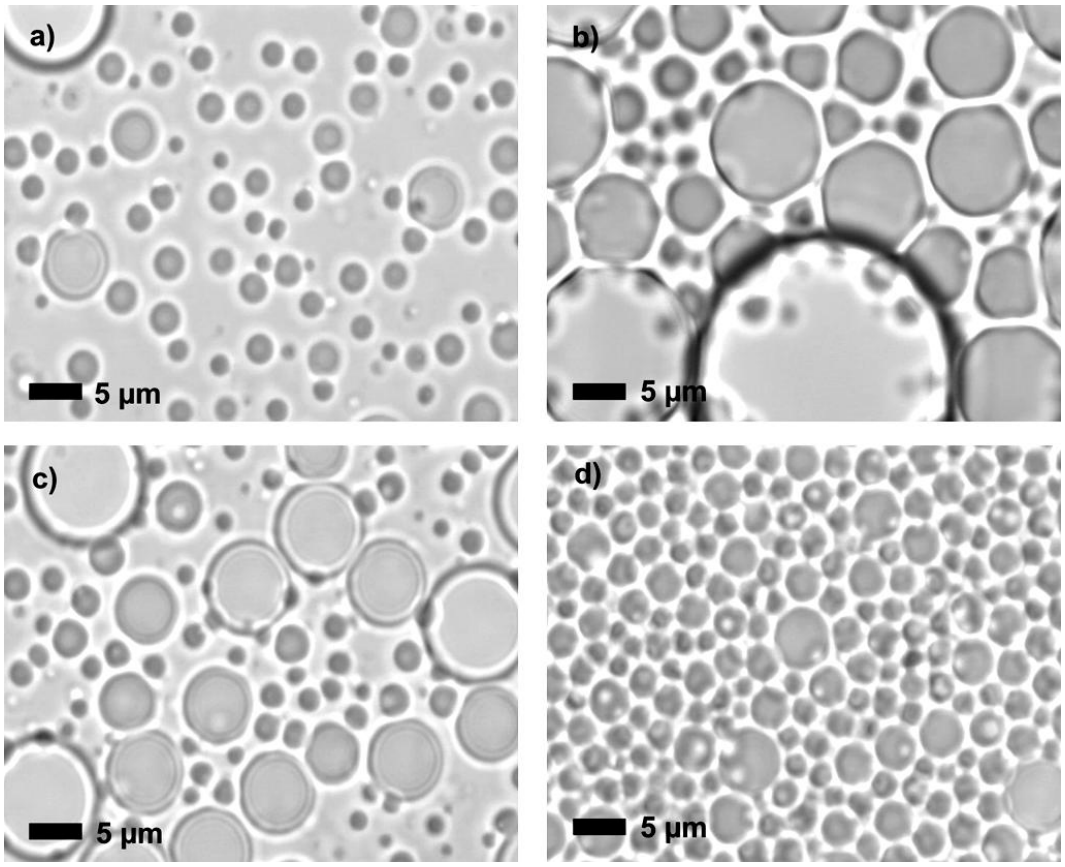

Figure 13: Samples of emulsion produced with 2 µm membrane at 20 ml per hour, using 0.03M NaCl/1mM AOT solution; a) Many 2-3 µm emulsion droplets were seen in the sample; b) very large droplets were seen around the edges of the sample; c) A small number of droplets in the 5 µm range were seen, mixed with much smaller droplets; d) Very concentrated areas of small emulsion droplets were seen around the edge of the sample.

Droplets of different sizes have a tendency to collect at different parts of the slide according to the space between the slide and the cover slip. Accordingly, the larger

droplets are found around the outside of the ring and inside the well, and many of the small droplets are found in the centre of the ring. The very concentrated regions are found outside the ring, towards the edge of the cover slip. These regions are a result of the flow of the emulsion between the cover slip and the glass slide, which tends to be in one direction across the slide. Each of these regions of the sample must be accounted for when assessing the polydispersity of the sample. system.

Overall the emulsions prepared with the 0.03M NaCl solution appear more concentrated than those prepared with the 0.05M NaCl solution. A possible explanation for this is that there were regions of ultra-low interfacial tension in the 0.05M NaCl samples, which were indistinguishable from the continuous phase. As previously mentioned, it is likely that the droplet break-up mechanism described by Vladisljevic was not active in the 0.05 M NaCl samples.

Figure 14 shows the results of the second experiment. The maximum flow rate achievable with the syringe pump was 23.7 ml per hour. This flow rate was not significantly faster than the 20 ml per hour used in the first experiment, so it was necessary to operate the syringes by hand to achieve a fast flow rate. It was estimated that the flow rate used was approximately 80 ml per hour. No large droplets were seen in the sample, which was contrary to the expected result that a faster flow rate would produce larger droplets. The emulsion appeared to be less polydisperse than for the slower flow rate, and there was certainly a smaller droplet size range. Very concentrated regions of small droplets were seen in the sample, and there were no regions of ultra-low interfacial tension. Although the average droplet size was smaller at the higher flow rate than at 20 ml per hour, there were still many droplets that were larger than the pore size of 2 μm.

Unfortunately, since the experiment with high flow rate failed to produce larger droplets, it was necessary to end the experiments with the extruder by concluding that 5 μm droplets could not be produced with the membranes available. It is possible that a good result could be obtained with a 5 μm Track-Etch membrane. Disadvantages of this technique include the long processing time required to produce an emulsion, and the difficulty in reproducing

the same flow rate if the syringes are operated by hand. Advantages include the small volumes of surfactant solution and oil that are required to make a great number of emulsion droplets.

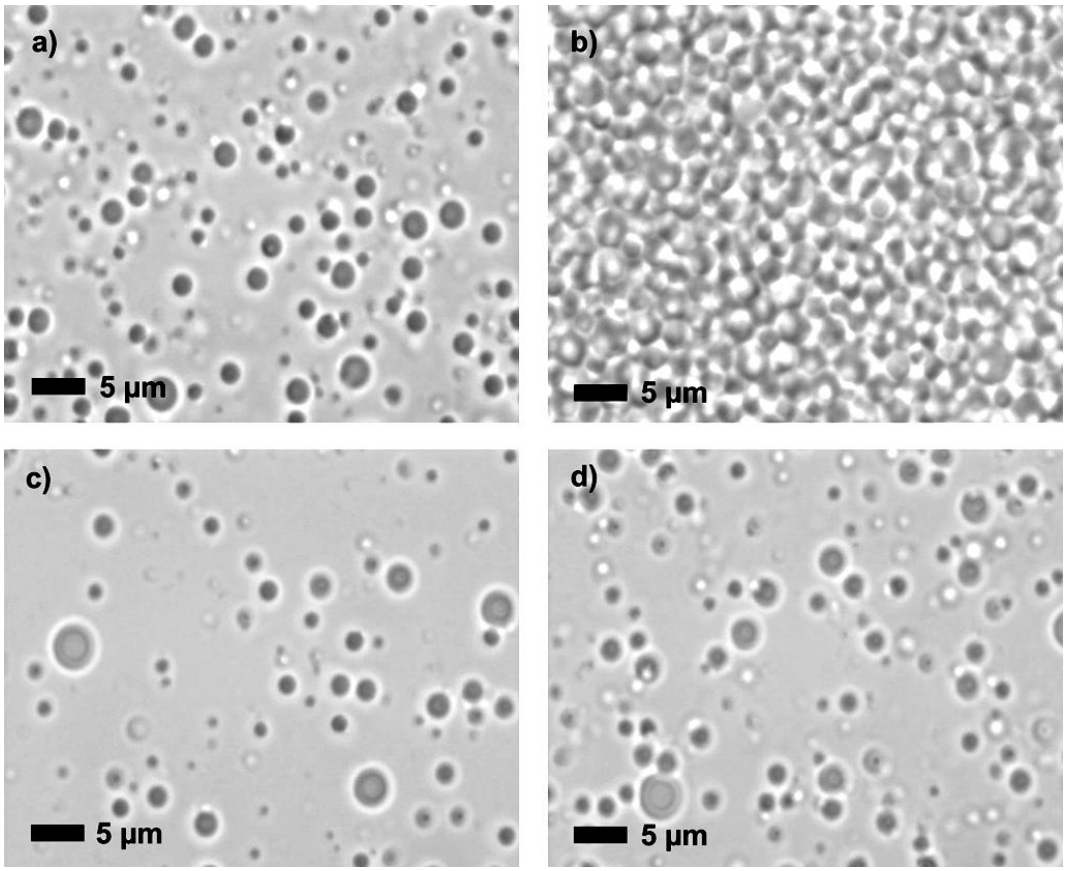

Figure 14: Samples of emulsion produced with 2 µm membrane at approximately 80 ml per hour, using 0.03M NaCl/1mM AOT solution; a) Much of the sample contained small (sub 5µm) droplets; b) Very concentrated areas of small emulsion droplets were seen around the edges of the sample; c) and d) Fewer drops per field of view were seen in the centre of the sample. Most were less than 4 µm in diameter.

3.17 Discussion

Despite the extruder having behaved as expected in terms of the dependence of droplet size on transmembrane pressure or flow rate, I was unable to produce a monodisperse emulsion using the extruder. In membrane emulsification, it has been shown that surfactant molecules adsorbed onto the surface of the membrane can lead to wetting of the membrane by the oil phase [18]. In the case of the droplet break-up mechanism described above, wetting of the membrane by the oil phase would lead to reduced friction between the pore

wall and the droplet, and therefore reduced shear stress. This would lead to the production of larger droplets. It is possible that a different droplet break-up mechanism would come into play under these conditions. In cross-channel membrane emulsification, droplet break-off occurs at the pore exit. If the oil phase does not wet the membrane, the contact line between the droplet and the membrane is restricted to the pore opening [18]. If the membrane is wetted by the droplet, it can spread out over the membrane beyond the pore opening, followed by detachment or droplet break-up. This mechanism would produce larger droplets than a clean break-off, and would lead to higher polydispersity. The interfacial tension between the disperse and continuous phases is often represented as a retaining force [1-4], but it could also act as a detaching force [9-10]. Sugiura *et al.* [10] presented a 'Spontaneous Transformation Based' (STB) mechanism for droplet detachment. A droplet forming at a pore is deformed by the geometry of the pore, and has a greater interfacial area than a sphere of the same volume [9]. By detaching from the pore and forming a sphere, the free energy of the droplet is reduced. If, however, the membrane is wetted by the disperse phase as a result of adsorbed surfactant molecules, the difference in free energy between an attached and detached droplet will be reduced, if not reversed. This may explain the production of larger droplets, and a more polydisperse emulsion than expected.

In assessing the success of the extruder as a means of producing emulsion droplets suitable for trapping and deforming, it is useful to compare the results with a sample of a hand shaken emulsion (see Figure 15). It is obvious from the images that the range of droplet sizes in an emulsion produced with the extruder is much smaller than the range of sizes produced by shaking the emulsion by hand. The emulsion produced with the extruder were also more concentrated, but this difference can be accounted for by the fact that slightly less heptane was used in making the hand shaken emulsion, and that due to the presence of very large droplets, the total number of droplets is expected to be fewer. In general, the droplets in the hand shaken emulsion are larger than those produced with the extruder, and there are more in the 5 μm region, which makes the emulsion more useful for the experiment.

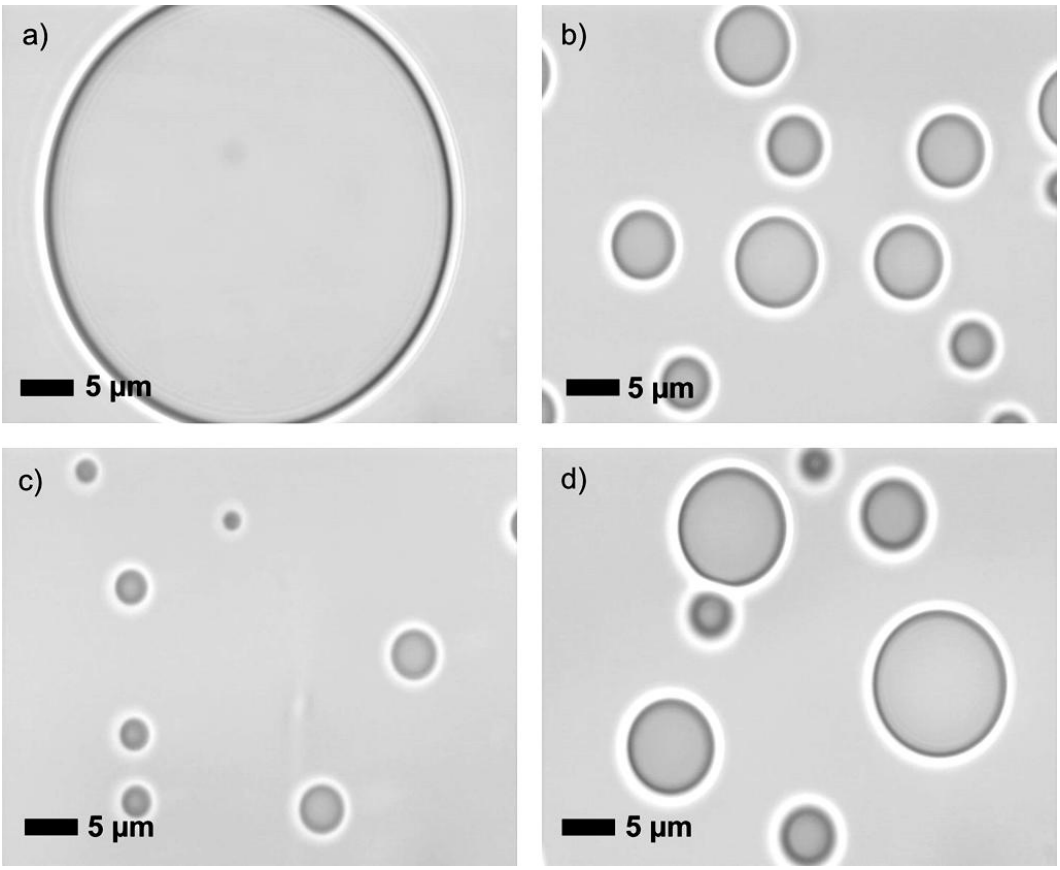

Figure 15: Samples of hand shaken emulsion made with 1 mM AOT/0.03 M NaCl solution at 23 ºC; a) Few very large droplets were present in the sample; b) Droplets of appropriate size for trapping were present; c) and d) Droplets ranging from less than 1 µm in diameter to more than 10 µm in diameter, well distributed throughout the sample.

It is possible that experiments with a 5 µm or larger membrane would yield good results.

It was expected that the emulsion produced with the 100 nm membrane would yield droplet sizes slightly smaller than 100 nm, but this was not the case. Since the same flow rate (20 ml per hour) was used for both the 100 nm and 2 µm membranes, the flow velocity through each individual pore in the 100 nm membrane would have been much higher than than through the 2 µm pores. Given that the droplets produced were larger than expected, it is reasonable to suppose that a different droplet break-up mechanism was at work. The fact that surfactant molecules adsorbed onto the surface of the membrane may have caused wetting of the membrane by the oil has already been mentioned, and this would certainly lead to larger droplets. Another possibility is that the flow of oil through the membrane

was in the jetting regime, and that the droplets that broke off from the jet were larger than the pore size.

References

1. Peng, S.J. and R.A. Williams, *Controlled Production of Emulsions using a Crossflow Membrane, Part 1: Droplet Formation from a Single Pore.* Trans IChemE, 1998. **76**(A): p. 894-901.
2. Rayner, M., et al., *Using the Surface Evolver to model droplet formation processes in membrane emulsification.* Journal of Colloid and Interface Science, 2004. **279**: p. 175-185.
3. Schroder, V., O. Behrend, and H. Schubert, *Effect of Dynamic Interfacial Tension on the Emulsification Process Using Microporous, Ceramic Membranes.* Journal of Colloid and Interface Science, 1998. **202**: p. 334-340.
4. Rayner, M. and G. Tragardh, *Membrane emulsification modelling: how can we get from characterization to design?* Desalination, 2002. **145**: p. 165-172.
5. Egidi, E., G. Gasparini, and R.G. Holdich, *Membrane emulsification using membranes of regular pore spacing: Droplet size and uniformity in the presence of surface shear.* Journal of Membrane Science, 2008. **323**: p. 414-420.
6. Lepercq-Bost, E., et al., *Use of the capillary number for the prediction of droplet size in membrane emulsification.* Journal of Membrane Science, 2008. **314**: p. 76-89.
7. Abrahamse, A.J., et al., *Analysis of droplet formation and interactions during cross-flow membrane emulsification.* Journal of Membrane Science, 2002. **204**(1-2): p. 125-137.
8. Yasuno, M., et al., *Visualization and characterization of SPG membrane emulsification.* Journal of Membrane Science, 2002. **210**: p. 29-37.
9. Rayner, M., C. Tragardh, and G. Tragardh, *The impact of mass transfer and interfacial expansion rate on droplet size in membrane emulsification processes.* Colloids and Surfaces A: Physicochemical and Engineering Aspects, 2005. **266**: p. 1-17.
10. Sugiura, S., et al., *Interfacial tension driven monodispersed droplet formation from microfabricated channel array.* Langmuir, 2001. **17**(18): p. 5562-5566.
11. Sugiura, S., et al., *Characterization of Spontaneous Transformation-Based Droplet Formation during Microchannel Emulsification.* Journal of Physical Chemistry, 2002. **106**: p. 9405-9409.
12. Kukizaki, M., *Shirasu porous glass (SPG) membrane emulsification in the absence of shear flow at the membrane surface: Influence of surfactant type and concentration, viscosities of dispersed and continuous phases, and transmembrane pressure.* Journal of Membrane Science, 2009. **327**: p. 234-243.
13. Kobayashi, I., M. Nakajima, and S. Mukataka, *Preparation characteristics of oil-in-water emulsions using differently charged surfactants in straight-through microchannel emulsification.* Colloids and Surfaces A: Physicochemical and Engineering Aspects, 2003. **229**: p. 33-41.
14. Kobayashi, I. and M. Nakajima, *Silicon Array of Elongated Through-Holes for Monodisperse Emulsion Droplets.* AIChE Journal, 2002. **48**(8): p. 1639-1644.
15. Kobayashi, I., S. Mukataka, and M. Nakajima, *Effect of slot aspect ratio on droplet formation from silicon straight-through microchannels.* Journal of Colloid and Interface Science, 2004. **279**: p. 277-280.

16. Vladisavljevic, G.T., I. Kobayashi, and M. Nakajima, *Generation of highly uniform droplets using asymmetric microchannels fabricated on a single crystal silicon plate: Effect of emulsifier and oil types.* Powder Technology, 2008. **183**: p. 37-45.
17. van der Graaf, S., et al., *Influence of dynamic interfacial tension on droplet formation during membrane emulsification.* Journal of Colloid and Interface Science, 2004. **277**: p. 456-463.
18. Dragosavac, M.M., et al., *Controlled production of oil-in-water emulsions containing unrefined pumpkin seed oil using stirred cell membrane emulsification.* Journal of Membrane Science, 2008. **322**: p. 178-188.
19. Vladisavljevic, G.T. and H. Schubert, *Influence of process parameters on droplet size distribution in SPG membrane emulsification and stability of prepared emulsion droplets.* Journal of Membrane Science, 2003. **225**: p. 15-23.
20. Zhu, J. and D. Barrow, *Analysis of droplet size during crossflow membrane emulsification using stationary and vibrating micromachined silicon nitride membranes.* Journal of Membrane Science, 2005. **261**: p. 136-144.
21. Joscelyne, S.M. and G. Tragardh, *Membrane emulsification - a literature review.* Journal of Membrane Science, 2000. **169**: p. 107-117.
22. Vladisavljevic, G.T., et al., *Shirasu Porous Glass membrane emulsification: Characterisation of membrane structure by high-resolution X-ray microtomography and microscopic observation of droplet formation in real time.* Journal of Membrane Science, 2007. **302**(1-2): p. 243-253.
23. Vladisavljevic, G.T. and H. Schubert, *Preparation and analysis of oil-in-water emulsions with a narrow droplet size distribution using Shirasu-porous-glass (SPG) membranes (vol 144, pg 167, 2002).* Desalination, 2002. **144**: p. 167-172.
24. Vladisavljevic, G.T., M. Shimizu, and T. Nakashima, *Permeability of hydrophilic and hydrophobic Shirasu-porous-glass (SPG) membranes to pure liquids and its microstructure.* Journal of Membrane Science, 2005. **250**: p. 69-77.
25. Joscelyne, S.M. and G. Tragardh, *Food emulsions using membrane emulsification: conditions for producing small droplets.* Journal of Food Engineering, 1999. **39**: p. 59-64.
26. Williams, R., A., et al., *Controlled production of emulsions using a crossflow membrane. Part II: Industrial Scale Manufacture.* Trans IChemE, 1998. **76**(A): p. 902-910.
27. Vladisavljevic, G.T., et al., *Production of O/W emulsions using SPG membranes, ceramic α-aluminium oxide membranes, microfluidizer and a silicon microchannel plate - a comparative study.* Colloids and Surfaces A: Physicochemical and Engineering Aspects, 2004. **232**: p. 199-207.
28. Kobayashi, I., S. Mukataka, and M. Nakajima, *Effects of type and physical properties of oil phase on oil-in-water emulsion droplet formation in straight-through microchannel emulsification, experimental and CFD studies.* Langmuir, 2005. **21**(13): p. 5722-5730.
29. Geerken, M.J., et al., *Micro-fabricated metal nozzle plates used for water-in-oil and oil-in-water emulsification.* Journal of Membrane Science, 2008. **310**: p. 374-383.
30. Nakashima, T., M. Shimizu, and M. Kukizaki, *Particle control of emulsion by membrane emulsification and its applications.* Advanced Drug Delivery Reviews, 2000. **45**(1): p. 47-56.

31. Vladisavljevic, G.T. and R.A. Williams, *Recent developments in manufacturing emulsions and particulate products using membranes.* Advances in Colloid and Interface Science, 2005. **113**: p. 1-20.
32. Yuan, Q., et al., *Manufacture of controlled emulsions and particulates using membrane emulsfication.* Desalination, 2008. **224**: p. 215-220.
33. Schroder, V. and H. Schubert, *Production of emulsions using microporous, ceramic membranes.* Colloids and Surfaces A: Physicochemical and Engineering Aspects, 1999. **152**: p. 103-109.
34. Kosvintsev, S.R., et al., *Liquid-Liquid Membrane Dispersion in a Stirred Cell with and without Controlled Shear.* Industrial & Engineering Chemistry Research, 2005. **44**: p. 9323-9330.
35. Vladisavljevic, G.T. and R. Williams, A., *Manufacture of large uniform droplets using rotating membrane emulsification.* Journal of Colloid and Interface Science, 2006. **299**: p. 396-402.
36. Massey, B., *Mechanics of Fluids*. 7th ed. 1998, Cheltenham: Stanley Thornes. 722.
37. Vladisavljevic, G.T. and H. Schubert, *Preparation of Emulsions with a Narrow Particle Size Distribution Using Microporous α-Alumina Membranes.* Journal of Dispersion Science and Technology, 2003. **24**(6): p. 811-819.
38. Apel, P., *Track etching technique in membrane technology.* Radiation Measurements, 2001. **34**: p. 559-566.
39. Aveyard, R., et al., *Interfacial Tension Minima in Oil-Water-Surfactant Systems.* Journal of the Chemical Society, Faraday Transactions 1, 1986. **82**: p. 125-142.
40. Ward, A.D., et al., *Optical sculpture: controlled deformation of emulsion droplets with ultralow interfacial tensions using optical tweezers.* Chemical Communications, 2006(43): p. 4515-4517.
41. Fischer, P. and P. Erni, *Emulsion drops in external flow fields - The role of liquid interfaces.* Current Opinion in Colloid & Interface Science, 2007. **12**(4-5): p. 196-205.
42. Vladisavljevic, G.T., M. Shimizu, and T. Nakashima, *Preparation of monodisperse multiple emulsions at high production rates by multi-stage premix membrane emulsification.* Journal of Membrane Science, 2004. **244**: p. 97-106.
43. Avanti, *The Mini-Extruder*.

4 Multiple Optical Tweezers

In order to describe the creation of multiple optical tweezers using a spatial light modulator (SLM), it is necessary to cover several aspects of the behaviour of light.

4.1 Interference and Diffraction [1]

A wave transports energy and momentum without transporting matter. A mechanical wave is a disturbance in a physical medium. An electromagnetic wave (such as visible light) is a disturbance in an electric and magnetic field, and does not require a medium for propagation. Electromagnetic waves are transverse waves, that is, the disturbance is perpendicular to the direction of propagation. Electromagnetic waves are sinusoidal in shape.

All waves can be approximated as a superposition of harmonic waves. The function describing displacements in a harmonic wave is

$$y(x) = A\sin\left(\frac{2\pi}{\lambda}x + \delta\right) \tag{4.1}$$

where A is the amplitude, λ is the wavelength, and δ is a phase constant that depends on the choice of the origin, at which $x = 0$. A simpler way to write this is

$$y(x) = A\sin(kx + \delta) \tag{4.2}$$

where k is the wavenumber, given by $k = \frac{2\pi}{\lambda}$. For a wave travelling in the positive x direction, we can write

$$y(x,t) = A\sin(kx - \omega t) \tag{4.3}$$

where $(kx - \omega t)$ is the phase, and $\omega = 2\pi\nu$ is the angular frequency, in which ν is the frequency.

When two or more waves overlap in space, their individual disturbances (represented by their wave functions) superimpose and add algebraically. When this overlap (called superposition) results in sustained waves in space, the effect is called interference. The result of the superposition of two waves (assuming they have the same amplitude and frequency) depends on the phase difference, δ, between the waves. Two waves are completely in phase when $\delta = 0$, or any integer multiple of 2π, and these waves interfere constructively to give an amplitude twice that of the original waves. Two waves with a phase difference of π (or any odd integer multiple thereof) interfere destructively, and result in zero amplitude. The intensity of a wave is proportional to the square of its amplitude. A phase difference between two waves is often the result of a difference in path length (distance travelled from the source). If the path difference is one wavelength, the phase difference is 2π, which is equivalent to no phase difference. A path difference of one half-wavelength produces a phase difference of π.

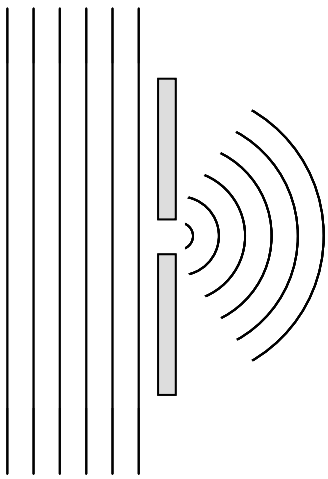

Figure 1: Plane wave encountering an aperture a few wavelengths across. The aperture acts as a point source for a new wave, and circular or spherical wavefronts emanate from the aperture.

Diffraction is the bending of a wavefront behind an obstacle, and almost all diffraction occurs for the part of the wavefront that passes within a few wavelengths of the obstacle's edge. When a wave encounters a barrier with an aperture only a few wavelengths wide, the part of the wavefronts passing through the aperture all pass within a few wavelengths of the edge. The aperture acts as a point source, with the wavefronts spreading out and bending, and becoming circular or spherical (see Figure 1). According to Huygen's principle each point on a wavefront acts as a source of spherical 'wavelets' that propagate with the speed and frequency of the primary wave. The wavefront at some time later is the envelope of these wavelets [1]. The Huygens-Fresnel principle accounts for the new wavefront by superposition of the wavelets to form a new wave.

Interference patterns are only seen for waves from two sources whose phase difference remains the same in time and space. This is called coherence. Interference patterns can be created from a single laser beam split into two and recombined. A plane wave encountering a barrier with two small apertures becomes two spherical or circular waves after passing through the aperture. The two new waves are from the same source, so they are coherent. The interference pattern is observed on a screen far away from the apertures.

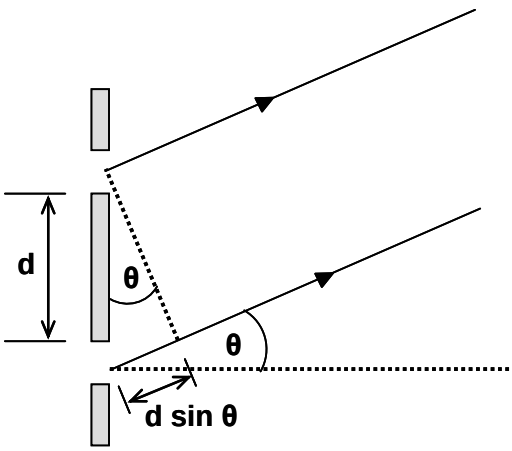

Figure 2: Path length difference of rays from two slits.

At very large distances from the apertures, lines drawn from the centre of each aperture to some point on the screen can be regarded as parallel. The path difference between these

lines, or rays, is approximately $d\sin\theta$, where d is the separation between the apertures, and θ is the angle made between each ray and the normal to the barrier (see Figure 2).

When $d\sin\theta = n\lambda$ (where $n = 0,1,2...$), i.e. the path difference is an integer number of wavelengths, the two waves will be in phase when they reach the screen, and they will interfere constructively to give interference maxima. Interference minima occur when $d\sin\theta = \left(n - \frac{1}{2}\right)\lambda$. In both these equations, n is called the order number. The position of these maxima and minima (called interference fringes) on the screen is given by θ. The zeroth order ($n = 0$) interference fringe occurs for $d\sin\theta = 0$, so $\theta = 0$. All the rays are therefore travelling straight forward towards the screen, and all arrive in phase, having travelled the same distance. The first order fringe occurs for $d\sin\theta = \lambda$, i.e. $\sin\theta = \frac{\lambda}{d}$, so all the rays are travelling at an angle θ to the grating. The spacing between apertures and the wavelength of the light determine the values of θ for which the interference fringes occur.

Light incident on a reflective diffraction grating strikes a series of grooves or rulings which act in the same way as the apertures or slits in a transmissive diffraction grating. The incident beam is split into several beams which continue to propagate beyond the grating.

4.2 Polarisation [1]

A transverse mechanical wave has vibrations perpendicular to the direction of propagation. If the vibrations are parallel to a plane the wave is said to be plane polarised. The same is true of an electromagnetic wave. A plane polarised light wave has disturbances of the electric field parallel to a plane.

Polarising materials (such as Polaroid) absorb and transmit light differently depending on the polarisation of the light. Polaroid contains long hydrocarbon chains that are aligned parallel to each other. Light with an electric field vector (direction of oscillations of electric field) aligned along the hydrocarbon chains is absorbed by the material as electric currents

are set up along the chains. Light with an electric field vector perpendicular to the chains is transmitted. This direction is called the transmission axis.

4.3 Spatial Light Modulators

A spatial light modulator is a reflective or transmissive device which alters the phase or amplitude (or both) of light. A 2-dimensional array of pixels is controlled by a computer, which inputs data into each pixel.

The manipulation of the phase and amplitude of incident light is done by a liquid crystal film. Liquid crystal molecules can be thought of as ellipsoids, with a single long axis. The molecules can stack next to each other in various ways. Smectic liquid crystals, such as the ones used in the Displaytech spatial light modulator, prefer to be aligned parallel to one another, with the centres of each molecule located in parallel layers. Ferroelectric crystals are a type of smectic crystal. Within a layer, the molecules are constrained to lie within a cone of angles relative to the layer normal (see Figure 3) [2].

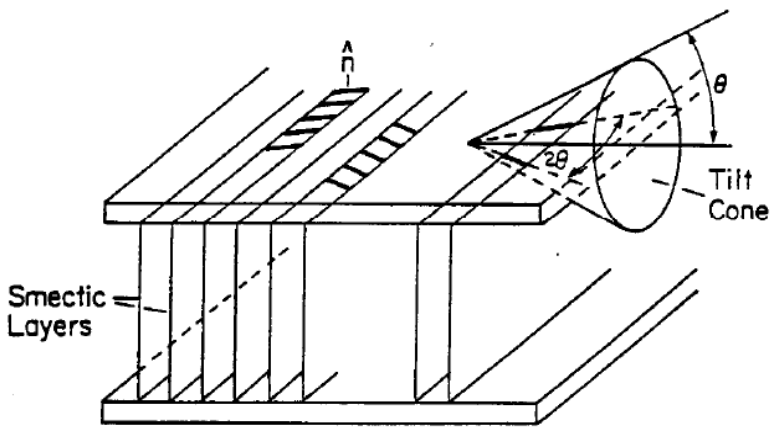

Figure 3: Diagram of liquid crystal smectic layers in an SLM, showing the orientation of the liquid crystal molecules within the layers. The FLC layer is sandwiched between two conducting layers. Image from [3].

In an SLM the liquid crystal film is contained between two glass plates. The glass is coated on the inside with a conductive material, indium tin oxide (ITO). The smectic layers of the

FLC material are approximately perpendicular to the surface of the glass plates. Ferroelectric liquid crystals (FLC) have a permanent dipole which is normal to the long axis of the molecule, so an applied electric field can be used to set the molecular axis to any particular direction on the cone. Reversing the direction of the applied electric field enables selection of one of two orientations, separated by 2θ, as shown in Figure 3. It is the restriction of the molecules to just two orientations that make FLC SLMs binary. Each pixel is either in an 'on' or 'off' state, depending on the orientation of the liquid crystals behind each pixel [2]. The FLC material can be switched rapidly between its two orientations [3].

4.4 Birefringence

An FLC film is birefringent and 'optically uniaxial' [4]. Birefringence is a phenomenon exhibited by some crystalline materials. Because of the structure of the material, the speed of light passing through depends on the direction of propagation of the light. Light striking such a material off the optic axis will be split into two rays with different speeds and directions. These rays are also polarised in mutually perpendicular directions. When light strikes the material along the optic axis, both rays propagate at the same speed. An optically uniaxial material has only one optic axis, which in FLCs is approximately parallel to the FLC molecule's orientation [3]. Applying a voltage to the FLC film selects one of two orientations for the optic axis, depending on the direction of the electric field. The two orientations are approximately 45º apart [4].

If light is incident on a birefringent material perpendicular to the optic axis (as in the case of an FLC SLM), the ordinary and extraordinary rays travel in the same direction but at different speeds, and they emerge with a phase difference that is a function of the optical path length of the material. A birefringent element with a thickness designed to give a phase difference of 180º is called a half-wave plate. Consider linearly polarised light incident on a half-wave plate, with its polarisation vector at 45º to the optic axis. If the wave is propagating along the z axis, the electric field has components in the x and y axes (Figure 4). Before entering the half wave plate, the two components have the same phase and amplitude, i.e. $E_x = E_y = E_0 \sin \omega t$.

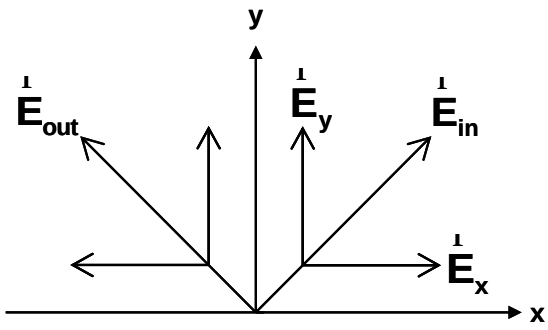

Figure 4: Electric field vector, $\vec{E}$, with components in the y and x axes. The direction of propagation is along the z axis, which lies perpendicular to the plane of the page.

Let us say that the optic axis of the half-wave plate is along the y-axis, since the polarisation vector is at $\pi/4$ to the optic axis. The component of the electric field along the y-axis (and therefore along the optic axis) will be unchanged on passing through the half-wave plate so $E_y = E_0 \sin \omega t$. The component in the x-axis will not travel at the same speed as the y-component, and will be shifted in phase by π by the time it leaves the half wave plate, becoming $E_x = E_0 \sin(\omega t + \pi)$, which is the same as $E_x = -E_0 \sin \omega t$. The x-component therefore points in the negative x direction and the net result is that the polarisation of the light is rotated by $\pi/2$ relative to the incident light [1].

The thickness of the FLC film on an SLM is designed so that it behaves as a half-wave plate. Consider light incident on a reflective SLM, with its polarisation vector parallel to one of the two optic axes of the FLC. By switching between the optic axis orientations which are 45º apart, the SLM either leaves the incident light unchanged, or rotates the polarisation of the incident light by 90º. Each pixel can be in either of the two states. Placing a polarizing filter in front of the SLM selects one polarisation of light, so one state of the SLM will be ‘bright’ (i.e. transmitted by the filter) and the other will be ‘dark’ [4]. An SLM can be used as a ‘diffractive optic element’, i.e. a reflective which acts as a diffraction grating to give a specific pattern of light intensity either on a far-away screen, or by focusing the light through a lens. An array of optical traps can be formed in this way.

4.5 Multiple optical tweezers

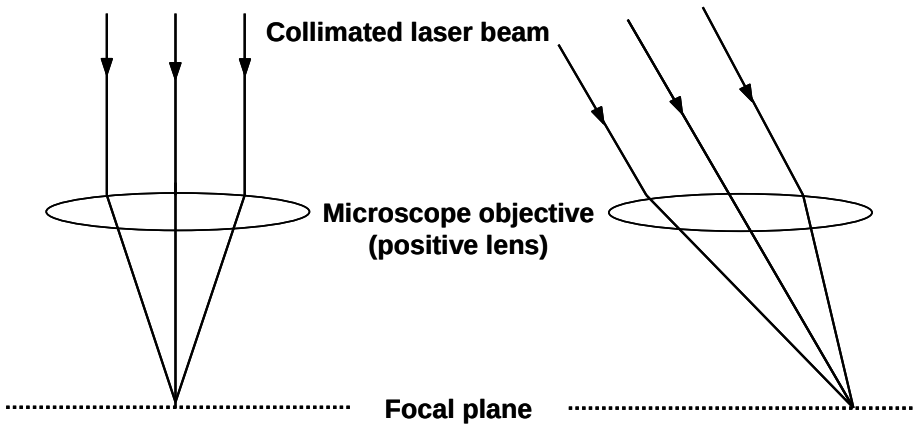

Figure 5: Microscope objective focusing a collimated laser beam. A beam entering the back of the objective off the optic axis will be focused to one side.

A microscope objective focuses a collimated laser beam into a tweezer, and provides a means of imaging a trapped particle or object. The optical tweezer can be moved across the focal plane of the objective by changing the beam's angle of incidence at the back aperture (Figure 5). Several collimated beams passing through the back aperture of the objective, at different angles of incidence, will be focused at different points on the focal plane, forming an array of tweezers. Dual optical tweezers can be created by splitting and recombining a single laser beam with a beam splitter and mirrors [5]. A simple set-up for a dual trap is shown Figure 6. The angle of incidence at the back aperture of the objective is controlled by angling and tilting each mirror.

Diffractive optical elements can also be used to form an array of tweezers [6]. Each beam from the diffraction grating enters the back aperture of the objective, and forms a single tweezer. A diffraction grating designed to produce a square array of beams will therefore produce a square array of tweezers.

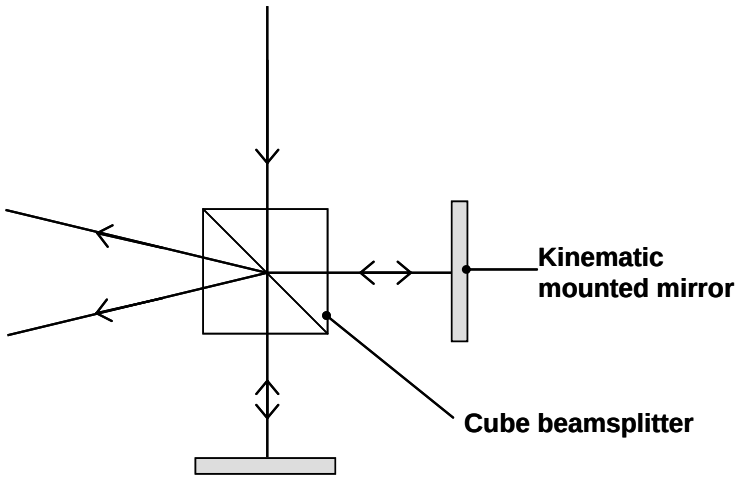

Figure 6: Splitting and recombining a laser beam using a cube beamsplitter and mirrors. Only the beams directed towards the microscope are shown.

4.5.1 Acousto-Optic Deflectors

When a sound wave propagates through a suitable crystal, the density and hence the refractive index of the crystal material is changed [7]. Acousto-optic modulators use this property to deflect light passing through the crystal. These devices can be used in optical trapping to steer a laser beam, so that it enters the objective at different angles. The acousto-optic modulator can be switched on and off very rapidly, so that the laser beam can be made to scan several positions in rapid succession. A droplet in a laser trap takes some time to wander away when the trap is removed, so scanning the laser to produce several traps around the droplet produces the effect of having several simultaneous traps. Ward *et al.* [8] made use of acousto-optic deflectors (AODs) in their work on optical deformation. Computer software enabled the generation and control of up to four traps. The authors assumed that dividing the traps into multiple positions would lower the power at each trap in the same way that splitting the beam into several beams would give each trap a fraction of the power of the single beam. The maximum force exerted by one trap was calculated to be 0.69 pN mW^{-1}. This was sufficient to deform emulsion droplets into ellipsoids, triangles and squares using two, three and four traps respectively.

Although the work by Ward *et al.* was very successful, AODs are expensive optical elements, and the number and positions of traps that can be generated are limited. A spatial

light modulator can generate an arbitrary array of traps, and the position of the traps can be controlled via a computer programme. The traps can be moved in the focal plane of the microscope objective.

4.5.2 Holographic Optical Tweezers

Holographic optical tweezers use a diffractive optical element (such as an SLM) to generate several beams, each of which is focused into a trap by a microscope objective. A computer-addressed spatial light modulator acts as a diffractive element.

As previously explained, multiple beams entering a microscope objective at different angles will be focused into a pattern of optical traps. The multiple beams entering the objective are mutually coherent because they are from the same coherent source. They will therefore form an interference pattern at the input pupil of the objective, consisting of amplitude and phase modulations. A spatial light modulator can be used to impose the same interference pattern on a single incident beam as it enters the objective, creating the same trapping pattern at the focal plane. This is the basis of holographic optical trapping [9]. Although the interference pattern consists of amplitude and phase modulations, the hologram only needs to modulate the phase of the beam since the scattering and gradient forces that contribute to the optical trap arise from the intensity and intensity profile of the beam. A normal Gaussian beam will form an optical trap without modulation of the intensity (which is proportional to the square of amplitude), so leaving the amplitude profile of the beam unchanged as it passes through the diffractive element will still create optical traps. This simplifies the holograms necessary for creating multiple traps [9]. The difficult step in creating the traps is calculating the hologram. The phase pattern associated with the interference of several beams can be computed, and the resulting pattern is known as a computer generated hologram (CGH).

4.6 Using the SLM as a Phase Grating

I am grateful to Dr Gordon Love and his research group in the Physics Department at the University of Durham for kindly lending us a Displaytech spatial light modulator. My thanks also go to Andy McKeague for his help with designing and undertaking the SLM

experiments. We did not compute the interference pattern as other authors have done, but used a simple pattern that acted as a diffraction grating when the SLM was used in reflection. The SLM is a binary system, so each pixel can be in a dark or light state. By placing a polarizing filter after the SLM, the SLM can act as a diffraction grating as only the light reflected from the 'bright' pixels will pass the filter. By rotating the incident light (or the SLM) such that the polarisation vector of the incident light is aligned with the optic axis of the FLC material, the SLM can be made to behave as a phase grating. Some of the pixels will have their optic axis aligned with the incident light's polarisation. The light reflected from these pixels is unchanged on being reflected from the SLM. Some of the pixels will be in the opposite state, so the light reflected off these pixels will effectively have travelled at a different speed to the light reflected from the other pixels. It will also leave the SLM 180º out of phase with the light from the bright pixels (see section on birefringence for an explanation of this).

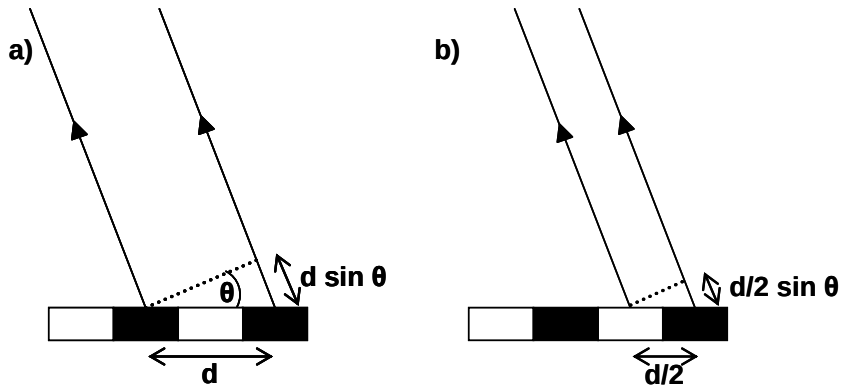

Figure 7: Diffraction from phase gratings.

A phase grating is similar to a normal diffraction grating, but a phase change is imposed on the light transmitted or reflected by the grating. The interference pattern created is therefore a function of the difference in phase imposed not only by the path length difference between interfering rays, but also the phase difference imposed by the grating.

For the phase grating shown in Figure 7, the path length difference is $d \sin\theta$ where d is the distance separating two sources (apertures or obstacles) with the same phase. The black and white blocks represent the phase change imposed on the light by the grating. In this

case adjacent blocks are 180º out-of-phase with one another. For rays from apertures of the same phase (Figure 7a), constructive interference occurs for $d\sin\theta = n\lambda$. For rays from adjacent apertures which are 180º out-of-phase with one another (Figure 7b), constructive interference occurs for

$$\begin{aligned} \frac{d}{2}\sin\theta &= n\lambda + \frac{\lambda}{2} \\ \frac{d}{2}\sin\theta &= \left(n + \frac{1}{2}\right)\lambda \\ d\sin\theta &= (2n+1)\lambda \end{aligned} \tag{4.4}$$

$(2n+1)$ gives only odd numbers, so only odd orders appear in the interference pattern from a phase grating. This means that the central bright spot, the zeroth order fringe, is absent. The first interference maxima from a phase grating therefore occurs for $\sin\theta = \frac{\lambda}{d}$, appearing either side of the centre of the screen. This can be understood by recalling that the central spot in a diffraction grating interference pattern arises from all the rays travelling straight forward, and having no path length difference (and therefore phase difference) when they reach the screen. Rays travelling straight forward from a phase grating also have no path length difference, but adjacent rays are 180º out-of-phase with one another, and interfere destructively when they reach the screen (Figure 8).

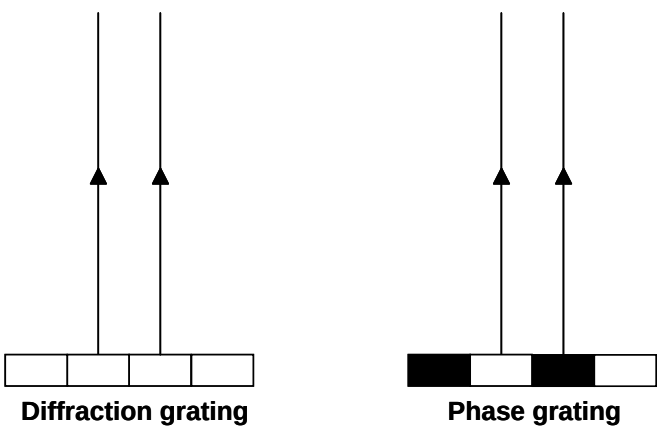

Figure 8: A phase grating does not produce a central spot.

Using the SLM as a phase grating enables the creation of two optical traps, without the large central bright spot that would occur if the SLM was used as a diffraction grating.

4.7 Creating phase grating patterns

A MATLAB program was used to create the patterns for the SLM. Since the SLM is binary and each pixel is either dark or light, the images were constructed from black and white pixels, forming a pattern of vertical stripes with widths according to the desired spacing of the two traps. The lateral displacement of each trap in the focal plane of the objective is proportional to the angle of incidence at the back aperture of the objective (see Figure 9).

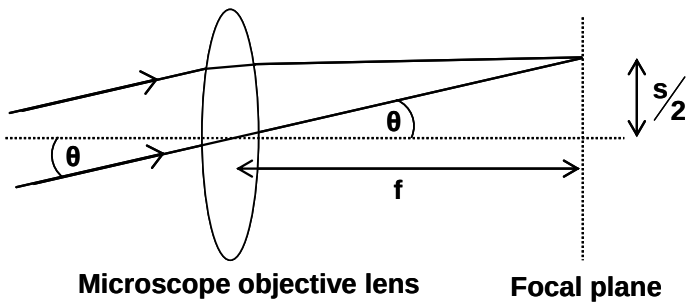

Figure 9: Ray diagram of geometry of optical trap. Only two rays are shown for clarity.

The focal length, f, of the objective in use for the trapping experiments is 2 x 10^{-3} m. The spacing between traps, s, is given by

$$s/2 = f \tan\theta \tag{4.5}$$

where θ is the angle between the optic axis and a ray travelling through the centre of the lens (i.e. the angle of incidence at the back aperture). Using the small angle approximation, $\tan\theta \approx \theta$, Equation (4.5) becomes

$$s/2 = f\theta \tag{4.6}$$

The first order diffraction fringes ($n = 1$) will form the optical traps, so we can write

$$n\lambda = d\sin\theta$$
$$\lambda = d\sin\theta$$
$$d = \frac{\lambda}{\sin\theta} = \frac{2\pi}{k\sin\theta} \tag{4.7}$$

where k is the wavenumber. The pattern of vertical stripes was made by a periodic function, varying between values of 1 and 0 for black and white. By creating a 'mesh' in MATLAB, the image space could be divided exactly as the SLM is divided into pixels. The cosine function $f(x) = \cos x$ is a periodic function beginning at 1, and provided a simple basis for the striped function required. The cosine function was rounded to a step function varying between +1 and -1, and made to vary between 0 and 1 by adding 1 and dividing by 2. Applying this function to the x variable of the mesh created a series of black and white alternating stripes, where the width of each stripe is the determining factor in the spacing between the traps. A normal cosine function has a wavelength of 2π, meaning that one black stripe and one white stripe fit into the space of 2π along the x axis. We required a wavelength of d, so that one black stripe and one white stripe fit into the space of 'd' along the x axis. This created a diffraction grating (or phase grating) with a spacing between apertures (either all the white stripes or all the black stripes) of d.

We can write

$$f(x) = \cos x$$
$$f(x) = \cos\left(k \cdot \sin\theta \cdot x\right) \tag{4.8}$$

and, since $d = \dfrac{2\pi}{k\sin\theta}$,

$$f(x) = \cos\left(\frac{2\pi}{d} \cdot x\right) \tag{4.9}$$

where d is the wavelength of the function. All that remained was to specify the variables to put into the program in order to create the series of images to give a range of trap distances. The minimum and maximum separations between the two traps were set at 0 and 10 μm respectively, since droplets bigger than 10 μm are unsuitable for trapping. Each image

would create two traps with slightly different separation, so the increment between each image had to be specified. This was set at 0.05 μm to give a reasonably smooth movement between trap positions. It was also necessary to instruct the program how to divide the image up into pixels. This was achieved by creating the mesh on a 6 mm square, with each vertical section of the mesh (x coordinate increments) measuring the same as the SLM pixel dimension. Running the program generated a series of images that, when loaded into the SLM as a diffraction grating, would give two traps with a separation ranging from 0 to 10 μm, with each new position 0.05 μm distant from the last. A selection of the images is shown in Figure 10.

Because the black and white step function is sampled finitely into the image, the widths of the stripes in the grating are somewhat uneven. This effect is most pronounced for higher trap separations. Fortunately the trap does not seem to be badly affected by the uneven diffraction grating, presumably due to the high focusing power of the microscope objective.

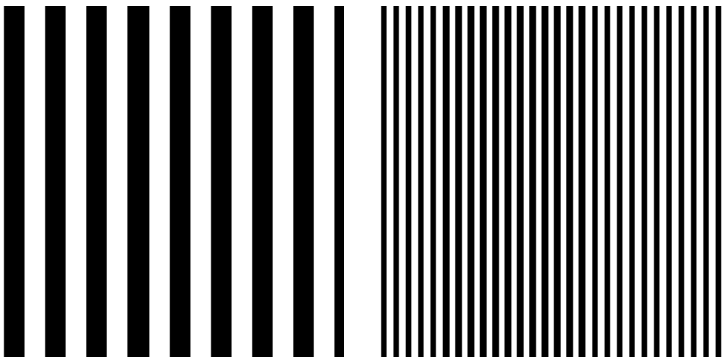

Figure 10: Samples of images created by MATLAB program, showing uneven stripe widths. Left: Trap spacing = 3 μm. Right: Trap spacing = 10 μm.

4.8 Experiments, Results and Discussion

The SLM was tested initially by observing the diffraction pattern at some distance away. The diffracted beams focused into spots on the screen, showing that the SLM was working as a diffraction grating.

The SLM was supplied to us with a PCI Bus interface and computer based control panel. The control panel enables the user to store, organize and upload images onto the SLM. Image sequences can be created, so that the traps can be made to move towards and away from each other by changing the phase grating displayed on the SLM. The control panel also enables the user to select 'Automatic DC balancing', which ensures that each pixel experiences zero voltage on average. An image alternates between the normal image and the inverted image, so each pixel changes rapidly between black and white to ensure that the average voltage across each pixel is zero. This prevents damage to the SLM.

The SLM was set up as shown in Figure 11. Apart from the central diffraction fringe, beams reflected from the SLM diverged away from each other, so that at a long distance from the microscope, they would not pass into the back aperture of the objective. To overcome this problem the optics were set up to position the SLM as close to the microscope as possible. This required the SLM and mirror being mounted on "stable" pillars, at the same vertical height as the upper mirror of the periscope.

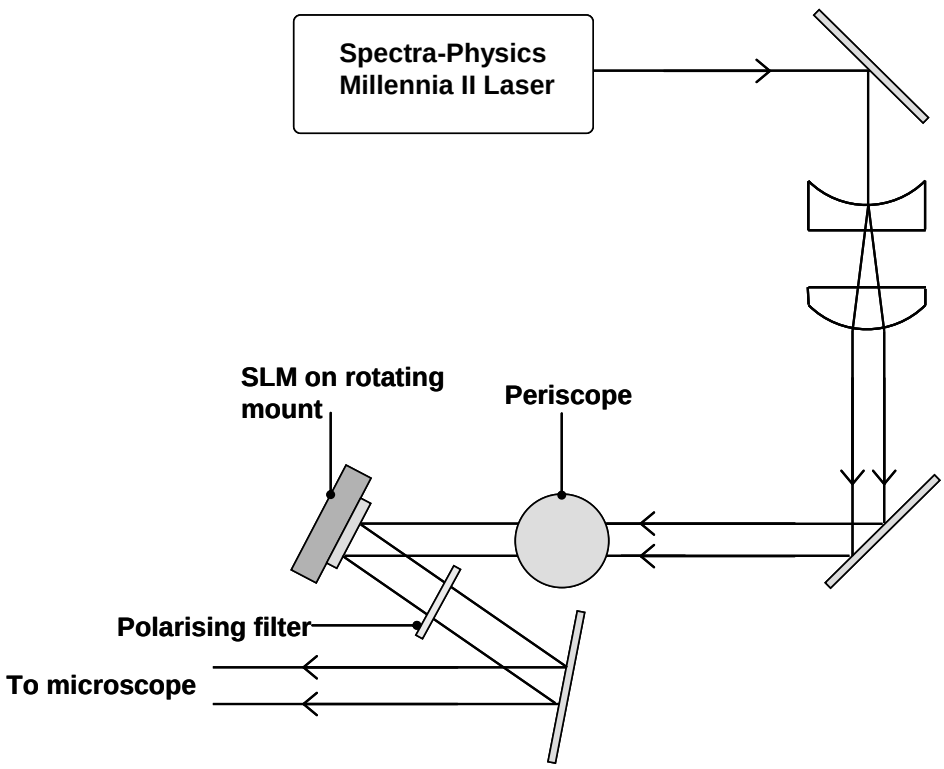

Figure 11: Position of SLM in optical set-up.

The polarizing filter was rotated to ensure that the polarisation vector of the incident light bisected the angle made by the two optic axes of the FLC. The simplest way to test this was to load an image into the SLM (for example the 3 μm separation image), and to focus the traps. Without the polarizing filter, the light reflected from the SLM formed a strong central trap. By inserting the polarizing filter and rotating it until the central trap was weakest, the system was optimized for use as a phase grating.

As previously mentioned, the easiest way to focus and align the trap is to place a mirror on the microscope stage and to use the periscope mirrors, the SLM, and the final mirror to centre the trap in the field of view and to ensure that the diffraction rings caused by the trap are symmetric about its centre.

The laser in use with the trapping experiments is a Spectra-Physics Millennia II frequency doubled Nd:YAG laser, with a wavelength of 532 nm. The maximum achievable laser power is approximately 0.45 Watts. The laser was always set to its highest power for the SLM experiments.

An optical trap is stable as long as the gradient forces are higher than the scattering forces [5-6, 9]. A high numerical aperture objective gives rise to a high number of rays providing a gradient force in optical trapping [5]. Completely filling (or slightly overfilling) the back aperture of the objective ensures that these forces are maximized, and that the trap is stable.

The PCI Bus interface and computer control panel enabled the uploading of a continuous series of images into the SLM, so that the traps could be moved smoothly apart and back together again. The maximum trap separation possible was in the region of 8 μm.

The shape of the traps was quite different to the shape formed with a single beam. It is likely that the beams did not fill the back of the objective, leading to geometric aberrations in the focus. The trap formed without the polarizing filter, i.e. from the reflection from the SLM surface, was almost round and the surrounding diffraction rings were nearly symmetrical. However even this trap was reduced in quality compared with one formed by a single laser beam, and the trap seemed to be quite weak when it was tested. The traps

formed by the diffracted beams were not quite round, and the diffraction rings surrounding the traps were not symmetrical. It is expected that the traps will not look the same as one created by a beam directed straight through the objective, and that the strongest part of the trap might not be exactly at its centre.

A 1 mM AOT/0.05 M NaCl solution was prepared as described in Microfluidics. An emulsion was made by adding 3 drops of heptane to approximately 6 ml of surfactant solution, and shaking in a small vial to disperse the oil. The emulsion was pipetted onto the haemocytometer slide and covered with a cover glass. Attempts to manipulate emulsion droplets with either or both of the traps were completely unsuccessful.

Increasing the angle between the two beams (and therefore the separation between traps) decreased the power of each trap. This would have implications in optical deformation experiments, since the power of the trap has to overcome interfacial tension forces. Large deformations would not be possible because the power of each trap fell off suddenly with increasing separation. The reason for this was that, even with the SLM as close to the microscope as possible, increasing the angle between the beams decreased the amount of light entering the back of the objective, which resulted in reduced intensity and reduced axial intensity gradient [6]. Even if the traps had been sufficiently strong to hold emulsion droplets, there would be a maximum separation between the traps that could be achieved with the optical set-up shown in Figure 11.

In order to assess the reflectivity and polarizing efficiency of the SLM, several measurements of laser beam power were taken before and after the SLM. The polarizing filter was removed from in front of the SLM, and placed to intersect the reflected light where necessary. A blank white image was loaded into the SLM. The results are presented in Table 5.

It is clear that the reflectivity is very similar to the value of 25 % quoted by the manufacturers [10]. The polarizing filter was tested for its efficiency at blocking a single polarisation, and it was found to block nearly all of the light when rotated correctly. If the SLM was 100% efficient at polarizing and reflecting light, the expected output from the

active SLM would be 3.0 mW. The image on the SLM was a white square (alternating with a black image for automatic DC balancing). For half the time, we would expect 6.0 mW of light to get through the polarizing filter, since it was rotated to allow one polarisation of light to pass. The average power would therefore be 3.0 mW. Turning the automatic DC balancing off had very little effect on the power output from the SLM. The fact that more power was measured with the polarizing filter than without is evidence that some of the light was being rotated to pass through the filter, but it was not enough to form a strong optical trap. From these results I concluded that the SLM was not working properly.

Table 5: Measurement of laser power before and after SLM.

Position of power meter	Measured Power / mW
Before SLM	23.0
After SLM, without polarizing filter	6.0
After SLM, with polarizing filter, SLM off	0.1
After SLM, with polarizing filter, SLM on	0.5

4.9 Conclusions and Future work

Given the many successful examples of SLMs employed in optical trapping applications, it seems likely that acquisition of a newer SLM, and perhaps little more work, would yield some positive results in this field. The first logical step would be to compute holograms for a series of trap separations, and to introduce a second telescope into the optical set up [6, 9, 11].

The principle of reversibility states that if rays from point A in Figure 12 are focused at point B, then rays travelling in the opposite direction, from B, will be focused at point A.

In an optical system, these points are known as conjugate points. If an object lies at A and is imaged at B by a series of optical elements, then the object would be equally well imaged at A if it was placed at B.

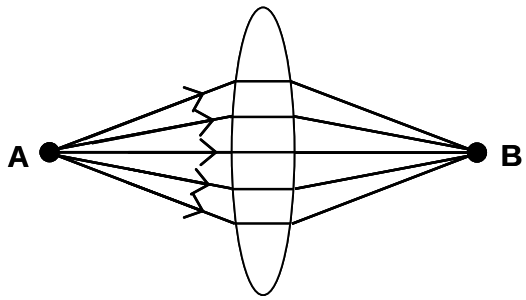

Figure 12: Conjugate points in an optical system.

Dufresne and Grier have reported the use of diffractive optical elements to create arrays of optical traps [6]. In their optical set up they use two Keplerian telescopes, to form two conjugate planes to the back aperture of the objective. Placing the diffractive element at the focus point of the first telescope creates the desired pattern at the focus point of the second telescope, which coincides with the back aperture of the objective. In this way, one can overcome the problem of diverging beams missing the back aperture of the objective. This is only appropriate for transmissive elements. A reflective SLM must be placed at a conjugate plane to the objective's input pupil, using a mirror to reflect the beam onto the SLM, as shown in Figure 11. A single telescope (aside from the beam expander) is required for this arrangement, as shown in Figure 13.

Grier and Roichman mention in their work [9] that not all of the input beam is diffracted by the SLM, even with computer generated holograms rather than simple diffraction gratings as used in this project. The undiffracted light (i.e. the light reflected from the front surface of the SLM) forms a bright trap in the middle of the field of view. Their solution to this was to make the incident beam slightly converging, so that the traps needed to be displaced along the optic axis to be formed in the focal plane. The undiffracted light focused in a plane different from the other traps.

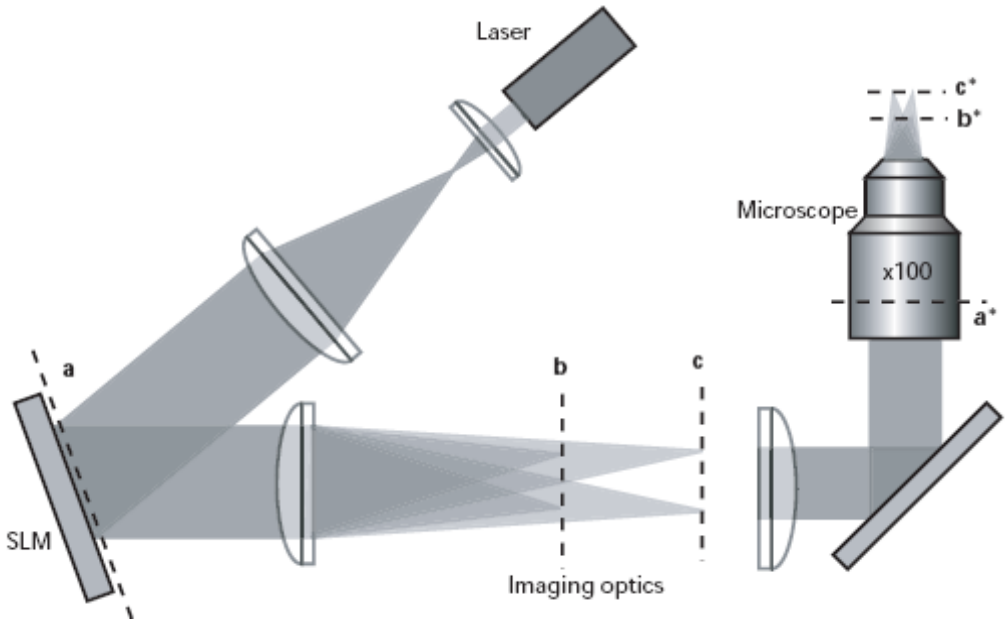

Figure 13: Diagram of holographic optical tweezers set-up, showing the SLM positioned at a, the conjugate plane of the objective's back aperture. Planes b and c are imaged at the focal plane [12].

Laser powers from several milliwatts to several watts are used in different optical trapping applications, the strength of the trap being proportional to the power of the light [13]. According to Dufresne and Grier [6] a milliwatt of visible light is ample to overcome the forces driving microparticle motion. Bronkhorst *et al.* [14] have reported using multiple optical traps to deform red blood cells, with a beam power of approximately 220 mW. It is difficult to define a minimum power necessary for the deformation of emulsion droplets, since the interfacial tension in microemulsion systems varies so much between different chemical systems. Given that the maximum laser power achievable with the laser in use for these experiments is in the region of 450 mW, it is clear that the huge reduction in laser power on reflectance from the SLM and transmission through the polarizing filter will reduce the power of the trap to a level that may not be sufficient to deform particles of the relevant size. It would certainly be worthwhile swapping the laser for a more powerful one for future experiments.

Although using a beamsplitter to create two diverging beams (and therefore two separated traps) is much simpler than using an SLM, creating more than two traps in this way

becomes cumbersome. Two traps created with a single beamsplitter each have a power equal to one quarter of the total beam power, and a reasonably powerful laser would be required to create a complex array of 4 or more traps, not to mention the space that would be required on the table. An SLM offers far more possibilities for creating arrays of traps for optical deformation, and has greater control on the movement of these traps. It takes up much less space on the optics table, and any arbitrary arrangement of a great number of traps can be created simply using the computer control panel. It is also possible to displace traps normal to the focal plane by using the SLM to change the curvature of the wavefront of the laser beam [6]. A diverging beam is focused downstream of the focal plane, and a converging beam is focused upstream. This provides a mechanism for positioning traps in three dimensions [9], and for deforming droplets in three dimensions.

References

1. Tipler, P. A., *Physics for Scientists and Engineers*. 4th ed.; W H Freeman: New York, 1999; p 1335.
2. Goodman, J. W., *Introduction to Fourier Optics*. 3rd ed.; Roberts & Company: Greenwood Village, 2005; p 491.
3. O'Callaghan, M. J.; Handschy, M. A., Ferroelectric liquid crystal SLMs - from prototypes to products. *Spatial Light Modulators: Technology and Applications, Proceedings of SPIE* **2001,** *4457*, 31-42.
4. Cotter, L. K.; Drabik, T. J.; Dillon, R. J.; Handschy, M. A., Ferroelectric-liquid-cyrstal/silicon-integrated-circuit spatial light modulator. *Optics Letters* **1990,** *15* (5), 291-293.
5. Fallman, E.; Axner, O., Design for fully steerable dual-trap optical tweezers. *Applied Optics* **1997,** *36* (1), 2107-2113.
6. Dufresne, E. R.; Grier, D. G., Optical tweezer arrays and optical substrates created with diffractive optics. *Review of Scientific Instruments* **1998,** *69* (5), 1974-1977.
7. Deblaquiere, J. A.; Harvey, K. C.; Hemann, A. K., Time-of-flight measurement of the speed of light using an acousto-optic modulator. *American Journal of Physics* **1991,** *59* (5), 443-447.
8. Ward, A. D.; Berry, M. G.; Mellor, C. D.; Bain, C. D., Optical sculpture: controlled deformation of emulsion droplets with ultralow interfacial tensions using optical tweezers. *Chemical Communications* **2006,** (43), 4515-4517.
9. Grier, D. G.; Roichman, Y., Holographic optical trapping. *Applied Optics* **2006,** *45* (5), 880-887.
10. Banas, D. B.; Handschy, M. A.; Crandall, C., 256 x 256 Ferroelectric Liquid Crystal Spatial Light Modulator. *Proceedings of SPIE* **1997,** *3015*, 114-124.
11. (a) Dufresne, E. R.; Spalding, G. C.; Dearing, M. T.; Sheets, S. A.; Grier, D. G., Computer-generated holographic optical tweezer arrays. *Review of Scientific Instruments* **2001,** *72* (3), 1810-1816; (b) Curtis, J. E.; Koss, B. A.; Grier, D. G., Dynamic holographic optical tweezers. *Optics Communications* **2002,** *207*, 169-175; (c) Martin-Badosa, E.; Montes-Usategui, M.; Carnicer, J. A.; Pleguezuelos, E.; Juvells, I., Design strategies for optimizing holographic optical tweezers set-ups. *Journal of Optics A: Pure and Applied Optics* **2007,** *9*, S267-S277.
12. Leach, J.; Sinclair, G.; Jordan, P.; Courtial, J.; Padgett, M., 3D manipulation of particles into crystal structures using holographic optical tweezers. *Optics Express* **2004,** *12* (1), 220-226.
13. Block, S. M., Making light work with optical tweezers. *Nature* **1992,** *360*, 493 - 495.
14. Bronkhorst, P. J. H.; Streekstra, G. J.; Grimbergen, J.; Nijhof, E. J.; Sixma, J. J.; Brakenhoff, G. J., A New Method to Studay Shape Recovery of Red Blood Cells Using Multiple Optical Trapping. *Biophysical Journal* **1995,** *69*, 1666 - 1673.5

5 Optical Deformation

Deformation of droplets is possible by creating multiple optical traps at a single point, then moving the traps apart. Since I was unable to form multiple optical traps using the SLM, I needed a simple optical set-up to create multiple optical traps. As discussed in the previous chapter, dual optical tweezers can be created by placing a cube beamsplitter in the optical set-up (see Figure 1).

5.1 Temperature-sensitive System

In order to test the optical tweezers before investigating temperature-insensitive systems, I studied the deformation of microemulsion droplets stabilised by the AOT/NaCl system that was used in previous work [1]. Ward *et al.* demonstrated large deformations of microemulsion droplets made possible by ultra-low interfacial tension, and also reported on the formation of stable nanometer-sized threads connecting droplets.

The surfactant solutions were prepared as described in 'Microfluidics'. All glassware and apparatus was sonicated in a 1% Deconex solution, rinsed in MilliQ water, and left to dry.

5.2 Control of Optical Traps

The optical set up is shown in Figure 1. Each trap could be moved up and down or side to side in the focal plane of the objective adjusting the kinematic-mounted mirrors either side of the beamsplitter. The traps were initially set close together. Once a droplet was trapped, either one or both of the traps were moved to deform the droplet.

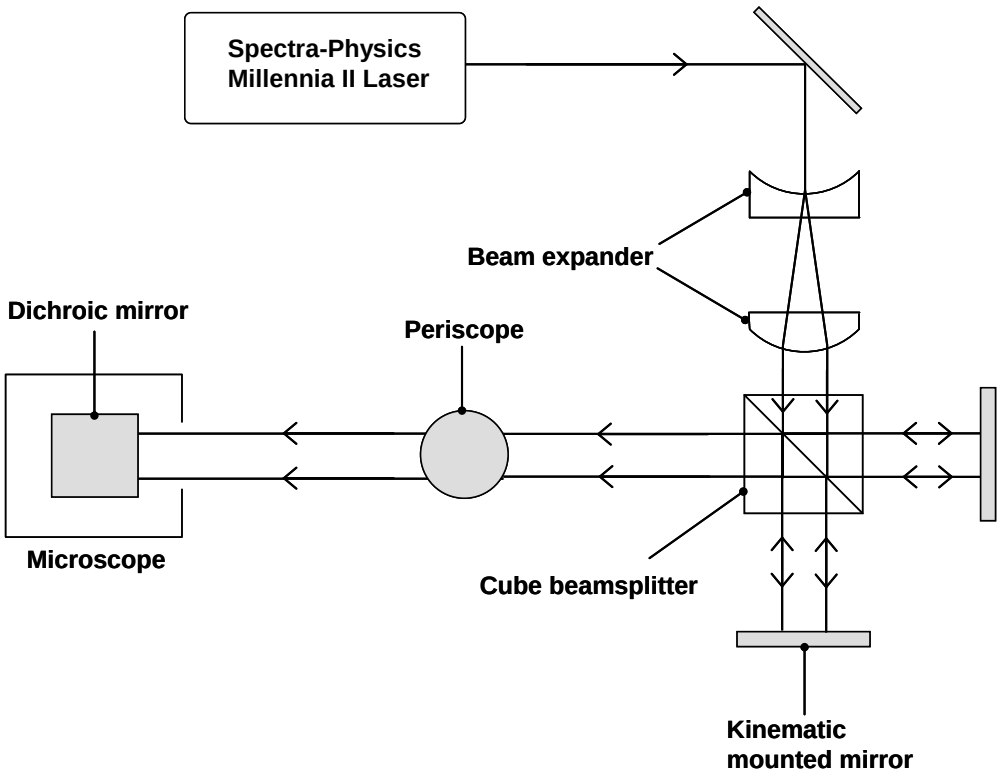

Figure 1: Optical set-up showing position of beamsplitter.

5.3 Results

5.3.1 Temperature Control

Due to problems with the air conditioning unit in the laser laboratory, the temperature in the laboratory was normally between 24º and 25º C. A thermocouple was fixed to the microscope stage such that it made contact with the lower face of the haemocytometer slide, and gave a reasonable estimate of the temperature of the sample. The temperature under the microscope objective (heated by the illumination lamp and by the laser) was between 25º and 28 ºC, very close to the temperature at which the region of ultra-low interfacial tension exists in the AOT system.

Ultra-low interfacial tension was achieved by heating the sample up from room temperature (if the room temperature was below the required temperature) with a heat gun directed at the microscope stage. The temperature around the ultra-low region will hereafter be called the critical temperature. It was clear that the tension could only be

controlled while increasing the temperature. If the sample was heated too high and left to cool, the droplets would pass through the critical temperature, but ultra-low interfacial tension was not observed and the droplets were not deformable. Reheating the sample had the same result. Neither could the sample be reheated to make it deformable.

5.3.2 Deformation

Several general observations that were made during the deformation experiments are presented here.

The critical temperature for deforming the droplets was between 26º and 27ºC, although there was slight variation of this temperature between samples. In the region of the critical temperature, the oil phase dissolved into the aqueous phase after a few minutes and no droplets remained in the sample. Droplets with ultra-low interfacial tension appeared different under the microscope to droplets with higher interfacial tension. This difference in appearance was likely to be caused by fluctuations in the surface separating the oil and aqueous phase. High interfacial tension prevents such fluctuations being large enough to be observed under the microscope, but as the interface 'softens' at low interfacial tension, the droplet appeared to be shimmering (see Figure 3). Droplets with a high refractive index (indicated by a dark ring surrounding the droplet, see Figure 2) were trapped easily, but they often did not have very low interfacial tension. Finding the right droplets to trap was a combination of looking for the right interfacial tension and refractive index. There were some very soft structures in the microemulsions. These were deformed very easily, but were difficult to hold in the trap. Nonetheless it was often possible to deform these structures where they were attached to the cover glass.

At the right temperature, small droplets could be deformed by moving each trap away from the centre of the droplet (see Figure 2). The extent to which each droplet could be deformed depended on the interfacial tension between the droplet and the continuous phase. It is clear that some droplets had lower interfacial tension than others.

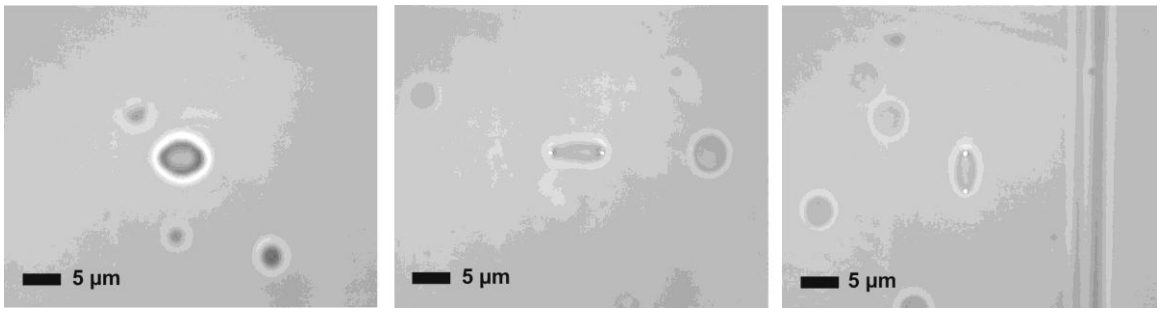

Figure 2: Varying degrees of deformation, depending on interfacial tension.

When a droplet was pulled apart completely by the two traps, there remained a thread attaching the two droplets (see Figure 3). These threads could be very long, 50 µm or more. When smaller droplets were broken up (see Figure 4), the threads were not always visible. The existence of a thread joining the two droplets was indicated by a pinch point on each droplet where the thread was attached. It was not possible to break up all the droplets that were studied because of the variation in interfacial tension. Large droplets tended to stick to the cover glass or to the bottom of the slide, so a single trap could be used together to pull off a small droplet.

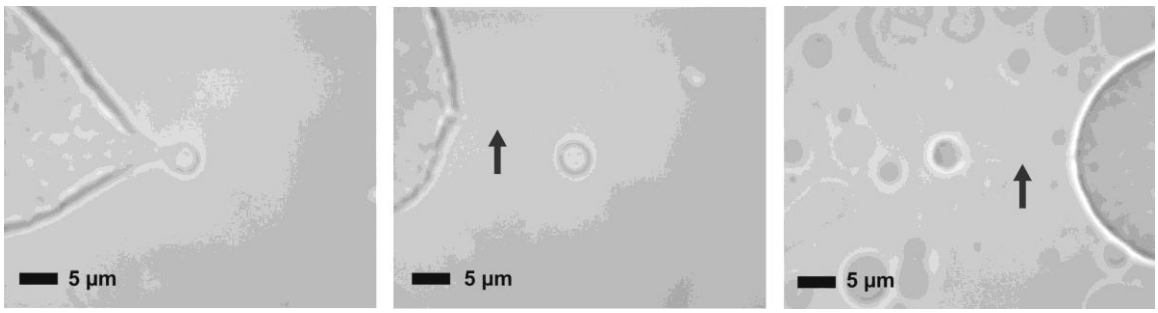

Figure 3: Images of droplet break-up and resulting threads. Arrows indicate position of thread. The surfaces of the droplets appear to be shimmering, because of the ultra-low interfacial tension.

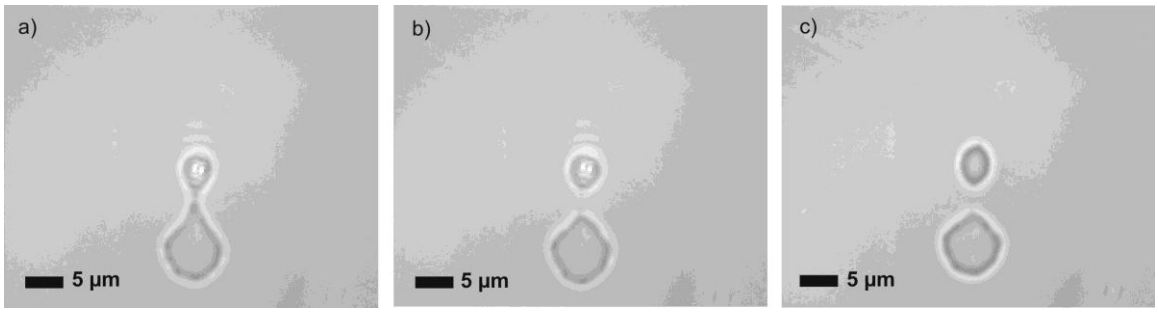

Figure 4: Droplet break-up and formation of thread. a) and b) show the two traps as bright dots; c) The droplet is pinched where the thread is attached.

If a droplet was broken up so that a thread joined the two new smaller droplets, the thread pulled one droplet back to the other. Figure 5 shows a droplet stuck to the cover glass, which has been broken up by pulling off a single satellite drop with both traps (two small bright dots in the image). When the traps were blocked, the thread contracted and pulled the released droplet back towards the other droplet. The two droplets eventually coalesced. This phenomenon was not seen for all the threads studied. Although there is very little variation in interfacial tension between different threads, it seems likely that the interfacial tension has a part to play in whether the released droplet is drawn back in or not. For the lowest interfacial tension, the thread did not contract, and the two droplets remained connected by the thread. For slightly higher interfacial tension, the thread contracted and the droplet was drawn back in to reduce the interfacial area.

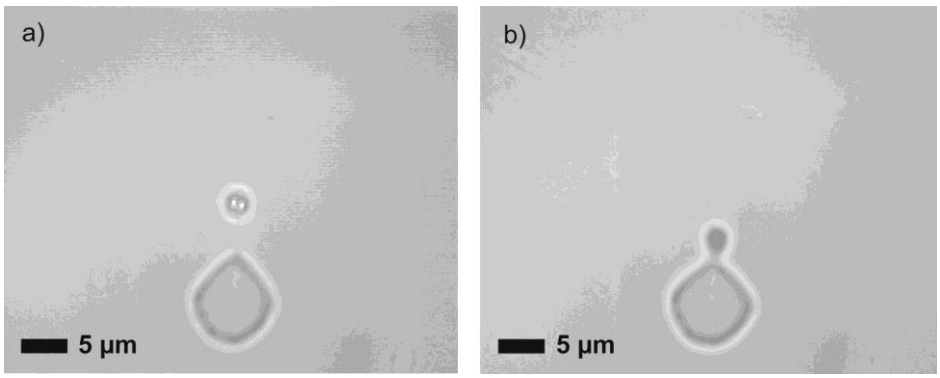

Figure 5: a) Droplet stuck to cover glass split into two using both traps; b) The traps are blocked, and the released droplet is drawn back by the thread.

Since the trapping and deforming experiments with the temperature-sensitive system were successful, I moved on to testing potential temperature-insensitive systems.

5.4 Microemulsion Phase Behaviour

Microemulsion phase behaviours present similarities regardless of the components of the system. These characteristics are best described by phase diagrams and the associated labels for each phase.

The phase behaviour of non-ionic surfactants such as polyoxyethylene glycols with temperature can be explained by a conformational change of the hydrocarbon chain with increasing temperature [2]. Ionic and non-ionic surfactants show opposing behaviour with a change in temperature. Ionic – non-ionic surfactant mixtures therefore offer the possibility of forming temperature-insensitive microemulsions.

Single phase microemulsions are formed only at surfactant concentrations in excess of a critical aggregation concentration, or 'critical microemulsion concentration' of surfactant (cμc). For oil-in-water microemulsions this value is usually similar in magnitude to the critical micelle concentration of the surfactant without oil [3].

Fletcher and Petsev summarise microemulsion phase behaviour as follows [3]. With equal volumes of oil and water, and for surfactant concentrations in excess of the cμc, the monomer concentration in each phase of a three phase body remains nearly constant (equal to the cμc), and any additional surfactant forms aggregates containing oil or water in either the water, the oil, or a third phase. If the surfactant forms aggregates in the water phase, oil-in-water emulsion droplets are formed, and this microemulsion phase coexists with the excess oil phase. If the surfactant forms aggregates in the oil phase, reverse micelles are formed, and the water-in-oil microemulsion coexists with an excess water phase. The type of microemulsion formed is determined by the preferred monolayer curvature of the surfactant. A bicontinuous structure has regions of oil and water separated by a surfactant monolayer with positive and negative curvature, and therefore has an overall curvature of zero. Lamellar liquid crystalline phases have zero monolayer curvature. A microemulsion

is a dynamic system, with surfactant molecules and oil and water molecules moving between domains and rearranging. The microemulsion aggregates are free to swell or shrink by solubilisation of more or less oil or water from the coexisting phases, and the curvature of the monolayer in the isotropic microemulsion is representative of the preferred monolayer curvature. The monolayer curvature is related to the relative sizes of the surfactant head and tail groups, which are affected by the addition of salt, change in temperature, and the nature of the oil.

The excess oil or water phases only exist in a microemulsion system when there are comparable volumes of each. The systems required for this project have a very small volume of oil in comparison with the volume of water, so no excess oil phase will be seen at the surfactant concentrations in use. All the oil will be solubilised in the surfactant aggregates in the continuous phase.

A single phase microemulsion stabilised by polyoxyethylene surfactants exists only within a certain temperature range. Below this temperature range the emulsion separates into oil solubilised in an aqueous surfactant solution and an excess oil phase. Above the temperature range, the microemulsion separates into water solubilised in an oil surfactant solution, and an excess water phase [3]. These solubilisation phase boundaries are known as the cloud and haze points for oil-in-water and water-in-oil systems respectively. Between the two boundaries lies an isotropic microemulsion. According to Fletcher [3] droplets at the boundaries generally behave as hard spheres, with the droplet radius indicating preferred monolayer curvature. Since I am aiming to produce oil-in-water droplets with ultra-low interfacial tension, the systems should be on or just below the lower boundary of the single phase microemulsion.

5.5 Temperature-insensitive Microemulsions

The choice of which systems to study was determined by the availability and cost of the components of each system, and by the results given in the literature. Sucrose monododecanoate features in a number of temperature-insensitive systems as noted in the Introduction [4], but it is an expensive surfactant. For these preliminary investigations, it

seemed prudent to choose less expensive surfactants. Similary, the system containing SDS and $C_{12}E_3$ [5] which is mentioned in the Introduction was not investigated because of the expense of purchasing $C_{12}E_3$. This system is very similar to the AOT and $C_{12}E_5$ system reported by Binks *et al.* [6], and so I chose to study just one of these systems.

Unless otherwise stated, the surfactant solutions were prepared as described in 'Microfluidics'. The microemulsions were prepared by pipetting approximately 6 ml of surfactant solution into a small vial, and adding 3 drops of oil from a pipette. The mixtures were shaken manually as required.

5.6 CTAB/Brij-58/Butanol/Heptane

Short chain lipophilic alcohols (called cosurfactants) work with surfactants to solubilise otherwise immiscible liquids. Like surfactants, they partition between oil and aqueous phases to stabilise microemulsions by controlling the bending elasticity of the interfacial layer [7]. At a fixed molar ratio of disperse phase to surfactant, a threshold amount of cosurfactant is required to stabilise the dispersion, and droplet diameter is controlled by the cosurfactant content. Increasing the amount of cosurfactant decreases the droplet size, and therefore increases the preferred monolayer curvature for an oil-in-water microemulsion, and decreases the preferred monolayer curvature for a water-in-oil microemulsion.

Mitra *et al.* [7] have studied a mixed surfactant system containing CTAB and Brij-58 (Polyoxyethylene (20) cetyl ether). The phase behaviour of water-in-oil microemulsions stabilised by mixtures of these surfactants, at different mixing ratios and different temperatures was investigated. The authors present their results in phase diagrams at a constant molar ratio of water to surfactant of 55.6, which is equal to a 1 mol dm^{-3} aqueous surfactant solution. Observation of the effects of butanol on the phase behaviour of the pure surfactant systems provides a good indication of how the mixed system will behave. Addition of 1-butanol to a mixture of CTAB, water and heptane changed the nature of the mixture from being viscous, to being biphasic. The two phases were likely to be an oil phase and a reverse micellar phase. Upon addition of more alcohol, the mixture became monophasic, with the curvature of the interfacial layer tending towards zero. The effect of

temperature on the phase behaviour of the CTAB and Brij-58 systems was observed. The single phase microemulsion region decreased in size with increasing temperature in the CTAB stabilised system, and increased in the Brij-58 stabilised system [7]. An equimolar mixture of CTAB and Brij-58 stabilised a microemulsion that appeared to be insensitive to temperature [7]. The phase diagram for this system is shown in Figure 6.

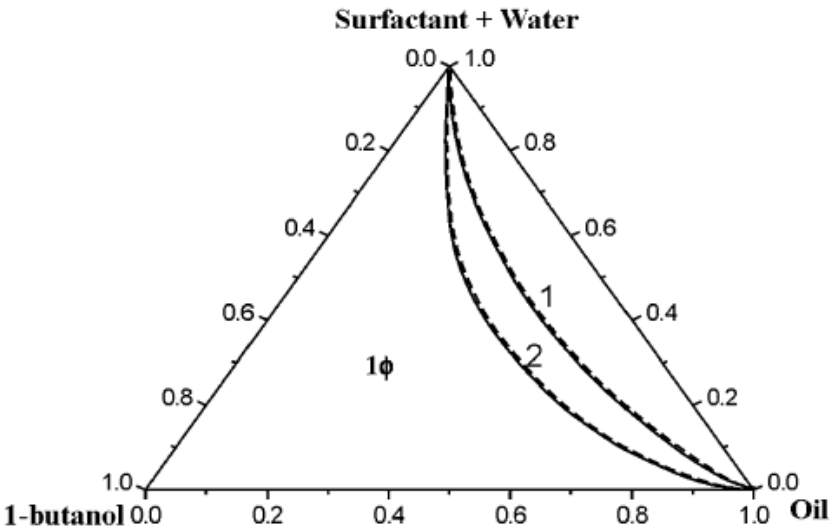

Figure 6: Phase diagram of CTAB/Brij-58/water/1-butanol/oil systems at 293 K (solid line) and 323 K (broken line). Molar ratio of surfactant to water = 1:55.6, and molar ratio of CTAB to Brij-58 = 1:1. Line labelled 1 refers to system with heptane, 2 refers to system with decane. 1φ indicates a single-phase microemulsion [7].

CTAB is a hydrophilic surfactant that spontaneously forms normal micelles in water (with positive interfacial film curvature) [8]. Palazzo *et al.* have found that adding a small amount of pentanol decreases the interfacial film curvature, but that it remains positive. It is reasonable to assume that a temperature-insensitive oil-in-water microemulsion could be formed with CTAB, Brij-58 and a small amount of butanol, or none at all. Addition of butanol presumably lowers the interfacial tension of the system by approaching a preferred curvature of zero.

The influence of alcohol in the microemulsion system can be explained as follows [7]. Butanol has limited aqueous solubility, so the alcohol molecules remain distributed between the oil phase and the oil-water interface. To stabilise a water-in-oil dispersion, a

threshold amount of butanol is required in the oil and at the interface. The distribution constant is a function of temperature. With increasing temperature the number of moles at the Brij-58 interface increased, and decreased at the CTAB interface. At the same time, the number of moles in the oil phase increased for CTAB and decreased for Brij-58. This explains the negligible effect of temperature on the phase boundaries of the mixed surfactant system. Increasing the oil content disrupts the equilibrium of the w/o system, and more butanol must be added to restore the monophasic region. The number of moles of alcohol at the interface did not follow a trend with the ratio of Brij-58 to CTAB in the surfactant mixture. There was more alcohol at the interface for the pure Brij-58 systems than for the pure CTAB systems.

5.6.1 Formulating the Microemulsions

In the paper by Mitra *et al.* [7] the combination of chemicals for each microemulsion system is given as follows:

Total surfactant to water molar ratios are kept constant at 1:55.6, which is equivalent to a 1 mol dm^{-3} aqueous surfactant solution. CTAB to Brij-58 molar ratios are kept constant at 1:1. A variety of oil to (water + surfactant) weight ratios are given. I have chosen to study emulsions along the 1:9 line (see Figure 6), since I only require a small amount of oil in the emulsions I am preparing. Since the volume of oil per mixture is reduced, the amount of surfactant will also have to be reduced to avoid completely dissolving the oil in the solution. Butanol to (water + surfactant) weight ratios are given. I will study microemulsions ranging from 0.1:0.9 to 0.5:0.5. The ratios of surfactant to butanol as are given in the paper in terms of weight rather than moles, so I will calculate the molar ratios here.

Table 6 gives formulations for 50g of solution. The span of weight ratios shown in Table covers the phase boundary from an oil-in-water microemulsion to a single phase microemulsion, and should provide an indication of the location of the interfacial tension minimum.

Each solution prepared contained 50 mL of surfactant solution. Butanol was added to the solution after it had been measured out. The smallest mass of butanol that can be measured out easily was approximately 0.01 g (the mass of one droplet from a pipette). It was be convenient if the smallest mass of butanol required was no smaller than this amount. For this reason, I used a 3 milli-molar surfactant solution, so that the minimum mass of butanol in the mixture was 0.029 grams. The molarity of the surfactant solution refers to the combined number of moles of CTAB plus moles of Brij-58 per volume of water.

Table 6: Formulations of surfactant solutions with varying weight fraction ratios of surfactant solution to butanol.

Solution label	A	B	C	D	E
Weight fraction ratio of surfactant solution to butanol	0.9 : 0.1	0.8 : 0.2	0.7 : 0.3	0.6 : 0.4	0.5 : 0.5
Molar ratio of butanol to CTAB + Brij-58	1 : 2.62	1 : 5.89	1 : 10.10	1 : 15.70	1 : 22.43

Butanol was obtained from Alfa Aesar, with a minimum purity of 99%, and used as received. Brij-58 was obtained from Sigma. CTAB was obtained from Aldrich. The sample I used had been recrystallised 3 times from ethanol and acetone. Heptane was used as received from Sigma, with a minimum purity of 99%.

5.6.2 Results

All of the dispersions formed with the mixed CTAB/Brij-58 system behaved in the same way. The heptane was not easily dispersed in any of the solutions. It is possible that a very small amount of deformation was possible at temperatures above 35ºC, but the optical system in use makes it difficult to assess whether the apparent deformation was the effect of diffraction rings, or whether the droplets were indeed being deformed.

The ratio of butanol to CTAB + Brij-58 in the emulsions had no visible effect on the mixtures.

It is possible that the total surfactant concentration was not high enough. However, the concentration of both CTAB and Brij-58 in the total mixture was above the c.m.c. for each surfactant, and as previously mentioned the 'critical microemulsion concentration' is normally in the region of the c.m.c. For this reason I did not continue to investigate this system.

5.7 AOT/NaCl/Brij-35/Butanol/ Eucalyptus Oil

Mitra *et al.* have investigated the phase behaviour of a mixed surfactant system containing AOT, Brij-35 (Polyoxyethylene (23) lauryl ether) and butanol [9]. According to the authors the role of the alcohol cosurfactant includes the prevention of formation of gels and liquid crystals, reduction of interfacial tension, and influencing the solubility of the aqueous and oil phases by its partitioning between the phases. Their results show that eucalyptus oil is immiscible in water but quite miscible in 1-butanol. A 1:1 (by weight) mixture of AOT and Brij-35, eucalyptus oil and 1-butanol forms a solution. Similar behaviour is exhibited by the AOT/Brij-35 mixture, water and 1-butanol. It should therefore be possible to make an oil-in-water two phase microemulsion using the 1:1 AOT/Brij-35 system, with a small amount of butanol. It was found that the largest regions of single phase microemulsion were formed for surfactant to cosurfactant ratios of 1:1 by weight. However, since this is likely to be a water-in-oil microemulsion [9] rather than the oil-in-water droplets that will be suitable for optical trapping, it will be necessary to reduce the amount of butanol in the system to ensure that the interfacial film curvature remains positive.

The authors report that increasing the amount of butanol in the system reduced the extent of the monophasic zone. This can be likened to the emulsification failure noted by Palazzo *et al* [8]. Increasing the amount of cosurfactant reduces the curvature of the interfacial film until it reaches zero curvature at the formation of a monophasic microemulsion. Further addition of cosurfactant leads to the curvature becoming negative and the formation of reverse micelles swollen with water. The mixed AOT/Brij-35 system showed some

temperature insensitivity, in that the monophasic zone changed little on increasing the temperature from 303 to 323 K.

Table 7 shows the formulations of surfactant solutions with varying concentrations of surfactant, and a surfactant to cosurfactant weight ratio of 1:1.

AOT (minimum purity 99%), NaCl (minimum purity 99.5%), Brij-35 and heptane (minimum purity 99%) were supplied by Sigma and used as received. Butanol (mimimum purity 99%) was obtained from Alfa Aesar and used as received. Eucalyptus oil (80-85% purity) was used as received from Sigma.

Table 7: Components of microemulsions with varying concentration of surfactant (given by concentration of AOT). The total volume of each solution is 50 ml. The concentration of NaCl in each solution is 0.2 mol dm $^{-3}$.

Solution label	A	B	C
Concentration of AOT (mol dm^{-3})	5 x 10^{-4}	5 x 10^{-3}	5 x 10^{-2}

5.7.1 Results

The microemulsion made with Solution A required vigorous shaking to disperse the eucalyptus oil. Very large droplets were visible in the sample. The sample was heated from 26 to 50ºC. A very slight increase in deformability was noticed at around 34ºC. Below this temperature, no deformation was seen. Deformability decreased again above approximately 45ºC.

The oil dispersed very easily in Solution B, forming a milky white emulsion with very little agitation. The sample was heated from 25º to 28ºC, at which point the droplets in the sample seemed to disappear. It is likely that they dissolved into the aqueous phase. I noticed that the eucalyptus oil droplets behaved quite differently to droplets of heptane, presumably because of the difference in refractive index and density. It was more difficult

to focus the trap to ensure that the eucalyptus oil droplets were not simply pushed away by the scattering force. The droplets also seemed to stick to the cover glass after a few minutes of being held in the trap. It was not possible to move them freely once this had happened.

The oil was dispersed instantly (without agitation) in Solution C, and dissolved shortly after being dispersed. More oil was added to the solution until it appeared blue and slightly cloudy. A sample was taken at this point. No droplets were seen in the sample, and there was no change in the appearance between 25º and 50ºC. After being left overnight, the sample became milky white. Large aggregates appeared in the sample, and completely dissolved at 40ºC. The vial was placed in the oven to warm to around 50ºC. It returned to a bluish, slightly cloudy dispersion. These experiments were repeated with a second vial of solution, and the same behaviour was observed. The system is clearly not temperature insensitive at these higher surfactant concentrations.

In order to ascertain what a suitable surfactant concentration would be, several more solutions were made up, with AOT concentrations between those of Solution B and Solution C. The formulations are shown in Table 8.

Table 8: Components of microemulsions with varying concentration of surfactant (given by concentration of AOT). The total volume of each solution is 25 ml. The concentration of NaCl in each solution is 0.2 mol dm^{-3}.

Solution Label	D	E	F	G
Concentration of AOT (mol dm^{-3})	6 x 10^{-3}	8 x 10^{-3}	1 x 10^{-2}	3 x 10^{-2}

At this point in the project, the Spectra-Physics Millennia II laser that I had been using failed. The maximum achievable power had been decreasing slowly for several days. The laser was swapped for a Laser Quantum Opus, with a wavelength of 532 nm and a maximum power of 2 W. I set the laser at 500 mW to ensure that deformation would be observed if it was possible.

5.7.2 Results

Eucalyptus oil dispersed quite easily in solution D. No deformation of the droplets was possible, and there was no change in appearance, behaviour or deformability on heating the sample from 25ºC to 50ºC. Similar results were obtained with Solution E.

A small amount of deformation was possible for the microemulsion made with solution F. This was unexpected. There was no change in deformability with increasing temperature from 25ºC to 50ºC.

No droplets were seen in the sample of microemulsion prepared with solution G. The microemulsion was bluish, cloudy and quite viscous. Some very small structures were seen in the sample, which could have been liquid crystal domains.

From these results I concluded that the ideal AOT concentration was 8 x 10^{-3} mol dm^{-3}, as in solution E.

5.7.3 Reducing the Interfacial Tension

Since this system displayed apparent temperature insensitive deformation I tried to further reduce the interfacial tension to find the optimum location in the phase diagram. The authors found that the 1:1 ratio of AOT to Brij-35 provided some temperature insensitivity, so I did not alter this ratio.

Increasing the salt concentration in a pure AOT-stabilised microemulsion system has the effect of changing the system from an oil-in-water to a water-in-oil microemulsion, with the associated region of low interfacial tension between these two phases [10-12]. The effect of concentration of NaCl in a pure Brij-35 stabilised system is much smaller [9], so it can be assumed that the behaviour of the mixed system will largely follow that of the pure AOT system. The authors noted that the extent of the monophasic region increased with increasing NaCl concentration up to 0.2 mol dm^{-3}. Further increase resulted in a decrease of the area of the monophasic region. This suggests that the system exists as an oil-in-water or three phase microemulsion up to salt concentrations of 0.2 mol dm^{-3}, and thereafter

changes to a water-in-oil microemulsion. For this reason I will not alter the concentration of NaCl in the surfactant solutions. However, the effect of temperature on the mixed surfactant system is most pronounced for the 0.2 molar solution, so the temperature insensitivity of the system may be reduced by working at these salt concentrations.

Butanol changes the curvature of the interfacial monolayer, and therefore changes the interfacial tension, reaching a minimum at the crossover point between the oil-in-water and water-in-oil phases. A monophasic zone was observed in the ternary water/surfactant/eucalyptus oil system, but only for low water content, indicating a water-in-oil microemulsion. The extent of the monophasic zone decreased in the mixed surfactant system with increasing cosurfactant content. This suggests a water-in-oil phase was dominating the phase diagram, with the decreasing curvature of the interfacial monolayer. For this reason, I have varied the surfactant to cosurfactant ratios from 1:0 to 1:1, in 0.25 increments (1:0, 1:0.25, 1:0.5, 1:0.75, 1:1). Since the 8 x 10^{-3} molar AOT solution dispersed the eucalyptus oil very easily, I will use this concentration of surfactant in the next solutions. Table 9 shows formulations of surfactant solutions with constant surfactant concentration, and varying weight ratios of surfactant to cosurfactant.

Table 9: Components of microemulsions with varying ratios of surfactant to cosurfactant. The total volume of each solution is 25 ml. The concentration of NaCl in each solution is 0.2 mol dm^{-3}.

Solution label	H	I	J	K
Ratio of surfactant to cosurfactant (by weight)	1 : 0.00	1 : 0.25	1 : 0.50	1 : 0.75

5.7.4 Results

The eucalyptus oil was very easily dispersed in each of the solutions. Very slight deformation was possible with solutions H, I and K. The droplets in the microemulsion formed with Solution J were slightly more deformable, so it seems that this is the ideal

microemulsion composition. However, given that the extent of deformation was so small as to be difficult to detect (see Figure 7), I concluded that this system would not provide low enough interfacial tensions.

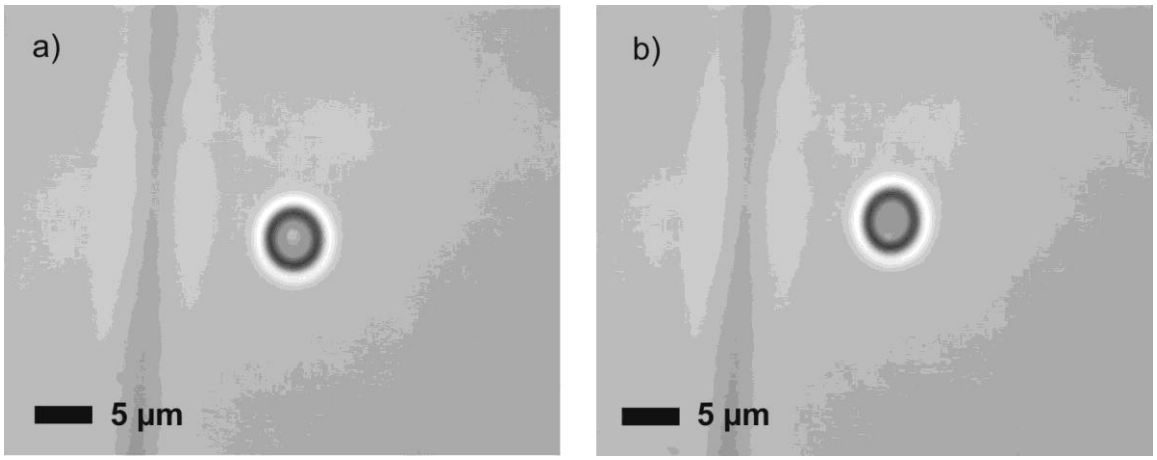

Figure 7: a) Droplet held in a single trap; b) Same droplet slightly deformed by moving two traps apart.

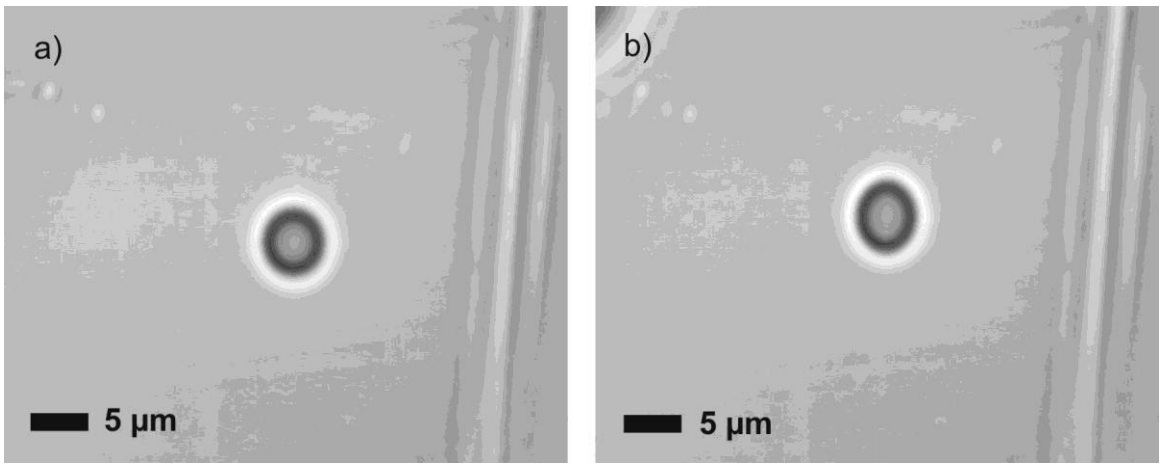

Figure 8: a) Droplet held in a single trap; b) Same droplet slightly deformed by moving two traps apart. Maximum deformation is greater than for solution H.

5.8 AOT/NaCl/$C_{12}E_5$/Heptane

Binks *et al.* have reported the formation of a temperature-insensitive microemulsion formed with a mixed surfactant system containing AOT and pentaethylene glycol

monododecyl ether ($C_{12}E_5$) [6]. The temperature dependence of the preferred interfacial monolayer curvature is similar in magnitude but opposite in sign for AOT and $C_{12}E_5$.

The molar ratio of solubilised component per surfactant is related to droplet radius, r, in Equation (5.1) [6]:

$$r = \left(3\frac{V}{A}\right)\left\{\left[\text{dispersed component}\right]/\left(\left[\text{surfactant}\right] - c\mu c\right)\right\} + \delta \qquad (5.1)$$

where V is the molecular volume of the dispersed component, A is the area per surfactant molecule on the curved droplet surface, $c\mu c$ is the 'critical microemulsion concentration' (surfactant monomer concentration in the continuous phase required for microemulsion formation), and δ is the thickness of the surfactant monolayer. Equation 1.1 predicts that the microemulsion droplet radius is proportional to the extent of solubilisation, and this has been observed experimentally [13].

The oil-water interfacial tension, measured at the planar interface separating the microemulsion from the excess water or oil phase scales approximately as $1/r^2$ [6], this value being at a minimum when the droplet radius is highest. Since monolayer curvature is inversely proportional to droplet radius, the interfacial tension is proportional to monolayer curvature. The interfacial tension therefore passes through a minimum value at the phase inversion when the preferred monolayer curvature is close to zero [6].

Karlström presented a theory for the phase behaviour of non-ionic, polyoxyethylene type surfactants with water [2]. Conformational changes in the polyoxyethylene chain of the surfactant with increasing temperature cause interactions with water to become less favourable, leading to the separation of phases, and eventually to the formation of reverse micelles.

Binks *et al.* presented a phenomenological model for finding the composition of a temperature insensitive microemulsion based on mixtures of AOT, NaCl and $C_{12}E_5$ [6]. For systems with comparable volumes of oil and water, the radius of a microemulsion droplet

is proportional to the extent of solubilisation. If the preferred droplet radius is labelled r_{nat}, the preferred monolayer curvature is given by $1/r_{nat}$. For single surfactant systems the preferred monolayer curvature is linearly dependent on temperature around the PIT:

$$1/r_{nat} = sT + i \tag{5.2}$$

where s and i are the slopes and intercepts of the plot of $1/r_{nat}$ against temperature. For a mixed surfactant system, with weight fraction X of ionic surfactant in total surfactant, Binks *et al* assume that s and i vary with X. It is therefore possible to calculate a value for X corresponding to temperature insensitivity (X^*) by noting that $s = 0$ for $X = X^*$. Since oil-water interfacial tension scales approximately as $1/r_{nat}$, it is also possible to calculate the interfacial tension for different values of X (see [6] for more details). The value of X^* was found to be 0.62. The authors noticed that a higher concentration of NaCl reduced the interfacial tension in the temperature-insensitive region, because the addition of salt to an ionic surfactant system changes the PIT. As a result, the optimum mixture for temperature insensitivity with low interfacial tension is a value of X of 0.62, and an NaCl concentration of 0.1 mol dm^{-3}. A range of total surfactant concentrations will be tested to find the lowest interfacial tension. It is important to avoid high surfactant concentrations that will lead to the formation of liquid crystal regions or isotropic microemulsions. These tend to be viscous liquids, and spherical droplets will be absent. Previous work in this project with AOT was carried out with a surfactant concentration of 1 mM, and this concentration seems ample for the formation of droplets with very low interfacial tension. However, the effect of mixing surfactants could require higher concentrations, so I will begin at 0.5 mM AOT (giving a total surfactant concentration of just over 1 mM) and study a range of concentrations.

Some important results on interfacial tension minima were presented by Aveyard *et al.* [11]. For AOT and NaCl containing systems, the following should be noted:

a) At a fixed salt concentration and temperature, increasing the surfactant concentration decreases the interfacial tension until the CMC is reached, at which point the tension remains constant at γ_C;
b) At low salt concentration surfactant resides in the aqueous phase, even above the CMC, and transfers to the oil phase at high salt concentration to form a water-in-oil microemulsion. The aqueous phase is left close to the CMC with no micelles present;
c) Varying temperature rather than salt concentration has similar effects to those in b), but surfactant resides in the oil phase at low temperatures (with the aqueous phase at the CMC), and in water above the CMC at high temperatures.

The presence of an interfacial tension minimum at a particular salt concentration and temperature can be explained by the dissociation of ionic surfactant molecules in the aqueous phase. A minimum in tension occurs for a salt concentration such that the degree of dissociation of surfactant molecules in the micelles and at the planar interface between the excess water phase and microemulsion phase is equal. A monolayer at a plane surface is almost completely associated, so the micelles prefer to reside in the oil phase where they too will be associated [11]. Tension minima occur with a phase transition from oil-in-water to a water-in-oil microemulsion. A similar explanation exists for the tension minimum observed at a certain temperature. The slope of tension against temperature is a function of the relative magnitudes of the entropy of surface formation per unit area and the entropy of micelle formation per moles of surfactant. The entropy associated with moving a mole of neutral (associated) surfactant is equal to the molar entropy of micelle formation at the tension minimum [11].

AOT (minimum purity 99%), NaCl (minimum purity 99.5%), $C_{12}E_5$ (minimum purity 99%) and heptane (minimum purity 99%) were obtained from Sigma and used as received.

Table 10: Components of microemulsions with varying NaCl concentrations. Each solution has a total volume of 100 ml.

Solution label	1	2
Concentration of NaCl (mol dm^{-3})	0.08	0.1
Concentration of AOT (mol dm^{-3})	5 x 10^{-4}	5 x 10^{-4}

5.8.1 Results

Neither of the two surfactant solutions in Table 10 dispersed the heptane quickly, but if the mixtures were left to equilibrate a bluish microemulsion was formed. Both microemulsions apparently exhibited very small deformation, which may well have been an optical effect. No change in phase behaviour or interfacial tension was seen on heating the samples from 25ºC to 50ºC. The system seemed to be temperature-insensitive but the interfacial tension was too high. Higher surfactant concentrations were studied. Table 11 shows formulations of surfactant solutions with varying surfactant concentrations, and constant NaCl concentration.

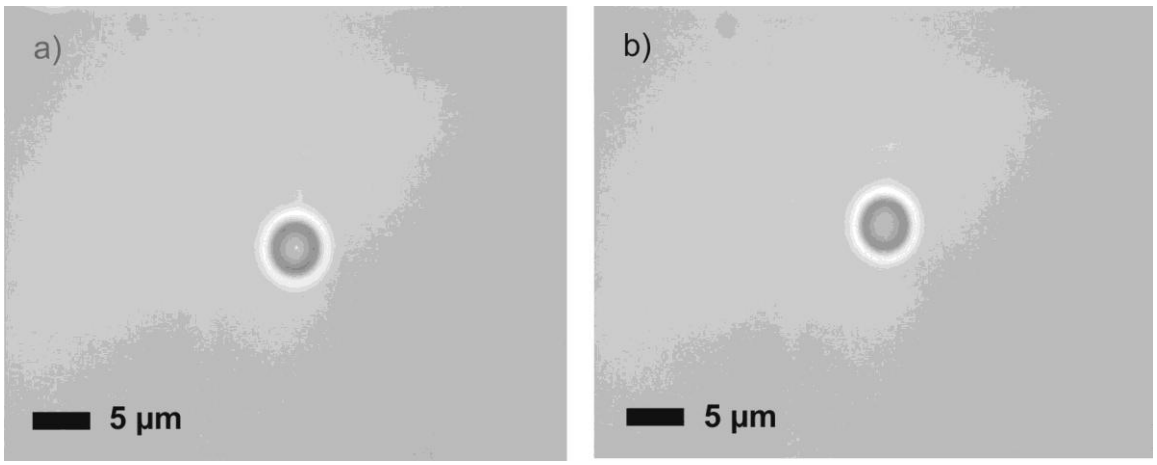

Figure 9: a) Droplet held in single trap; b) Same droplet, showing negligible maximum deformation.

Table 11: Components of microemulsions with varying surfactant concentrations (given by AOT concentration). The concentration of NaCl in each solution is 0.1 mol dm^{-3}.

Solution label	I	II	III
Concentration of AOT (mol dm^{-3})	1 x 10^{-3}	5 x 10^{-3}	1 x 10^{-2}

5.8.2 Results

Unlike solutions 1 and 2, Solutions I, II and III were not transparent in appearance. They were all slightly cloudy. The reason for this is likely to be a small amount of aggregation between the surfactant molecules at these higher concentrations. I was concerned that this would affect the emulsification behaviour of the surfactants, so each solution was sonicated for several hours before being used.

Agitation was required to disperse heptane in Solution I, but a stable microemulsion was formed once the oil was fully dispersed. The sample was heated from 25ºC to 50ºC, and deformation of the droplets was possible throughout the temperature range. Figure 10 shows examples of the deformation achieved.

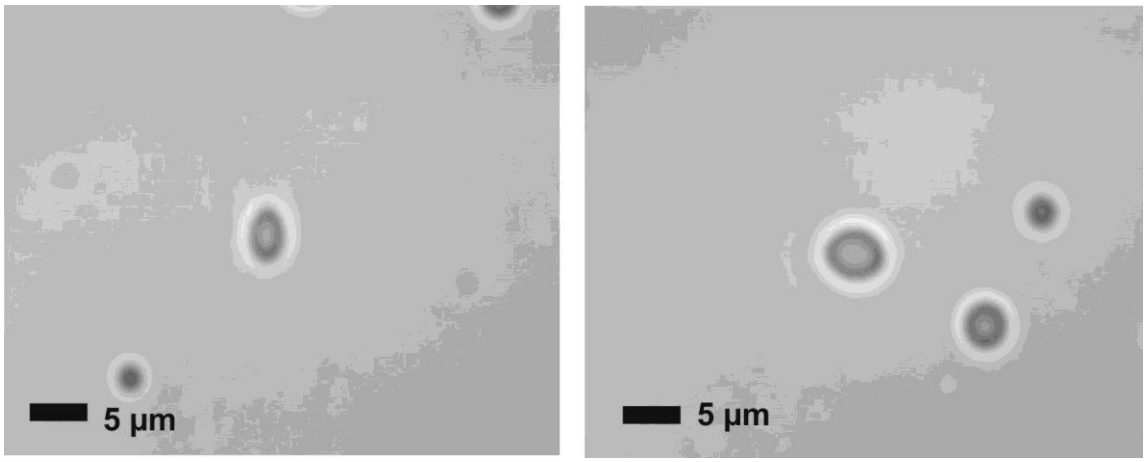

Figure 10: Deformation of microemulsion droplets made with solution I.

Heptane dispersed instantly in Solution II, and the droplets proved to be very deformable. Comparison with the deformation of droplets made with the pure AOT system shows that the interfacial tension in the mixed system is not as low, but it was certainly low enough to produce large deformations. The sample was heated from 25ºC to 50ºC, and no change in deformability was seen with increasing temperature. Examples are shown in Figure 11.

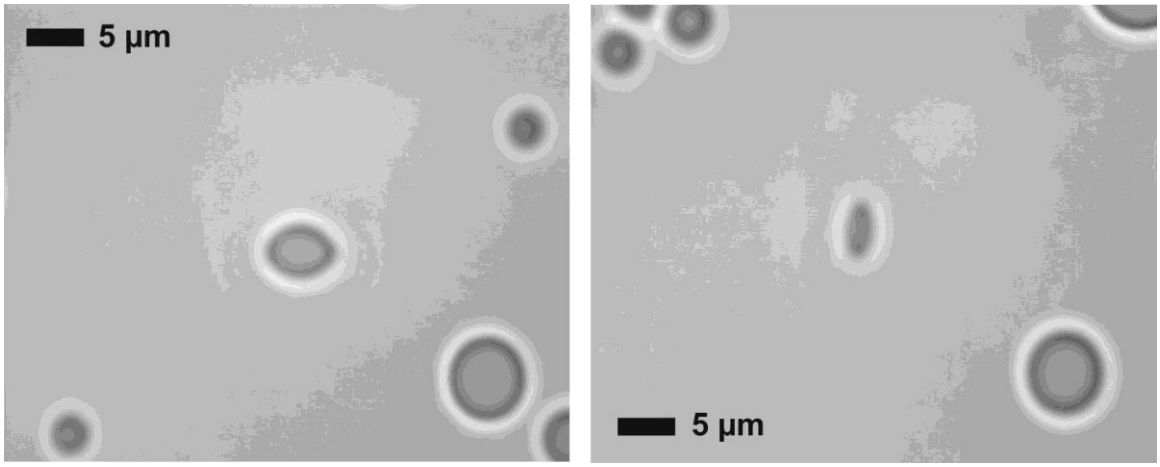

Figure 11: Deformation of microemulsion droplets made with Solution II.

It was possible to pull droplets apart, but it was unclear whether threads were formed between the droplets. I did not observe any droplets being drawn back in when released from the trap. The microemulsion made with Solution III produced very similar results to Solution II.

Solutions I, II and III were tested with the Opus laser, at a higher power than Solutions 1 and 2. To check whether the increased deformability of Solutions I, II and III was the result of the chemical composition rather than the higher laser power, Solution 2 was reexamined with the new laser. The droplets were deformed slightly more with the higher laser power, but not sufficiently that the positive results with Solutions I, II and III should be discounted.

5.9 Alkyl Glucoside Surfactants

Temperature-insensitive microemulsions can be achieved by using sugar surfactants such as alkyl glucosides. Alkyl glucosides (C_mG_n) are sugar surfactants with m carbons in a hydrocarbon chain, and n glucose units in the hydrophilic head group [14]. The hydration of headgroups in these surfactant molecules display weak temperature dependence, which is an advantage when searching for temperature-insensitive microemulsions, but can be a problem when trying to alter the curvature of the monolayer in microemulsion systems [14]. This behaviour contrasts that of polyoxyethylene glycol type surfactants.

Penders and Strey [15] have studied the effects of adding 1-octanol to a ternary microemulsion system containing water, *n*-octane and C_8E_5. The hydrophobic alcohol acts as a cosolvent to make the oil more polar, and acts as a cosurfactant to increase the hydrophobicity of the surfactant mixture. These results also apply to C_mG_n systems [14].

Adding a hydrophobic cosurfactant such as 1-octanol to a ternary system of water, *n*-octane, and C_8G_1 causes a phase inversion from an oil-in-water microemulsion to a water-in-oil microemulsion, with the characteristic region of ultra low tension associated with phase inversion [14]. The middle region between the normal and reverse microemulsions is either a microemulsion phase coexisting with excess water and oil phases, or, at sufficiently high surfactant concentrations, a single phase microemulsion. For the purposes of this project, it is important to avoid the one-phase microemulsion region to ensure that the oil exists as droplets in the surfactant solution. Low surfactant concentrations will be used. Increasing the volume fraction of the cosurfactant in the total surfactant (surfactant plus cosurfactant) mixture changes the structure of the microemulsion from oil-in-water droplets, through a bicontinuous structure, to water-in-oil droplets [14]. The addition of 1-octanol changes the curvature of the surfactant monolayer from positive to negative, with the crossover point occurring at a volume fraction of 0.27 [16].

The phase behaviour of alkyl glucosides is different to that of polyoxyethylene glycol surfactants [16]. The binary water-alkyl glucoside system displays a miscibility gap which does not change with temperature. In contrast, polyoxyethylene glycols do not show a

miscibility gap with water. A Krafft point is also observed for some C_mG_n/water systems, where the surfactant crystallises out of solution to form a cloudy mixture. Alkyl glucosides are nearly insoluble in *n*-alkanes, unlike the alkane/C_iE_j systems, which are usually completely miscible. Despite these differences, the phase behaviour of the ternary and quaternary microemulsion systems show many similarities [16].

A water, *n*-octane and *n*-octanol system displays a water-in-oil microemulsion region, and a water, *n*-octane and *n*-Octyl β-D-Glucopyranoside (C_8G_1) system displays an oil-in-water region. A phase inversion is expected to exist in a mixture of these systems [16].

The addition of an alcohol cosurfactant to an alkyl glucoside system acts in the same way as changing the temperature of a polyoxyethylene glycol system [15].

Figure 12 [17] shows a section through the phase tetrahedron of a quaternary system of water (A), oil (B), non-ionic surfactant (C) and alcohol (D) at constant temperature and equal volume fractions of oil and water, i.e. $\phi = \frac{V_B}{V_A + V_B} = 0.5$. The diagram represents the different phases in the system as a function of the composition of the interface, $\delta_{V,i} = \frac{V_{D,i}}{V_{C,i} + V_{D,i}}$, and the total surfactant volume fraction $\phi_{C+D} = \frac{V_C + V_D}{V_A + V_B + V_C + V_D}$. Increasing the total surfactant volume fraction in the system changes the three phase region (**3**) (microemulsion coexisting with excess oil and water phases) into a one-phase region (**1**). This forms a 'fish' shape which is characteristic of many microemulsion systems. At low volumes of alcohol in the interfacial layer, the system exists as an oil-in-water microemulsion (**2**). At high volumes of alcohol, the system exists as a water-in-oil microemulsion ($\bar{\mathbf{2}}$). X% denotes the minimum amount of surfactant required to solubilise equal amounts of oil and water. The diagram demonstrates the changing of the interfacial monolayer curvature from positive to negative with increasing amounts of alcohol in the interfacial layer.

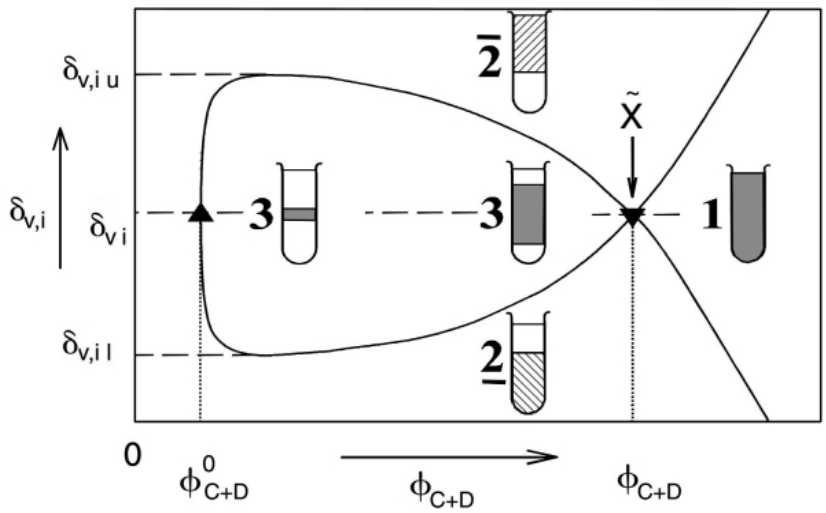

Figure 12: Schematic phase diagram at constant temperature and a constant water-to-oil volume fraction of $\varphi = 0.5$ for the quaternary system water/oil/surfactant/alcohol as a function of the total surfactant volume fraction φ_{C+D} and the composition of the interface $\delta_{V,i}$ [17].

Stubenrauch *et al* have made a detail study on the role of alcohol in the interfacial layer [18]. When incorporated into the interfacial monolayer, alcohol acts to change the curvature of the layer. Hydrophobic alcohols will be incorporated into the oil and cause the oil to become more polar, encouraging a hydrophilic surfactant to partition more into the oil.

Although it is possible to form a temperature-insensitive microemulsion with alkyl glucosides and alcohol cosurfactants [19-20], the high price of the pure sugar surfactants means that I have sought alternatives to these systems.

Ryan *et al.* have investigated mixed surfactant systems containing alkyl glucosides and polyoxytheylene glycol ethers [22]. Increasing the fraction of sugar surfactant in the total surfactant mixture raises the temperature at which the three phase region exists, and also increases the temperature range over which the three phase region exists. There is also a ‘temperature insensitive’ section of the three phase region, the extent of which increases with increasing fraction of sugar surfactant in total surfactant. Although the three phase

region does indeed exist across a broad temperature range, the lower edge of the three phase region, adjacent to the oil-in-water microemulsion, is still sharply defined by temperature and total surfactant concentration.

5.10 Plantacare/Cetiol S/GMO

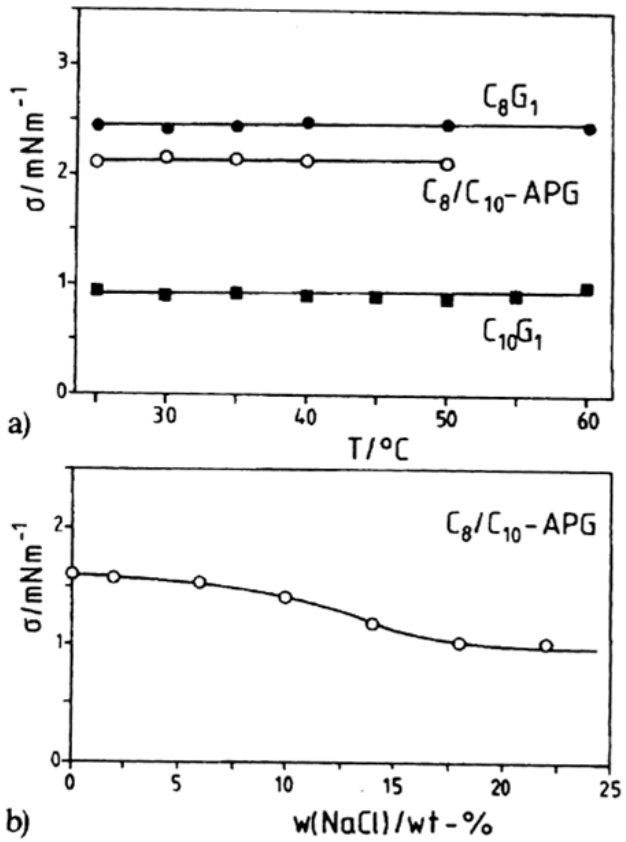

Figure 13: a) Negligible temperature dependence of different alkyl glucoside surfactant systems; b) Interfacial tension as a function of NaCl concentration for an aqueous solution of C_8/C_{10} alkyl polyglucoside with decane at 40ºC [23].

Von Rybinski *et al* have reported a very temperature-insensitive microemulsion system consisting of C_{12}/C_{14} alkyl glucosides, glyceryl monooleate and dioctyl cyclohexane [23]. These chemicals are available as Plantacare 1200 UP, GMO and Cetiol S respectively. Figure 13a shows the interfacial tension between water and decane, in systems stabilised with different alkyl glucosides. It is clear that the pure surfactant systems are very temperature-insensitive, and that increasing the alkyl chain length reduces the plateau value

of the interfacial tension. Figure 13b shows the effect of adding salt to the alkyl polyglucoside system. A small reduction in interfacial tension is observed with increasing concentration of NaCl.

The authors made a model emulsion system with which to compare a range of co-emulsifiers. Figure 14 shows the phase diagram for the model system. A translucent microemulsion is formed for mixing ratios of alkyl polyglucoside (APG) to glyceryl monooleate (GMO) between 6:4 and 7.5:2.5. To ensure that a one-phase microemulsion was formed, the total surfactant concentration was 15%. The addition of GMO to the alkyl glucoside surfactant has the same effect as adding alcohol to polyoxyethylene glycol surfactants, in that it brings about a phase inversion from an oil-in-water to a water-in-oil microemulsion. The vertical line separating the o/w and o/w ME regions shows that the change between these regions is independent of temperature and dependent only on the fraction of GMO in total surfactant.

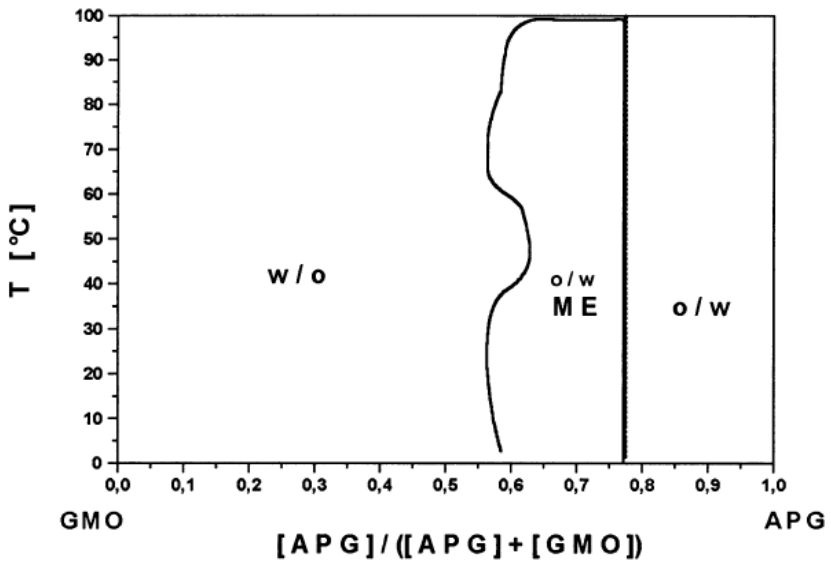

Figure 14: Phase diagram of microemulsion system containing C_{12}/C_{14} alkyl polyglycoside and GMO, 42.5% water and 42.5% dioctylcyclohexane [23].

Assuming that the value of 15% for the concentration of the surfactant solution is given in terms of weight, and that the total volume of each emulsion mixture was 50 ml, I can calculate the molar concentration of the surfactants in the solution. It is unlikely that total

surfactant concentration will have a great effect on the phase behaviour of the microemulsion, other than producing a 3-phase or 1-phase microemulsion region between the two 2-phase regions.

Since the amount of oil in the microemulsion system will be very small compared to the volume of surfactant solution, I will ignore the oil when calculating concentrations of surfactants in the whole system.

Plantacare 1200 UP is an aqueous solution of $C_8 - C_{16}$ alkyl glucosides. I will assume that the average molecular mass of the alkyl glucoside (active material) content is the same as that of lauryl glucoside (C_{12} alkyl glucoside), which is 348 g mol^{-1}. The product data sheet supplied with the Plantacare 1200 UP states that the solution consists of 50.7% active matter and 49.3% water. This is equivalent to a 1.56 mol dm^{-3} solution of C_{12} alkyl glucoside. GMO is supplied as a paste with a minimum 90.0% monoglyceride content, and a molecular mass of 356.54 g mol^{-1}.

The microemulsions prepared in the paper contain equal volumes of oil and water. The authors note that for total surfactant concentrations below 10% a three phase microemulsion exists. I will be using a much smaller fraction of oil in the microemulsions I prepare, and I will make a surfactant solution that is lower in concentration.

5.10.1 Calculating Molar Ratios

Ratios of APG to GMO are given in the paper in terms of the number of moles of APG, n_{APG}, as a fraction of the total number of moles of surfactant, $n_{APG} + n_{GMO}$:

$$X = \frac{n_{APG}}{n_{APG} + n_{GMO}} \tag{5.3}$$

where X is the ratio given in the paper.

Table 12: Formulations of surfactant solutions with varying APG to GMO ratios.

Solution Label	1a	2a	3a	4a	5a
$X = \frac{n_{APG}}{n_{APG} + n_{GMO}}$	0.70	0.75	0.80	0.85	0.90
$Y = n_{GMO} : n_{APG}$	1 : 2.33	1 : 3.00	1 : 4.00	1 : 5.67	1 : 9.00

Plantacare 1200 UP (APG, lauryl glucoside), Cetiol S (dioctyl cyclohexane) and Monomuls 90-O 18 (glyceryl monooleate) were kindly supplied by KemCare Ltd., and used as received.

5.10.2 Results

None of the solutions 1 to 5 were able to disperse dioctyl cyclohexane. Better results were found with heptane, but this was likely to be caused by heptane having a much lower viscosity. Samples of each microemulsion were examined, and no deformation was seen in any of them. There was no change in behaviour with increasing temperature between 25ºC and 50ºC.

References

1. Ward, A.D., et al., *Optical sculpture: controlled deformation of emulsion droplets with ultralow interfacial tensions using optical tweezers.* Chemical Communications, 2006(43): p. 4515-4517.
2. Karlstroem, G., *A new model for upper and lower critical solution temperatures in poly(ethylene oxide) solutions.* Journal of Physical Chemistry, 1985. **89**(23): p. 4962-4964.
3. Fletcher, P.D.I. and D.N. Petsev, *A model for the temperature-dependent interactions in uncharged droplet microemulsions.* Journal of the Royal Chemistry Society, Faraday Transactions, 1997. **93**(7): p. 1383-1388.
4. Pes, M.A., et al., *Temperature-Insensitive Microemulsions in a Sucrose Monoalkanoate System.* Journal of Colloid and Interface Science, 1996. **178**: p. 666-672.
5. Aramaki, K., O. Kazuyo, and H. Kunieda, *Effect of Temperature on the Phase Behaviour of Ionic-Nonionic Microemulsions.* Journal of Colloid and Interface Science, 1997. **196**: p. 74-78.
6. Binks, B.P., P.D.I. Fletcher, and D.J.F. Taylor, *Temperature Insensitive Microemulsions.* Langmuir, 1997. **13**: p. 7030-7038.
7. Mitra, R.K., B.K. Paul, and S.P. Moulik, *Phase behaviour, interfacial composition and thermodynamic properties of mixed surfactant (CTAB and Brij-58) derived w/o microemulsions with 1-butanol and 1-pentanol as cosurfactants and n-heptane and n-decane as oils.* Journal of Colloid and Interface Science, 2006. **300**: p. 755-764.
8. Palazzo, G., et al., *The role of the cosurfactant in the CTAB/water/n-pentanol/n-hexane system: Pentanol effect on the phase equilibria and mesophase structure.* Physical Chemistry and Chemical Physics, 2004. **6**: p. 1423-1429.
9. Mitra, R.K. and B.K. Paul, *Physicochemical investigations of microemulsification of eucalyptus oil and water using mixed surfactants (AOT + Brij-35) and butanol.* Journal of Colloid and Interface Science, 2005. **283**: p. 565-577.
10. Mitani, S. and K. Sakai, *Observation of interfacial tension minima in oil-water-surfactant systems with laser manipulation technique.* Faraday Discussions, 2005. **129**: p. 141-153.
11. Aveyard, R., B.P. Binks, and J. Mead, *Interfacial Tension Minima in Oil + Water + Surfactant Systems.* J. Chem. Soc., Faraday Trans. 1, 1985. **81**: p. 2169-2177.
12. Aveyard, R., et al., *Interfacial Tension Minima in Oil-Water-Surfactant Systems.* J. Chem. Soc., Faraday Trans. 1, 1986. **82**: p. 125-142.
13. Fletcher, P.D.I., *Characterisation of Aerosol OT-stabilised Oil-in-water Microemulsions using a Time-resolved Fluorescence Method.* J. Chem. Soc., Faraday Trans. 1, 1987. **83**: p. 1493-1506.
14. Reimer, J. and O. Soderman, *Microstructure of Alkyl Glucoside Mircoemulsions; Control of Curvature by Interfacial Composition.* Langmuir, 2003. **19**: p. 10692-10702.
15. Penders, M.H.G.M. and R. Strey, *Phase Behaviour of the Quaternary System H_2O/n-Octane/C_8E_5/n-Octanol: Role of the Alcohol in Microemulsions.* Journal of Physical Chemistry, 1995. **99**: p. 10313-10318.

16. Sottmann, T., K. Kluge, and R. Strey, *General Patterns of the Phase Behaviour of Mixtures of H_2O, Alkanes, Alkyl Glucosides, and Cosurfactants.* Langmuir, 2002. **18**: p. 3058-3067.
17. Stubenrauch, C., *Sugar surfactants - aggregation, interfacial, and adsorption phenomena.* Current Opinion in Colloid & Interface Science, 2001. **6**: p. 160-170.
18. Stubenrauch, C., B. Paeplow, and G.H. Findenegg, *Microemulsions Supported by Octyl Monoglucoside and Geraniol. 1. The Role of the Alcohol in the Interfacial Layer.* Langmuir, 1997. **13**: p. 3652-3658.
19. Ryan, L.D. and E.W. Kaler, *Role of Oxygenated Oils in n-Alkyl β-D-Monoglucoside Microemulsion Phase Behaviour.* Langmuir, 1997. **13**: p. 5222-5228.
20. Kahlweit, M., G. Busse, and B. Faulhaber, *Preparing Microemulsions with Alkyl Monoglucosides and the Role of n-Alcohols.* Langmuir, 1995. **11**: p. 3382-3387.
21. Ryan, L.D. and E.W. Kaler, *Alkyl polyglucoside microemulsion phase behavior.* Colloids and Surfaces a-Physicochemical and Engineering Aspects, 2001. **176**(1): p. 69-83.
22. Ryan, L.D., K.-V. Schubert, and E.W. Kaler, *Phase Behaviour of Microemulsions Made with n-Alkyl Monoglucosides and n-Alkyl Polyglycol Ethers.* Langmuir, 1997. **13**: p. 1510-1518.
23. von Rybinski, W. and T.H. Guckenbiehl, *Influence of co-surfactants on microemulsions with alkyl polyglucosides.* Colloids and Surfaces A: Physicochemical and Engineering Aspects, 1998. **142**: p. 333-342.